EXPERIMENTAL INVESTIGATION OF FLEXURAL BEHAVIOR OF ULTRA HIGH PERFORMANCE CONCRETE STRENGTHENED CONVENTIONAL RC BEAM

BY

MUHAMMAD NURA ISA

A Thesis Presented to the

DEANSHIP OF GRADUATE STUDIES

KING FAHD UNIVERSITY OF PETROLEUM & MINERALS

DHAHRAN, SAUDI ARABIA

In Partial Fulfillment of the
Requirements for the Degree of

MASTER OF SCIENCE

In

CIVIL ENGINEERING

MAY 2016

KING FAHD UNIVERSITY OF PETROLEUM & MINERALS

DHAHRAN- 31261, SAUDI ARABIA

DEANSHIP OF GRADUATE STUDIES

This thesis, written by **MUHAMMAD NURA ISA** under the direction of his thesis advisor and approved by his thesis committee, has been presented and accepted by the Dean of Graduate Studies, in partial fulfillment of the requirements for the degree of **MASTER OF SCIENCE IN CIVIL ENGINEERING.**

Dr. Mohammed A. Al-Osta
(Advisor)

Dr. Salah U. Al-Dulaijan
Department Chairman

Dr. Mohammed H. Baluch
(Co-Advisor)

Dr. Salam A. Zummo
Dean of Graduate Studies

Dr. Shamshad Ahmad
(Member)

22/5/16
Date

Dr. Kalimur Rahman
(Member)

Dr. Salah U. Al-Dulaijan
(Member)

Dedicated to

My beloved **parents**, for their **love** and **support,**

my **brother** and **sisters**

for their **support** and **encouragement.**

ACKNOWLEDGMENTS

Thanks be to Almighty Allah who gave me the opportunity, health, strength and patience to carry out this research work.

I will first like to show my gratitude to King Fahd University of Petroleum and Minerals, for providing me with the opportunity to undergo my Master's degree. I will also like to send my gratitude and appreciation to my thesis advisor Dr.Mohammed Al-Osta for his tremendous effort, help, presence, guidance, motivation and feedback during the course this work. He provided me all the necessary assistance while conducting this work.

I would like to express my appreciation to my co-advisor Dr. Mohammed Baluch for his guidance and useful comments which helped us in improving our work. My gratitude also to my committee members Dr. Shamsad Ahmed, Dr. Kalimur Rahman and Dr. Salah U. Al-Dulaijan who gave useful comments and feedback on my work.

I am also thankful to PRAINSA PRECAST CONCRETE who helped us prepare our concrete beams. Thanks to the laboratory staffs and personal Engr. Omer Hussein, Engr. Syed Imran Ali & Mr. Syed Khaja Najamuddin.

I would also like to thank my friends, brothers and senior colleagues, Saheed Adekunle, Abdulmajid Lawan Abba Abubakar, Dr. Adamu Lawan, Dr. Faisal Mukhtar, Ibrahim Mansur and Zubair whose consistent support and encouragement made my life in Saudi Arabia a lot easier. Many thanks to the members of Nigerian community who through guidance and advice have made my stay more pleasant.

Lastly, My thanks and prayers go to my family for their tremendous support, love and care they provided during the course of my entire studies. My sisters for always supporting and encouraging. May Almighty Allah bless us all.

TABLE OF CONTENTS

LIST OF TABLES

LIST OF FIGURES

LIST OF ABBREVIATIONS

2 SJ : Two sides jacketing

3 SJ : Three sides jacketing

d : Distance from extreme compression fiber to the centroid of steel in tension

x : Location of neutral axis

BOT SJ : Bottom side jacketing

EP : Epoxy

FEM : Finite Element Model

PC : Plain concrete beam

RC : Reinforced Concrete beam

SB : Sand blasting

UHPFRC : Ultra-high performance fiber reinforced concrete

b_c : Width of concrete beam

b_u : Width of side UHPFRC jacket

$b_{u,b}$: Width of UHPFRC bottom jacket

h_c : Height of concrete beam

h_u : Height of UHPFRC bottom jacket

$f_{c,c}$: Concrete compressive stress

$f_{c,t}$: Concrete tensile stress

$f_{u,c}$: UHPFRC compressive stress

$f_{u,t}$: UHPFRC tensile stress

f_s : Steel stress

f_{yt} : Yield stress of steel in tension

C_c : Concrete compressive force

C_u : UHPFRC compressive force

E_{st} : Modulus of elasticity of steel in tension

E_{cc} : Modulus of elasticity of concrete in compression

E_{ct} : Modulus of elasticity of concrete in tension

E_{uc} : Modulus of elasticity of UHPFRC in compression

E_{ut} : Modulus of elasticity of UHPFRC in ctension

T_c : Concrete tensile force

T_u : UHPFRC side jacket tensile force

$T_{u,bot}$: UHPFRC bottom jacket tensile force

T_s : Steel tensile force

$\sigma_{c,c}$: Concrete compressive stress

$\sigma_{u,c}$: UHPFRC compressive stress

$\sigma_{c,t}$: Concrete tensile stress

$\sigma_{u,t}$: UHPFRC tensile stress

σ_{s} : Steel tensile stress

$\varepsilon_{cc,ult}$: Ultimate strain of concrete in compression

$\varepsilon_{ct,ult}$: Ultimate strain of concrete in tension

$\varepsilon_{uc,ult}$: Ultimate strain of UHPFRC in compression

$\varepsilon_{ut,ult}$: Ultimate strain of UHPFRC in tension

ABSTRACT

Full Name : [Muhammad Nura Isa]

Thesis Title : [Experimental Investigation of Flexural Behavior of Ultra High performance Concrete Strengthened Conventional RC Beam]

Major Field : [Civil Engineering]

Date of Degree : [April 2016]

Ultra-high performance fiber reinforced concrete have provided us with enormous opportunities in the area of repair and strengthening of concrete structures, by utilizing its excellent material properties to improve the performance of both existing and new structures. This research was undertaken to develop and investigate the behaviors of reinforced concrete (RC) and plain concrete (PC) beams strengthened with UHPFRC jackets in different configurations. Two concepts were used to apply the UHPFRC jackets (i) by sandblasting the concrete beams surfaces and casting UHPFRC in-situ around the desired surfaces (ii) by applying prefabricated UHPFRC strips to beams surfaces using epoxy adhesive. Both concepts were applied to RC beams while only the first concept was applied to PC beams. Bond strength test conducted to ascertain the bond performance of the two concepts shows promising results. The beams specimens were tested in flexure under a four point loading arrangement. Test results regarding crack propagation, stiffness and failure load shows great enhancement for all types of strengthening technique and configuration. Finite element and analytical model were developed to predict the behavior of the strengthened beams. The results show good agreement with experimental results as the model was able to predict the behavior of the beams specimens with high accuracy.

ملخص الرسالة

الاسم الكامل: **محمد نورا عيسى**

عنوان الرسالة: التحقيق التجريبي لسلوك الانحناء للجسور الخرسانية العادية المقواة باستخدام خرسانة فائقة الاداء والمعززة باستخدام الياف الحديد

التخصص: هندسة مدنية

تاريخ الدرجة العلمية: **ابريل 2016م**

وفرت الخرسانة الفائقة الاداء والمعززة باستخدام الياف الحديد لنا فرصا هائلة في مجال إصلاح وتقوية الهياكل اجري هذا .الخرسانية، من خلال الاستفادة من خصائصه المادةالممتازة لتحسين أداء كل من الهياكل القائمة والجديدة والجسور الخرسانية العادية بدون (RC) البحث إلى تطوير والتحقق من سلوك الجسور الخرسانية المسلحة العادية وبتكوينات UHPFRC) والمقواة باستخدام سترات من الخرسانة الفائقة الاداء والمعززة باستخدام الياف (PCتسليح على الجسور الخرسانية العادية (أ) وذلك UHPFRCوقد تم استخدم مفهومين لتطبيق هذا النوع من السترات .مختلفة بتعريض الأسطح الخرسانية الى قاذف رملي وبعد ذلك صب الخرسانة فائقة الاداء والمعززة باستخدام الياف الحديد ومن ثم تطبيقها على UHPFRC حول الأسطح المطلوبة (ب) عن طريق صب شرائط منUHPFRCلتكوين سترات من الأسطح الخرسانية باستخدام لاصق الايبوكسي.طبقت كل من الطرق أ و بوالسابق ذكرها على الجسور الخرسانية . أظهرتنتائج اختبار قوة PC بينما تمتطبيق الطريقة ب فقط علىالجسور الخرسانية العادية بدون تسليحRCالمسلحة التماسك التي أجريت للتأكد من أداء التماسك للطريقتين نتائج ممتازة.كما تم اختبار عيناتالجسور تحت الانحناء وذلك بتطبيق الحمل على أربع نقاط. أظهرت نتائج الاختبارات فيما يتعلق بتطور الشروخ، وصلابة و قوة التحميل لجميع الجسور المقواة باستخدام الطرق المختلفة تعزيزا كبير لجميع أنواع تقنية التعزيز.كما تم تطوير نموذج باستخدام العناصر المحدودة ونموذج تحليليللتنبؤ بسلوك الجسور الخرسانية المقواة باستخدام الخرسانة الفائقة الاداء والمعززة باستخدام الياف الحديد.أظهرت النتائج تطابق جيد ما بين النتائج المعملية والنتائج التي تم الحصول عليها من النماذج المطورة،

حيث وجد ان النموذج كان قادرا على التنبؤ بسلوك الجسور الخرسانية المقواة باستخدام الخرسانة الفائقة الاداء والمعززة باستخدام الياف الحديد بدقة عالية

CHAPTER 1

INTRODUCTION

1.1 General

Reinforced concrete is the most commonly used material for construction. Its versatility economy and ability to be molded and finished into different shape makes it a very suitable construction material. Reinforced concrete consists of plain concrete and steel reinforcement. Plain concrete is brittle material that has good compressive strength but low tensile strength; this makes it crack at even low loads. However reinforcing the plain concrete with steel at the tension side improves it tensile strength and hence the name ‘’Reinforced Concrete’’.

Reinforced concrete (RC) structures are usually designed to efficiently perform their functions over a design service life. However, due to human errors (e.g. design error, change of usage, and lack of maintenance), material defect or change in environmental conditions, most structures has to undergo repairs and rehabilitation over their design service life. Repair and strengthening of RC structures have become so important not only for deteriorating RC structures but also for strengthening new RC members so that they perform much better under service. Initially, research in this area started in order to preserve historical structures and later to important structures such as power stations, nuclear plants, marine structures etc. which are economically and technically unfeasible for demolishing except if the rehabilitation and strengthening techniques failed to secure the needed performance.

Reinforced concrete structures are highly prone to deterioration especially due to human activities and environmental conditions. This tends to reduce the load-bearing capacity of the structure, causing physical damage/deterioration thereby making its physical appearance aesthetically unappealing and a reduction in its service life.

In the last two decades, researchers have developed different materials and techniques for repair and rehabilitation of existing structures as well as strengthening new RC members. Among the most widely used is the Carbon Fiber Reinforced Polymer (CFRP). Research works conducted on strengthening with CFRP have yielded many positive results. El-Enein et al [1] investigate the flexural strengthening of an RC slab-column joint using CFRP on the tension side and the result shows a significant increase in the flexural load carrying capacity and reduction in deflection of joints. Monti and Liotta [2] through an experimental and analytical study on CFRP strengthening in shear of RC beams came up with closed-form design equations for shear strengthening with CFRP. A lot more research works have been and are currently been conducted on the effectiveness of using CFRP as a strengthening material.

A more recent material developed and used for both repair, rehabilitation, and strengthening of RC structures is the Ultra-high performance fiber reinforced concrete (UHPFRC). Ultra-high Performance Concrete has been developed in a number of countries including Korea, France, USA, Japan and here at KFUPM, Saudi Arabia. UHPFRC's high strength was achieved through using improved concreting techniques, materials (ultra-fine pozzolan), very low water-cement ratio, high quality and higher dosage of superplasticizer, high cementations material content, and sometimes involves use of synthetic or steel fibers to decrease brittleness and increase energy absorption capacity as clarified by Rahman et

al [3] Its similarity in physical and some mechanical properties to conventional reinforced concrete, has fetched to it, attention in the repair and rehabilitation research industry. Research works conducted on both its durability and structural performance has so far shown very promising results. Works have also been conducted on its potentials and effectiveness to rehabilitation and strengthening of RC structures.

Hakeem [4] studied the mechanical properties of the UHPFRC. It was found that the compressive strength was 163 Mpa, with an elastic modulus of 57 Gpa. The results showed that the flexural strength increases from 15.2 MPa with no fiber to 24.4 MPa with 3.1% fiber and 31.4 MPa with 6.2% fiber. Lubbers [5] indicated that the compressive strength and flexural strength of UHPC could be 2 to 3 times and 2 to 6 times greater than high-performance concrete (HPC), respectively. Hussein [6] studied the flexural capacity of ultra-high performance concrete – normal strength concrete composite beams without stirrups. The beam specimen has the UHPFRCC in tension and the normal concrete layer in compression. The test results revealed that the performance of the proposed composite system was successfully enhanced in both flexural and shear capacity. Habel et al [7] conducted a study on the structural response of 12 – full-scale UHPFRC –normal RC-beams composite, having (UHPFRC) layer in tension. It was observed that, the UHPFRC significantly improved structural capacity of the composite member. Martinola et al [8] studied the effect of fibre reinforced concrete in strengthening and repair of full scale reinforce concrete beams. Both experimental and numerical techniques were adopted in this investigation. The results showed that the effectiveness of the proposed technique both at ultimate and serviceability limit state.

In this proposed work, we investigate into the behavior of both RC and plain concrete (PC) beams strengthened with UHPFRC using different configurations as well as checked the effectiveness of two different methods of applying the UHPFRC to the RC beams.

1.2 Need for Research

Despite these valuable research studies on using UHPFRC in repairing and strengthening of RC beams, it was observed these studies overlooks the individual contribution of longitudinal sides strengthening on flexural strength of concrete beams.

Also, information regarding comparison of the various techniques for which UHPFRC can be used to strengthened RC beams is lacking in the literature.

Another aspect which has not been given attention was the effect of UHFRC strengthening on plain concrete beams. The objective of this investigation is to evaluate the individual as well as combined effect of sides jacketing of both RC and plain concrete beams with UHPFRC. Additionally, comparison of two methods used to apply UHPFRC strengthening to RC beams will be made.

1.3 Objectives of these Research

The aim of this research is to "Assess the strengthening potential of our locally made UHPFRC on conventional RC and PC Beams"

To achieve the above aim, the following objectives need to be achieved;

1) Check the Ultimate Strength of a conventional RC beam strengthened with UHPFRC at various locations

2) Assess the effect of strengthening with UHPFRC on the midspan deflection of RC beam

3) Study crack propagation pattern and assess crack with and crack spacings.

4) Assess the possibility of substituting tensile reinforcement with UHPFRC strengthening for adoptability in corrosion prone areas.

5) Develop a finite element model of a similar conventional or normal RC beam strengthened with UHPFRC the FEA package ABAQUS.

6) Suitably extend existing mechanistic model behavior of RC beams to account for partial jacketing provided by UHPFRC. The model will be able to predict failure load both control and strengthened beam specimens.

CHAPTER 2

LITERATURE REVIEW

2.1 General

Over the last decade, a large number of research studies on repair and strengthening of concrete members using various types of high strength and high performance concretes have been carried out by engineers and researchers worldwide. Although most of these studies were carried out for the sake of research, quite a number of them have been put into practice and have shown promising performance.

Most of the research works were conducted to ascertain the effectiveness of these types of concrete in the repair of damaged RC members while others were conducted on strengthening of undamaged RC members in either flexure, shear, torsion or both. However, others investigate into the performance of normal RC-high strength concrete composite members where the high strength/high-performance concrete represents a large percentage of the total volume of the member

2.2 Ultra-high performance fiber reinforced concrete (UHPFRC)

Ultra-high performance fiber reinforced concrete (UHPFRC) is a highly dense, steel fiber reinforced cementitious composite material having a compressive strength in excess of 130 MPa, tensile strength in excess of 5 MPa and first cracking strength in excess of 4 MPa. In addition to strength, UHPFRC has excellent durability properties.

The high strength of UHPFRC is achieved through the use of improved concreting techniques, materials (addition of ultra-fine pozzolans), very low water-cement ratio, high quality and higher dosage of superplasticizer, high cementitious material content and optimum volume of high strength ductile steel fibers.

2.2.1 Properties of UHPFRC for Effective Performance as a Repair And Strengthening Material

The properties and behavior of a repair material should fulfill requirements pertaining to strength and durability. Knowledge of such properties and behavior under certain load conditions is essential for the design of a repair, rehabilitation or strengthening techniques using UHPFRC.

2.2.1.1 Tensile Behavior of UHPFRC

UHPFRC under a direct tension test has an increase tensile strength and shows a more strain hardening response when compared to conventional reinforced concrete. Graybel [11] developed an idealized stress-strain response of UHPFRC under direct tensile test by dividing the behavior into four different phases as shown in Figure 1.

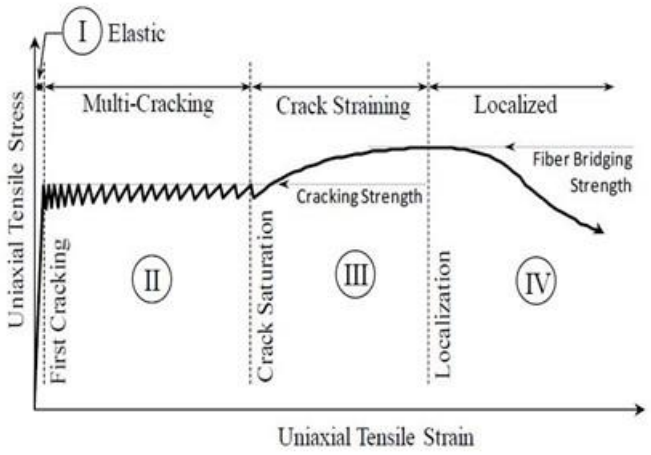

Figure 1: Phases in uniaxial tensile behavior of UHPFRC (Graybeal [11])

Under phase, I, the UHPFRC behave in an elastic manner while phase II indicates the formation of closely spaced cracks within the specimen. Phase III begins at strain level when additional crack formation between existing cracks is unlikely, thus causing existing cracks to increase in width. Phase IV represents the time when individual cracks have reached its strain limit and steel fiber bridging the gap created by the crack starts to get pulled out.

2.2.1.2 Flexural Behavior

Figure 2 shows a flexural strength test of UHPFRC prism. It can be observed that the behavior is linear at the initial stages up to the first crack. After the first crack, a decrease in the rate of load increase is observed while deflection increases at a faster rate.

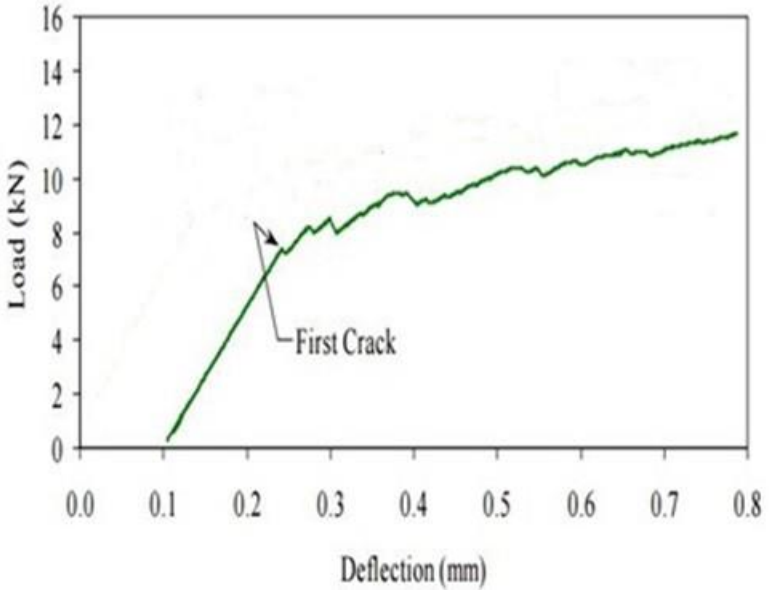

Figure 2: Load-deflection response of UHPFRC prism (UDT [12])

2.2.1.3 Fatigue Behavior

Tensile fatigue tests conducted by Makita and Bruhwiler [14] on steel reinforced ultra-high performance fiber reinforced concrete (R-UHPFRC) shows that it possesses a significant amount of fatigue resistance that makes it an effective fatigue strengthening material for RC structures. At the initial stage of the test, UHPFRC material was the most active in determining the fatigue behavior. However in the later stages, reinforcing bars determines the fatigue behavior of the R-UHPFRC. Therefore, for high fatigue deformations, it is recommended to add reinforcing bars to the UHPFRC layer.

2.2.1.4 Durability Performance

The high dense microstructure of UHPFRC has made it possible for foreign substances to penetrate through it. This made UHPFRC to be highly resistive to chloride penetration,

sulfate attack, carbonation etc. Experimental tests conducted by Voort [15] shows that UHPFRC has a high scaling, abrasion, freeze-thaw and alkali-aggregate reaction resistance as shown in Figure 3.

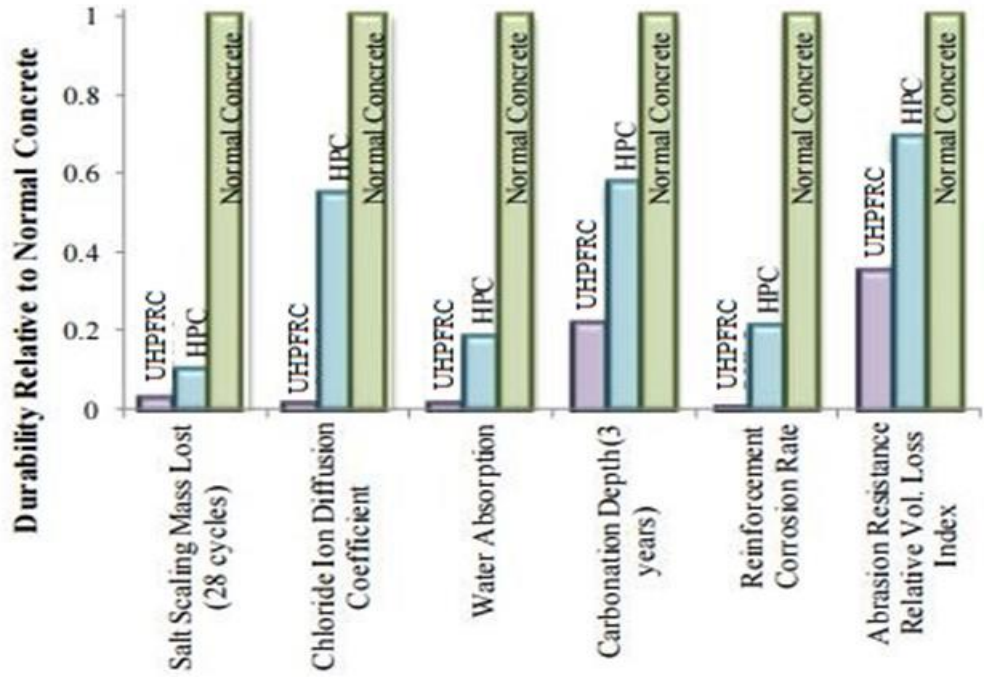

Figure 3: Durability Performance of UHPFR relative to High-performance concrete and normal concrete (Voort [15]).

2.2.1.5 Coefficient of Thermal Expansion

The coefficient of thermal expansion of UHPFRC was found to be slightly higher than that of a normal concrete Ahlborn et al [16]. This is because the coefficient of thermal expansion for concrete is controlled the coefficient for its constituents aggregate. Fine sand and cement been the main constituents in UHPFRC will determine its coefficient of thermal expansion while coarse aggregates (usually gravels) will determine that of normal concrete.

Because the coefficient of thermal expansion of UHPFRC and of normal concrete a very close, it can be suitably used as a repair material since differential thermal expansion between UHPFRC and the host concrete will be avoided.

2.2.1.6 Fire Resistance

Fire resistance tests conducted on high-performance concrete (HPC), ordinary concrete (OC) and UHPFRC specimens show that explosive spalling of UHPFRC occurs at a temperature of 790˚C which is 100˚C and 190˚C more than for HPC and OC respectively Liu and Hang [27]. Compressive strength of UHPFRC increases at a temperatures between 200-300˚C but starts to fall above this range Tai et al [28]. Residual strength of UHPFRC after 60min of fire test at temperatures between 450-550˚C is 62.2% while that for HPC and OC is 46.7% and 58.5% respectively. Additionally, loss of mass in HPC and OC was considerably more than that of UHPFRC for the same fire testing conditions Liu and Hang [27]. As such, the high fire resistance of UHPFRC will make it a suitable repair and rehabilitation material for RC structures.

2.3 Review of works conducted Using UHPFRC as a Repair Material

2.3.1 Flexural Strengthening of RC Structural Members using UHPFRC

Flexural strengthening of RC beams with high-performance fiber reinforced concrete (HPFRC) was carried out by Martinola et al [8] to ascertain the potential of HPFRC in strengthening both damaged and undamaged RC beams. The strengthening material (HPFRC) used was a self-flowing mortar having a 28days cube compressive strength of 177 MPa and having a strain hardening behavior in tension. A layer of HPFRC was cast at

the bottom and the two sides RC beam specimens that have been roughened by sandblasting. Four (4) different specimens were tested; one RC beam as control, one strengthened RC beam, one strengthened plain concrete beam and one repaired damaged RC beam. The beams were tested in flexure under a four point loading arrangement at a constant displacement rate.

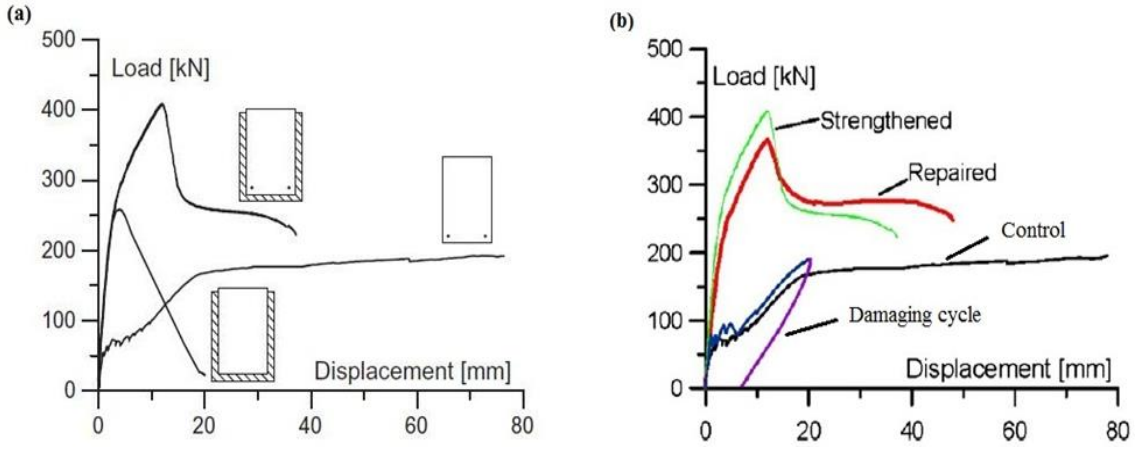

Figure 4: Load Displacement Curves for (a) strengthened beams (b) strengthened, repaired RC beam and damaging cycle (Martinola et al [8])

The strengthened RC beam shows a sudden failure, but due to the hardening of steel reinforcement, the load stabilizes at a lower load below the failure load as shown in Figure 4. While the strengthened plain concrete beam shows a brittle failure at a load level much lower than the strengthened RC beam, however due to the presence of HPFRC some strain softening was observed as shown in Figure 4. For the repaired beam which has been already damaged to the yielding of the tensile reinforcement and then unloaded, the failure behavior was much like that of the strengthened RC beam only that the failure load is 11% lower for the repaired beam. In addition, the yielding behavior is similar to that of the strengthened RC beam. Strengthening with HPFRC jacket has proved effective in increasing the load

bearing capacities of RC beam, damaged RC beam and plain concrete beam by 2.15 times, 1.9 times and 1.55 respectively in addition to reduced crack opening of when compared with the control as reported by.

Ranjan et al [17] studied the behavior of repaired damaged RC beams retrofitted with UPFRC strips as overlays at the tension sides of the beams and the effect of curing type (hot air curing, steam curing, and moist curing) on the strength of UHPFRC. Damage was introduced to the RC beams by loading some specimens to 80% of their ultimate load while others to 90 % of the ultimate load to cause flexural cracking. To retrofit the damaged RC beams, 20mm thick UHPFRC strips were cast and cured, then bonded to the required surface of the concrete using an epoxy adhesive and tested under a four point loading arrangement at a displacement rate of 0.5mm/min. Results of the effect of curing type on compressive strength shows compressive strengths for all the methods is equal at 3 days of curing. However, at 7 and 14 days curing, hot air curing (HC) gives the highest compressive strength while moist curing gives the least. Nevertheless, for 28 days curing period hot air highest strength while steam curing gives the least strength as shown in Figure 5.

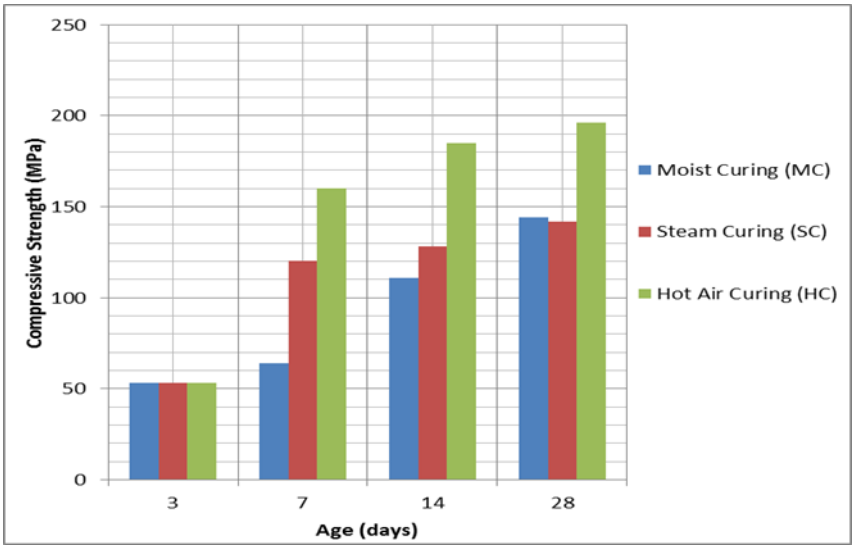

Figure 5: Compressive strength of cubes cured by moist, steam and hot air curing (Ranjan et al [17])

The retrofit was found to increase the load carrying capacity of the damaged beams, reduces the midspan deflection and crack openings when compared to the control specimen. The failure load for all the repaired beams was found to be more than that of the control for all cases of curing methods.

Experimental investigation and numerical modeling of the mechanical properties of ultra-high performance fiber reinforced concrete was carried out by Lampropoulus [9] to determine its effectiveness in strengthening reinforced concrete beams compared to other existing strengthening techniques. The UHPFRC material used contains a relatively higher volume of steel fibers of 3% compared with 2% commonly used and has a compressive and tensile strength of 164 and 30 MPa respectively. A direct tensile test on dog bone specimens, flexural testing on beam specimens and shrinkage strain test on prisms were

experimentally and numerically (using FEA package ATENA) conducted as shown in Figure 6. Strengthening of the RC beam is made by applying a layer or jacket of UHPFRC over the required surface of the RC beam. Three strengthened beam models in addition to the initial (control) beam model were developed; one was strengthened at the tension side (bottom), another strengthened at the compressive side (top) while the last one strengthened at the bottom and around the two faces of the beam

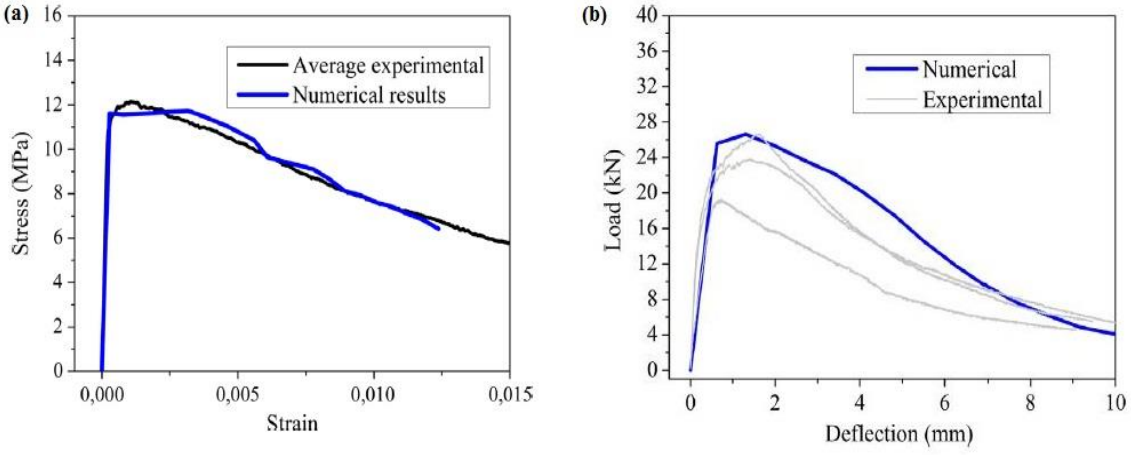

Figure 6: Experimental and numerical test results (a) Tensile test (b) Flexural test (Lampropoulus [9])

The result of shrinkage test indicates that shrinkage of UHPFRC is greatly reduced by the presence of steel fibers. Overall, the response of the strengthened beams was insignificantly affected by the difference in shrinkage strain of the UHPFRC layer. Slip at the interface of beams specimens was maximum near the ends of the beam. Specimen strengthened at the tension side experienced the highest slip while the beam specimen strengthened at its three sides has very small and least slip. Both yielding and ultimate moment of the beam specimens was found to be significantly increased compared to the control specimen. The beam strengthened at the three sides (ST_UHPFRC_3SJ) has the highest increment while

the beam strengthened at the tension side (ST_UHPFRC_TS) and the beam strengthened at the compression side (ST_UHPFRC_CS) has approximately equal increments. This results of yielding and ultimate moment were compared to similar RC beam specimens strengthened by adding a layer of reinforced concrete at tension side beam strengthened at the tension side (ST_RC_TS) for one beam and plain concrete at the compression side beam strengthened at the tension side (ST_PC_CS) for another beam. It was found that beam strengthened at with RC layer at tension side (ST_RC_TS) has higher moments when compared to the corresponding beam strengthened with UHPFRC (ST_UHPFRC_TS). While beam strengthened with plain concrete at compression side (ST_PC_CS) has relatively lower moments compared to the corresponding beam strengthened with UHPFRC (ST_UHPFRC_CS). However, Beam strengthened with UHPC over its 3 sides (ST_UHPFRC_3SJ) has the highest moment increment compared to all.

A high-performance fiber reinforced concrete known as CARDIFRC developed by Alaee and Karihaloo [18] at Cardiff for the purpose of strengthening and rehabilitation of damaged reinforced concrete beams in a number of different retrofitting arrangements as shown in Figure 7. Two types of RC beams were investigated; Type I RC beams reinforced only in flexure and type II reinforced in both flexure and shear. Four Types I beams and three Type II beams were tested until failure under a three point loading and four point loading arrangement respectively to serve as controls. While the remaining beams each for Type I and Type II were loaded in a similar manner to 75% of their respective average control failure load. The damaged beams were then retrofitted based on three parameters namely; retrofit thickness (16mm, 20mm), CARDIFRC mix (mix I having water/binder =

0.18, mix II having water/binder = 0.16), retrofitting configurations (4 – configurations for Type I and 3 – configurations for Type II beams).

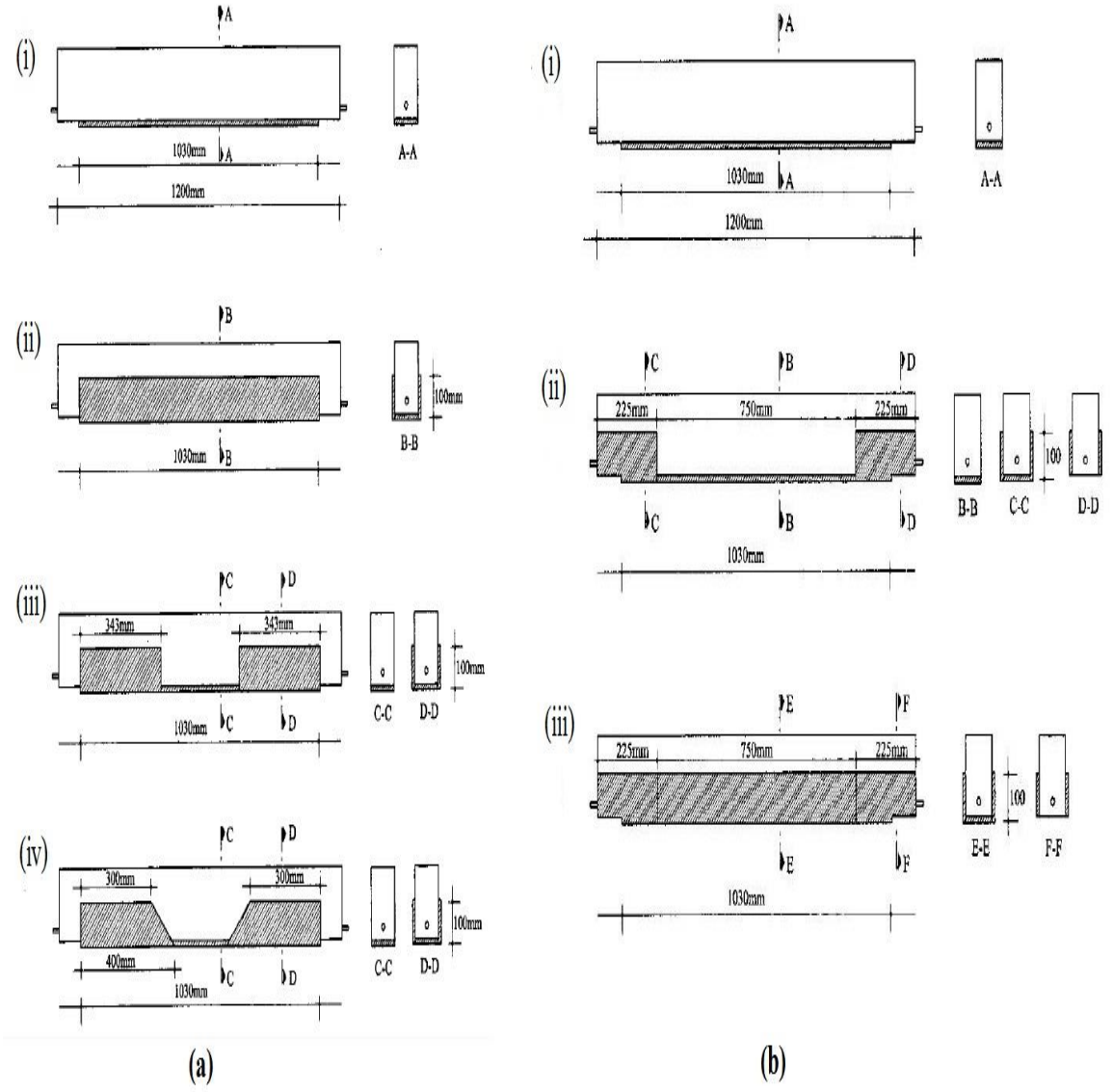

Figure 7: Configurations of retrofitting (a) Type I beams (b) Type II (Alaee and Karihaloo[18])

The CARDIFRC mixes were cast as flat strips of desired dimensions separately and cured. Bonding to the beam surface is achieved by using epoxy adhesive. Test results show that all strengthening configurations have proven to be effective in increasing the failure load of the specimens above that of the control for all cases. Strengthening configuration in which beams are retrofitted with CARDIFRC strip at the bottom and the two sides as shown in Figure 11(a)(ii) and (b)(iii) gives the highest increase in failure load compared to other configurations, while type of mix and thickness of CARDIFRC strips does not significantly affect the failure load.

2.3.2 Shear Strengthening of RC Structures using UHPFRC

The flexural-shear response of reinforced concrete (RC) beams strengthened with either reinforced ultra-high performance fiber reinforced concrete (RU) or ultra-high performance fiber reinforced concrete (UHPFRC) was studied by Noshirivani and Bruhwiler [19]. The specimens were classified into three (3) groups based on type of composite materials; first group made up of RC beams only, another group (RU-RC) consisting of RC members strengthened with RU at the tension side and the last group (UHPFRC-RC) consists of RC beams strengthened with UHPFRC layer at the tension side also. Each group was further subdivided based on cantilever span (long, medium and short span), based on stirrup spacing (narrow or wide spacing) and based on reinforcement content.

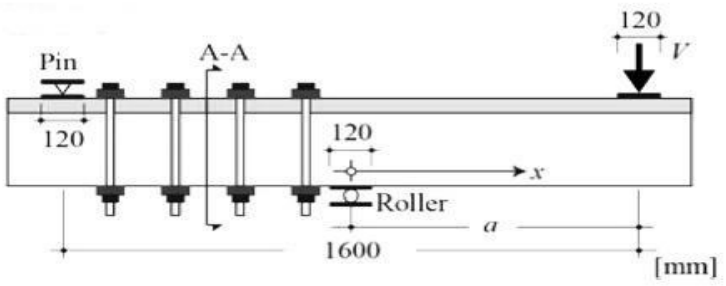

Figure 8: Specimen Test Set-up (Noshirivani and Bruhwiler[19])

Test results show that all RU-RC beams having long and short cantilever span failed in flexure while most of the medium cantilever span beams had a flexure-shear failure after reaching their maximum bending resistance. The increase in transverse reinforcement and a corresponding decrease in stirrup spacing improves both ultimate resistance and rotation capacity of the specimens. However, the bond strength between the UHPFRC element and the reinforcing bars depends on tensile strength and strain softening of the UHPFRC material. While crack propagation in the composite beams is affected by both longitudinal and transverse reinforcement, UHPFRC-RC beams show lesser no of cracks and crack width than the RU-RC specimens. In specimens with higher stirrups spacing's, flexure-shear cracks tend to interrupt the spread of flexural cracks in competing to become the collapse crack. In addition, beams having larger stirrup spacing has more irregular horizontal crack spacing compared to beams with smaller stirrup spacing. In summary, failure of an RU-RC beam depends on softening behavior of the reinforced RU layer at the tip of the crack that determines which crack (i.e. flexure or flexure-shear) becomes the collapse crack. Longitudinal reinforcement in the RU layer increases the beam's moment of resistance. Both RU-RC and UHPFRC-RC specimens improve beams resistance to both tensile and bending stresses compared with their reference RC beams.

The performance of reinforced concrete (RC) beams retrofitted by fiber reinforced concrete (FRC) jacketing under shear was reported by Ruano et al [20] to determine the effectiveness of FRC as a shear repairing and strengthening material. RC beams with and without stirrups were cast. Some of the beams with stirrups were damaged to a certain extent before strengthening. One RC beam without stirrups was used as a control specimen. While, different mixes of high-performance concrete were prepared; plain concrete, FRC with 30 kg/m^3 of steel fibers and FRC with 60 kg/m^3 of steel fibers to assess the effect of steel fiber content on the performance of the strengthening. The specimens were jacketed at the bottom and the two sides of the beam and were tested under load controlled at the initial stages and then under displacement control at the later stages. Beams having stirrups and strengthened with FRC were found to have an increase in shear strength while those strengthened with plain concrete shows no significant increase. However for RC beams with no stirrups and retrofitted with plain concrete or FRC shows greater stiffness and shear strength compared to their control specimen, despite having a sudden failure with development of wide cracks. In addition, beams repaired with FRC shows greater increase in shear capacity for both types of beams as such prove effective for shear strengthening. Beams strengthened or repaired with plain concrete experienced debonding of the jackets. Therefore, the addition of steel fibers to the jacketing mix prevents debonding of jackets from the RC beams.

2.3.3 Torsion Strengthening of RC Structures

The performance of reinforced concrete beams strengthened with ultra-high performance fiber reinforced concrete (UHPFRC) under torsion was investigated by Mohammed et al [21]. The RC beams were strengthened with UHPFRC using three different configurations. Finite element model was also developed to prove and justify the effectiveness of the strengthening technique. The RC beams were produced with only longitudinal steel reinforcement (i.e. with no stirrups) whiles the UHPFRC was reinforced with 2% steel fiber volume. Three different strengthening configurations were used; jacketing on two, three and four sides jacketing. One RC beam was used as a control while 10 others were strengthened with varying thickness of the UHPFRC layers. They use four beams each for the four sided and three sided jacketing with each beam having a different jacket thickness i.e. 10, 15, 20 and 25mm respectively. While 15 and 25mm thick layer were used to strengthened the two-sided jacket beams. The specimens were tested under pure torsion created by loading the specimens at an eccentricity from the longitudinal axis of the beam. Test results show that all beam specimens shows a significant increase in torsional strength as shown in Figure 9. Beams jacketed on all the four sides' shows the highest increase in strength while beams jacketed at the two faces shows lowest increase in torsional strength. The torsional strength was found to increase with increase in UHPFRC layer thickness for all jacketing configurations as in Figure 9(b). However, beams jacketed at three sides despite showing a significant increase in strength shows hairline cracks at the unjacketed face, which further increase in size with increased loading until they reach the UHPFRC jacket layers ultimately causing debonding of the layer from the main beam. Similar crack propagation pattern was reported for the two-sided jacketed beams. While the cracking

behavior four sides jacketed beams was similar to that of the control beam where the cracks propagate from the larger face of the rectangular section since these faces experience greater shear stresses

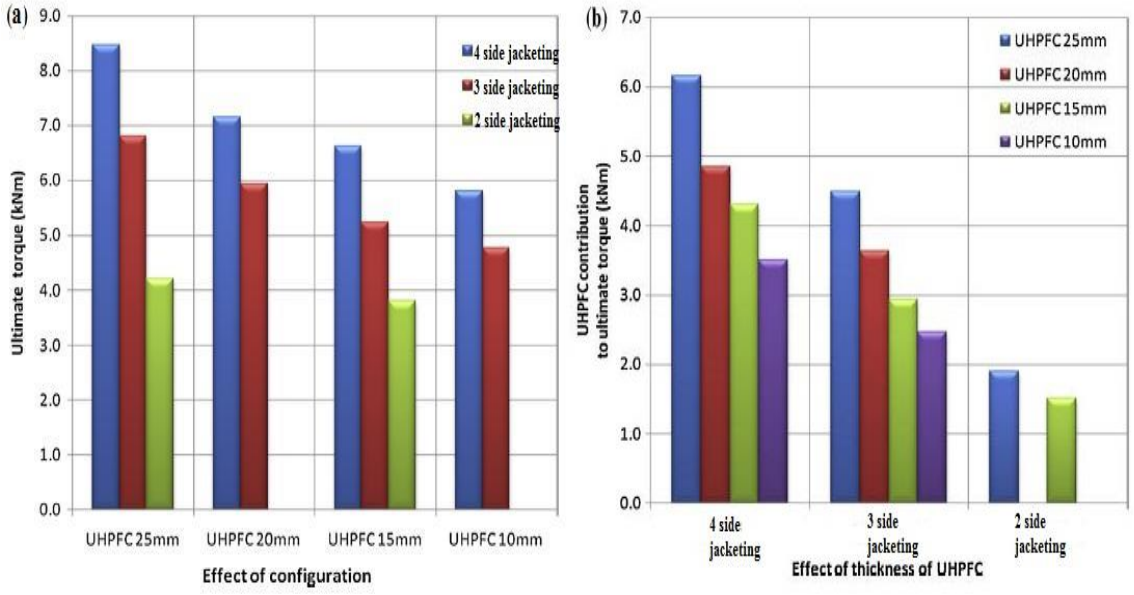

Figure 9: (a) Effect of (a) configuration (b) UHPFRC layer thickness on the ultimate torque of tested beams (Mohammed [21])

The results of finite element model show good agreement with the experimental test values for all specimens. It was therefore observed that RC beams fully jacketed on all its four sides is more effective in increasing the torsional strength and also preventing cracks that might cause debonding of jackets made using other configurations. However, jacketing beams on all its four side is impractical in existing structures.

2.3.4 Composite Normal Concrete- UHPFRC Structures

To improve the load bearing capacity of reinforced concrete member. A two-layer reinforced concrete beam was developed by Ishakov et al [22] with steel fiber high-performance concrete (SFHPC) in the compression zone and normal strength concrete (representing the original member) in tension zone. The thickness of the SFHPC was selected to be equal to the depth of compression zone of the composite member. However, the reinforcement in the upper part of the original member was assumed ineffective, as it will be located close to the neutral axis of the composite member. SFHPC cubic specimens having different steel fiber contents were tested to ascertain the optimum fiber content for highest compressive and split tensile strength while corresponding cylindrical specimens were tested to assess the development of poison deformation. The beam specimens were tested under a four point loading arrangement. Results and findings from the tests conducted on SFHPC specimens show that steel fiber content of 30 – 40 kg/m^2 gives the optimum compressive and tensile strength as well as poison coefficient. Beam specimens show more ductile behavior up to failure when compared to some strengthening techniques where the repair material is applied in the tension zone i.e. shown in Figure 6 which a sudden and sharp decrease in load after reaching the load is experienced indicating a rather lower ductility. However, at high deflections, horizontal cracks were found to propagate between the SFHSC and the normal concrete layer thereby causing de-bonding of the two layers.

Experimental and analytical study on the improvement in flexural and shear capacity of reinforced concrete composite members consisting of either normal strength concrete

(NSC) or high strength concrete (HSC) at the compression zone and ultra-high performance fiber reinforced concrete (UHPFRC) at the tension Hussein and Amley [6]. Sets of beams each for NSC-UHPFRC and HSC-UHPFRC in addition to two control specimens one each for NSC and HSC. All specimens were reinforce with both tension and compression steel but adequate stirrups were only provided on the right-hand span of the beams so as to ensure shear failure on the left support. Stud connectors and or dowels were used to connect the layers and their effect been studied. The volume of steel fibers in UHPFRC and type of connector used were used to distinguish between specimens of the same composite materials. Compressive strength and split tensile strength, tests were conducted on NSC, HSC, NSC-UHPFRC and HSC – HSC cylindrical specimens, flexural strength test carried out on NSC, HSC, NSC-UHPFRC, and HSC – HSC prisms while bond strength was carried out on 150mm cubes of NSC-HPFRC and HSC-UHPFRC. Beams specimens were tested under a three point loading arrangement. Results of flexural strength test on prism specimens show that failure load increases with increase in steel fiber for both composite specimens as shown in Figure 10. This results due to increase in ductility due to the presence of more steel fibers around cracks causing more effective transfer of stress. However, Ultimate load for NSC was found to be more than that of HSC likely due to HSC been more brittle than NSC.

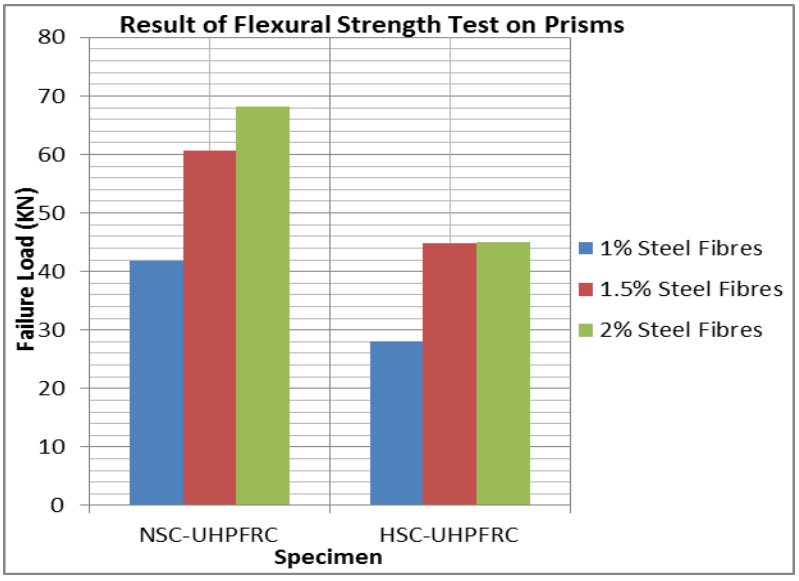

Figure 10: Results of flexural strength test on prisms (Hussein and Amley [6])

Split tensile tests show that there is a strong bond between the composite layers. However, the bond strength was not affected by the amount of steel fibers. Shear resistance test shows a significant increase in shear capacity of the composite beam specimens compared to their control specimens as shown in Figure 11. The test results further revealed that the addition of stud connector or dowels does not have any major effect on the shear capacity of the specimens.

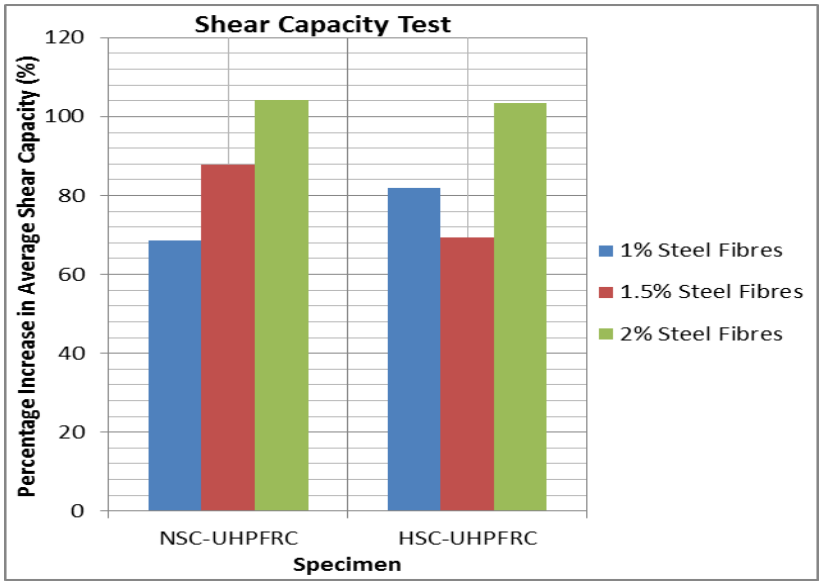

Figure 11: Results of shear capacity test (Data sourced from Hussein and Amley [6])

The result of three-point load tests on beam specimens' shows that all beams fail in shear at the left-hand side of the beam as required at a higher applied load than their corresponding control with NSC-UHPFRC beams having 1.6-2.0 times higher than NSC beam and HSC-UHPFRC beams having 1.7-2.0 times higher than HSC beam. Values of maximum deflections measured show no significant difference with increase in the steel fiber volume content as shown in Figure 12. The addition of shear stud connector or dowels also shows no effect w=on measured deflections This indicates that the ductility of the composites members is not affected by the variation in the fiber content present in the UHPFRC layer.

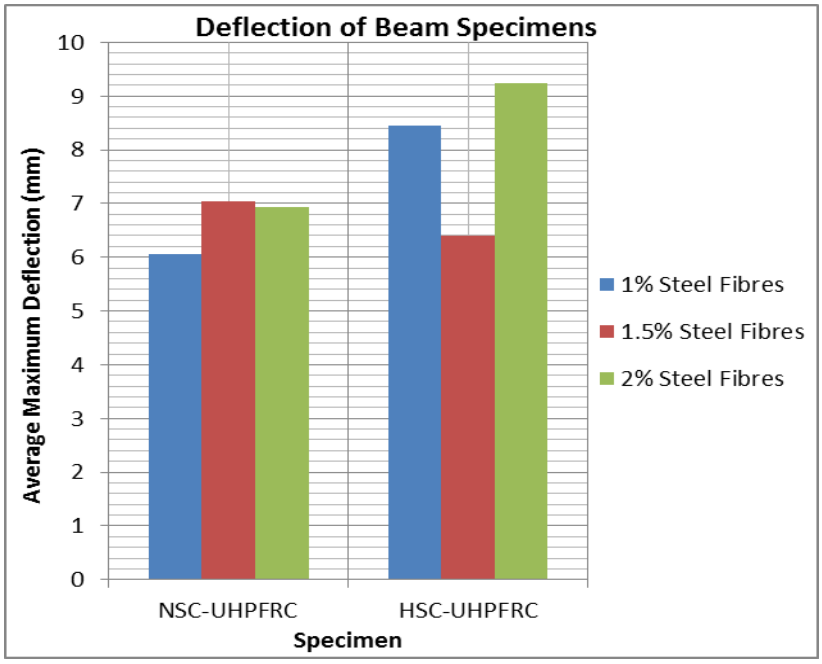

Figure 12: Deflection of composite beam specimens (Hussein and Amley [6])

The analytical model operates based on the assumption that shear capacity of the of the composite beams is equal to the shear resistance provided by the NSC/HSC beam neglecting shear reinforcement and shear resistance provided by the steel fibers in the UHPFRC layer. The model shows some reasonable ability to predict the shear strength of the specimens. However, all the predicted results are lower than the experimental results, which is likely due to neglecting the shear resistance contribution of the solid ultra-high performance concrete (without the fibers) in the prediction model.

Ishakov et al [23] investigate the behavior of conventional concrete and ultra-high performance fiber reinforced composite members. Two types of the composite members were investigated; those having reinforcing bars in UHPFRC layers (R) and those without (NR). An analytical model for predicting the behavior of the composite beams was also

developed. The test specimens consist of an RC substrate (at the bottom in compression) and UHPFRC layer at the top (in tension). Experimental parameters are the; UHPFRC layer thickness and presence of steel reinforcing bars in the UHPFRC layer. The specimens were tested under a four point loading arrangement. Both beams with and without reinforcing bars in their UHPFRC layer show increase in both stiffness and ultimate force with the once having the reinforcing bars showing the most significant increase. Beams having no reinforcing bars in their UHPFRC layer shows interface cracks, which later developed into a debonding crack thereby changing the behavior of these beams. Reinforcing bars in UHPFRC layer shows an increased hardening, which improves not only the ultimate resistance of the beams but also reduces crack propagation. The analytical model was developed based on the bending beam theory. The model was able to predict the behavior of the composite members in flexure within some acceptable range.

2.3.5 Repair and Strengthening of Existing Structures with UHPFRC

Bastien-Masse and Bruhwiler **[**24] reports on the performance of bridge deck slabs strengthened with ultra-high performance fiber reinforced concrete. Results of flexural testing conducted by Oesterlee [25] indicating an increase in flexural strength of up to 165% of the control RC beam and cantilever test on such composite beams by Noshirivani and Bruhwiler [19] reports an increase in shear resistance were used. Punching test on composite two-way slabs with and without reinforcing bars inside the UHPFRC layers was conducted. Test results show that UHPFRC layers increases the punching resistance by 67% without reducing rotation capacity and that addition of reinforcing bars in UHPFRC layer does not affect the punching resistance of the specimens. Suitability of this technique

proved through the above series of tests, prompt its adoption in strengthening of an old slab bridge at Lausanne, Switzerland. The slab bridge was strengthened to meet the safety requirements in both bending and shear in accordance to the Swiss Standard for existing structures (SIA 2011). The upper layer of the slab was first scrapped off under water pressure jet to remove damaged top surface and create the needed roughness. The UHPFRC layer was cast over the slab while a thicker layer reinforced with steel bars was cast over the columns supports since more strengthening is required as such locations.

Figure 13: (a) view of Bridge (b) placing of UHPFRC on bridge slab [24]

The technique was found to effectively increase the load bearing capacity of the bridge. In the year 2014, more than 20 bridges were undergoing rehabilitation and strengthening using this technique

A strengthening technique using UHPFCR used to strengthen an existing bridge known has Husine Bridge in the City of Le Mans, France was reported Thibaux [26]. The bridge was initially having two parallel decks originally designed to support a three lane dual carriageway was strengthened to support four road traffic lanes at its downstream deck and

a bicycle and tram lane at its upstream deck. Strengthening was achieved by providing an external prestressing to the load bearing I-beams supporting the bridge decks. The bridge spans were supported by I-beams having a web thickness of 200mm. To increase the load carrying capacity, two layers of UHPFRC 200mm thick and 900mm high, one at each side were laid along the length of the I-beams. The cross sections of the composites were held together using prestressed crossed bars at several locations along the beams length. Strengthening is achieved by transverse prestressing of the UHPFRC elements provided at the faces of the web as shown in Figure 14.

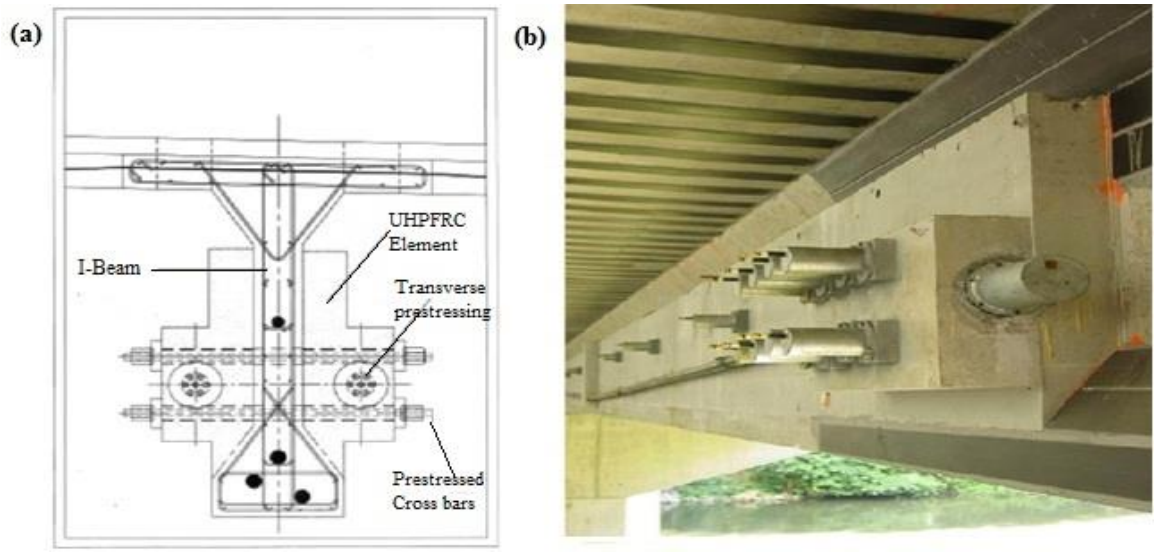

Figure 14: Fully strengthened beam (a) section (b) side view (Thibaux [26])

The technique has proved to be effective in eliminating the difficulty and challenges in laying reinforcement and formworks in the case of conventional reinforce concrete. The technique was carried out at a low cost and in a shorter period without need to stop or divert moving traffic and most importantly, the bridge performance under re-designed load was positive.

CHAPTER 3

EXPERIMENTAL PROGRAM

3.1 General

Experimental investigations comprising of material strength tests, bond strength test and flexural strength test were conducted. The material strength tests were conducted to determine the uniaxial stress-stress behavior of both UHPFRC and normal concrete in compression as well as in tension. The material behavior gives a clear idea of the likely behavior of the beam specimens under flexural test. In addition, these behavioral data were used to develop the FEA model of the beam specimens. Bond strength tests; slant shear test and split cylinder tensile strength test conducted on composite UHPFRC-normal concrete composite cylinders were conducted to ascertain the suitability of using sandblasting or epoxy adhesive in achieving the necessary bond strength. Beams specimens were strengthened with UHPFRC jackets either by casting fresh UHPFRC to sandblasted surface or by bonding UHPFRC strips using epoxy adhesive in different strengthening configurations. The prepared beams specimens were tested under four point loading arrangement after curing for 28 days.

3.2 Preparation of Normal Concrete Beams

Two types of normal concrete beams were prepared; reinforced concrete (RC) beams and plain (unreinforced) concrete (PC) beams. A total of twelve (12) beams were prepared comprising of eight (8) RC beams and four (4) PC beams. The RC beams were reinforced with two (2) 12mm diameter bars at both top and bottom and 8mm diameter stirrups spaced

at 50mm center to center as shown in Figure 15. To ensure quality control, molds fabrication, reinforcement bending, and concreting works were all done at a precast concrete company "PRAINSA PRECAST CONCRETE" as shown in Figure 16, 17 and 18. In the case of RC beams, strain gauges were attached to the reinforcing bars and stirrups to monitor the strain of the reinforcement when performing the test.

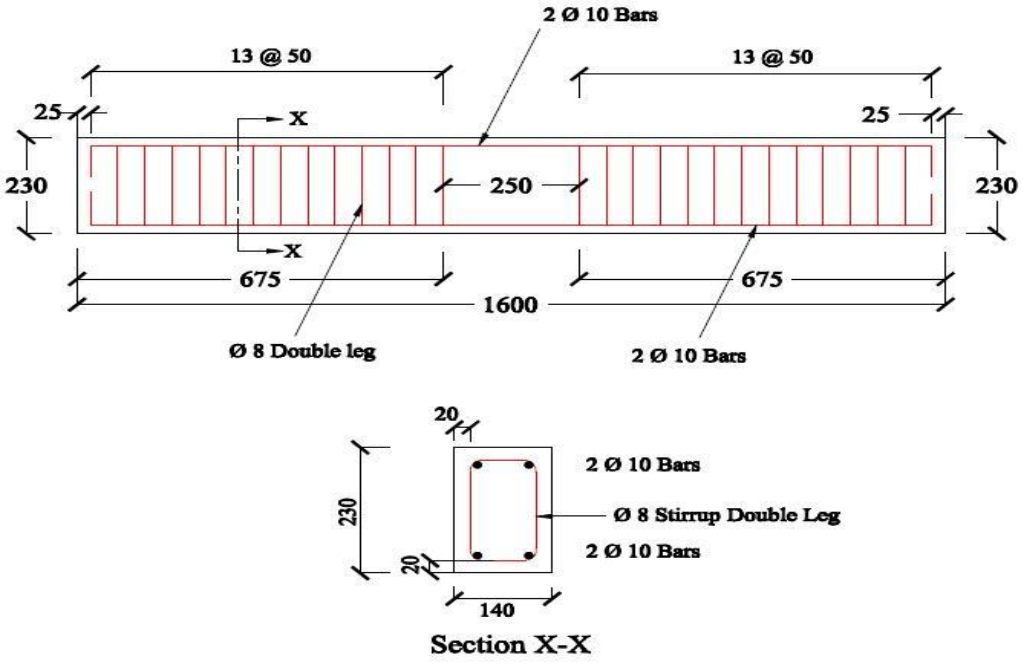

Figure 15: Geometry and details of concrete beam specimens

Figure 16: Molds and reinforcement preparation

Figure 17: Casting of reinforced concrete beams

Figure 18: Demolding of reinforced concrete beams

3.3 Preparation of UHPFRC

The UHPFRC used in this research is prepared locally in the university laboratory.

3.3.1 Materials

The constituents' materials used to prepare the UHPFRC used in theses research work comprises of Type I Portland cement, micro-silica, dune sand, steel fibers, water and superplasticizer as shown in Figure 19. The dune sand has a maximum aggregate size of 300microns.

Figure 19: UHPFRC constituent materials

A mixture of two different sizes of steel fibers as shown in Figure 20 i.e. hooked end and straight fibers were used in the ration of 1:1. The hooked end steel fibers are of 0.2mm diameter, 25mm long and has a tensile strength 2500MPa. While the straight steel fibers has a length of 0.1mm, 12.5mm in diameter and a tensile strength of 2500MPa

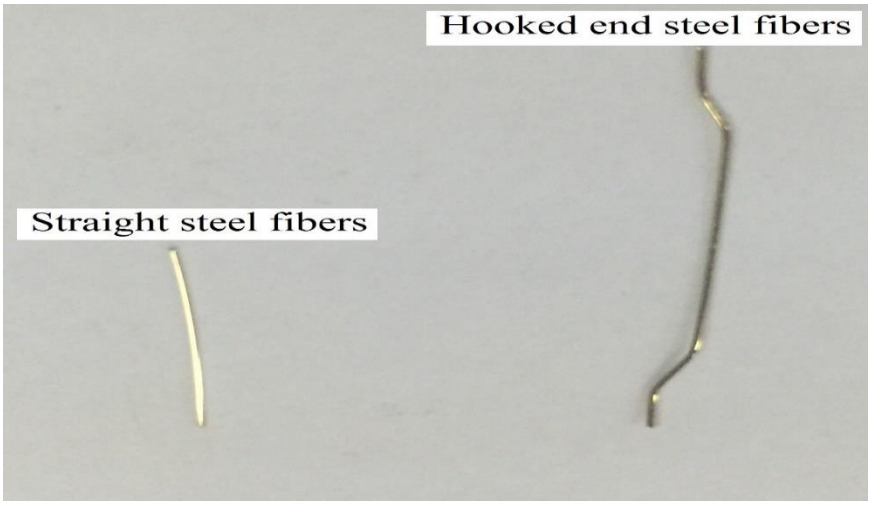

Figure 20: Types of steel fibers used

3.3.2 Mix Design Proportioning

Table 1: Proportion of each of the constituent material to produced **1 m^3** of UHPDRC

Material	**Mix Proportion** (kg/m^3)
Cement	900
Micro-silica	220
Dune sand	1005.13
Steel fibers	157
Superplasticizer	40.32
Water	162.40

3.4 UHPFRC Material Testing

3.4.1 Uniaxial Compression Test

Uniaxial compression test of UHPFRC was conducted on cylinders having dimensions of 75mm * 150mm in a uniaxial compression testing machine. The specimens were inserted into a metal ring set-up for measuring the axial deformation of the specimen as shown in Figure. 21. The test gives values of stress-strain behavior of UHPFRC under uniaxial compression from which modulus of elasticity and compressive strength of UHPFRC can be deducted.

Figure 21: Uniaxial Compression Test

3.4.2 Uniaxial Direct Tensile Test

The tensile behavior of UHPFRC is determined by a direct uniaxial test on dog bone specimens. In other to restrict failure only to the web and avoid failure of the flanges during testing, CFRP was used to strengthen the flanges up to one-third of the web length as shown in Figure 22. This technique ensure that failure occur within the range covered by the extensometer used to measure the extension.

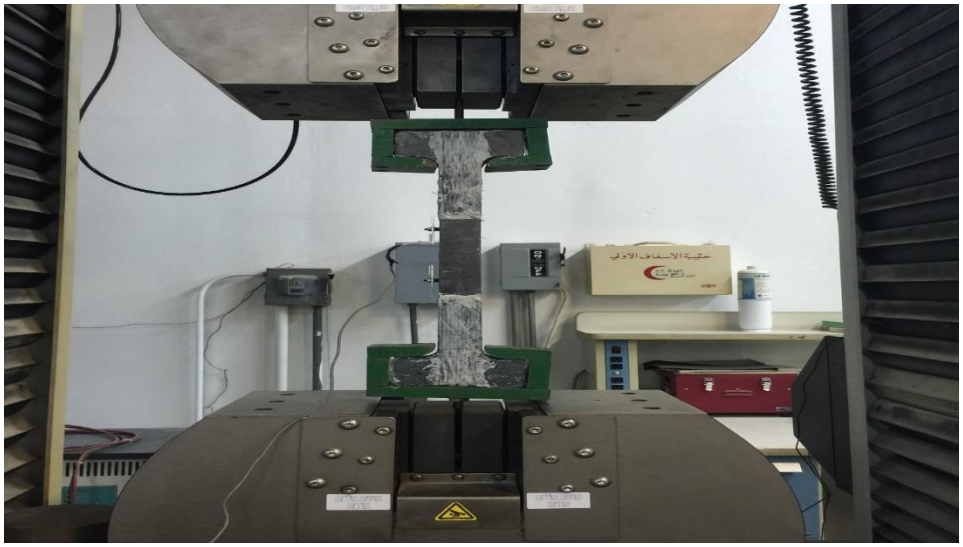

Figure 22: Uniaxial direct tensile test

3.4.3 Bond Strength Test

To ensure adequate bond strength between UHPFRC and normal concrete substrates, two types of bond strength test were conducted i.e. split cylinder tensile strength test and slant shear test on composite UHPFRC-normal concrete cylinders. The UHPFRC is bonded to the normal concrete substrate shown in Figure 23 using two methods

1) By sandblasting of concrete beam surface then casting fresh UHPFRC to the required surface.
2) By using epoxy adhesive to apply prefabricated UHPFRC strips to the concrete beams.

(a) (b)

Figure 23: (a) Half split cylinders (b) Slant cut cylinders

3.4.3.1 Split Cylinder Tensile Strength Test

This test was conducted along the UHPFRC-normal concrete interface of the 75mm*150mm composite cylinder to determine the split tensile strength of the bond. The test was conducted in accordance with ASTM C 496/C 496M after 28 days curing as shown in Figure 24. The split tensile strength of UHPFRC cylinders and normal concrete cylinders were also measured for comparison with that of the bond.

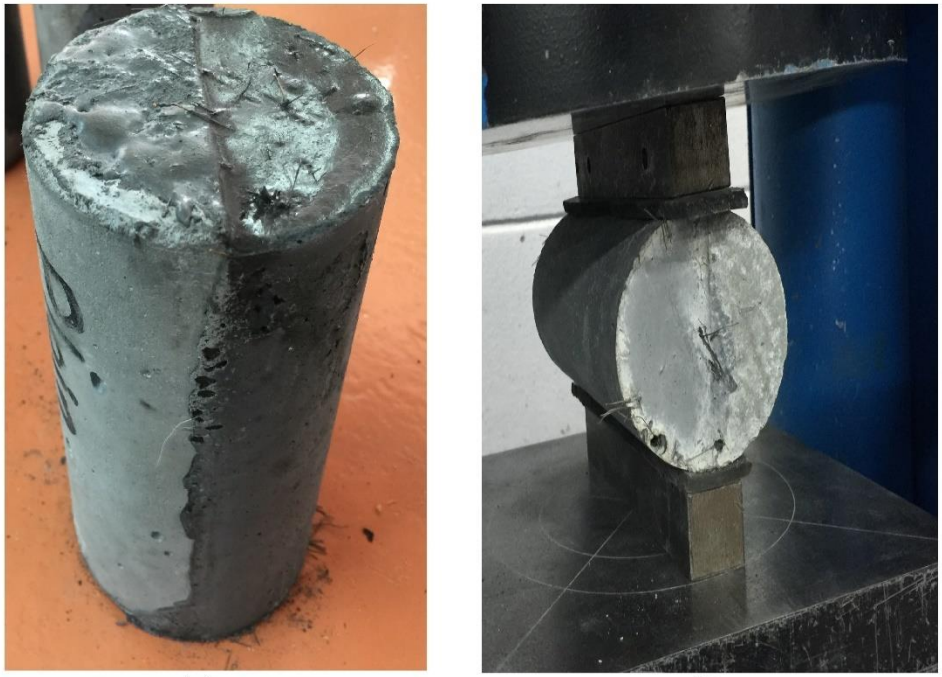

(a) (b)

Figure 24: (a) bonded composite cylinder (b) pic during test

The split tensile strength is calculated as

$$T = \frac{2P}{\pi\, d\, l} \tag{1}$$

where

T = Split tensile strength

P = Maximum applied load from compression testing machine

l = Length of cylinder

d = Diameter of cylinder

3.4.3.2 Slant Shear Test

Slant shear test was conducted by performing compressive strength test on UHPFRC-normal concrete composite 75mm*150mm cylinders cut and bonded at a slant elliptical plane at an angle of 30° to the vertical in accordance with ASTM C882 test procedure as shown in Figure 25. The bond strength for the slant shear strength was calculated by dividing the maximum load taken by bond divided by the bond area.

$$S = \frac{P}{A_b} \quad (2)$$

where

P = Maximum load

A_b = Area of bonded surface (an ellipse in this case)

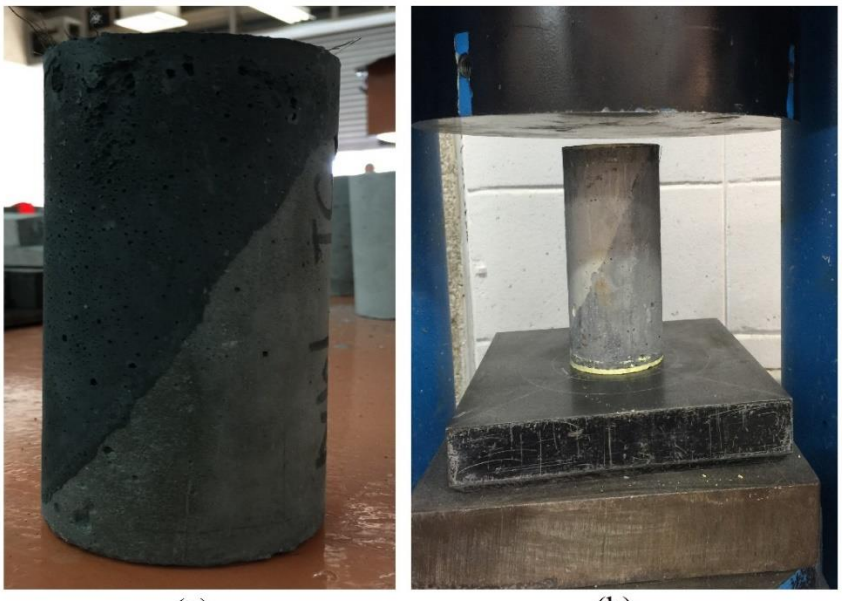

(a) (b)

Figure 25: (a) UHPFRC-concrete substrate composite cylinder (c) slant shear test

The compressive strength and mode of failure of the composite cylinders were compared to the specifications and standard available in the. The test is conducted after curing both the UHPFRC and normal concrete for 28 days.

3.5 Preparation of Test Specimens

The test specimens were prepared using the selected the strengthening methods (i.e. casting UHPFRC on sandblasted surfaces or attaching UHPFRC strips using epoxy adhesive) in addition to using a variety of strengthening configurations.

3.5.1 Types of Test Specimens

A total of twelve concrete specimens were prepared, out of which eight are RC beam while four were PC beams. Among the eight RC beams, two were used as a control specimen while the remaining were divided into two groups. One group represent RC beams to be strengthened by casting UHPFRC on sandblasted surfaces while the other group represents RC beams strengthened by bonding prefabricated UHPFRC strips to the beam surfaces using epoxy adhesive. Three of the four plain concrete (PC) formed another group where strengthening is done by sandblasting technique.

Beams are distinguished from each other by the strengthening configurations as shown in Table 2 (one configuration for each beam) namely;

- Bottom (tension) side jacketing
- Two sides Jacketing
- Three sides jacketing

Table 2: Strengthening schemes of beams specimens

Strengthening Configurations (Jacket thickness = 30mm)	Specimen Identification
	RC - Control
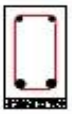	RC - BOT SJ
	RC - 2 SJ
	RC - 3 SJ
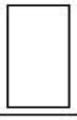	PC - Control
	PC - BOT SJ
	PC - 2 SJ
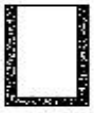	PC - 3 SJ

The following nomenclature is used to distinguish between specimens. Example;

$$\mathrm{RC-SB-BOT\ SJ}$$

where

The first item represents type of beam:

$$\mathrm{RC-Reinforced\ concrete\ beam}$$

PC – Reinforced concrete beam

The second item represents type of strengthening:

SB – By sandblasting technique

EP – Attaching UHPFRC strips using epoxy adhesive

The third item represents configuration/positions of Jacketing

BOT SJ – Bottom side

2 SJ – Two longitudinal sides

3 SJ – Three (Bot + Two longitudinal) sides

3.5.2 Applying UHPFRC Jackets

Two techniques of applying UHPFRC strengthening to the beams were used;

1. By sandblasting the concrete beams surfaces to an average depth of 2mm and casting UHPFRC around it inside a mold
2. By bonding prefab UHPFRC strip using epoxy adhesive

3.5.2.1 Sand Blasting Technique

The surfaces of the beams were to be strengthened were sandblasted to a depth of 3mm after 14 days of curing at the precast concrete plant as shown in Figure 26

Figure 26: (a) Sandblasting of concrete beams (b) sandblasted surface

The beams were transported to the lab for strengthening. Wooden molds having the required dimensions of the strengthened beams were prepared.

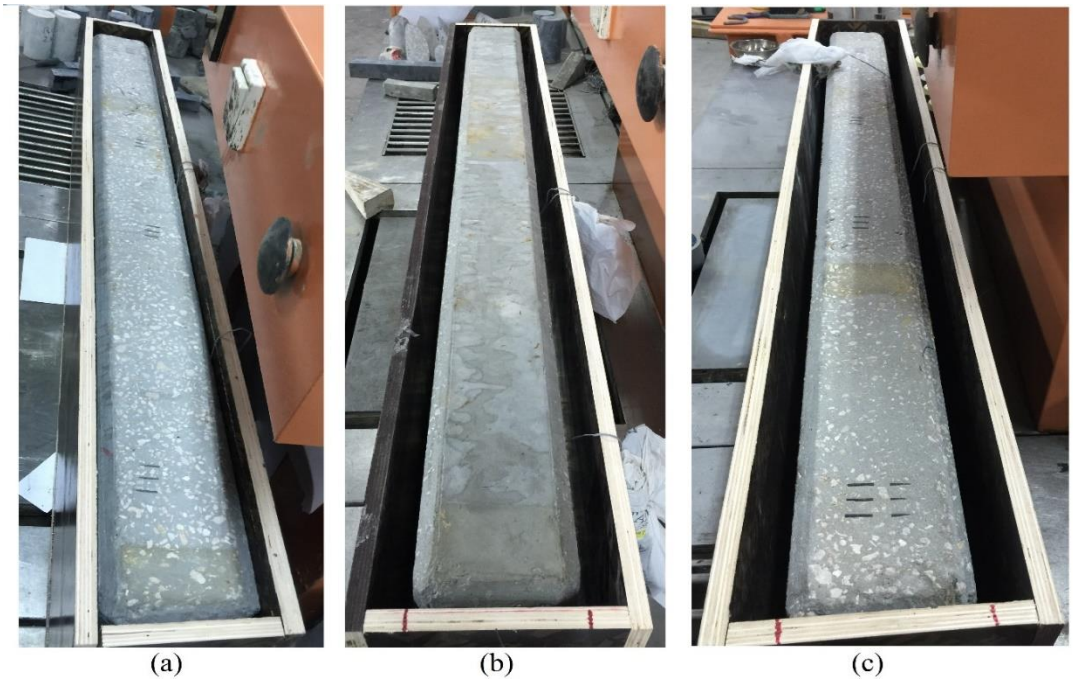

Figure 27: Beams prepared for (a) Bot side (b) 2-sided (c) 3-sided strengthening

After inserting the beams into the mold and adjusting it to the right position to give the precise thickness of the jacket of 30mm as shown in Figure 27, freshly prepared UHPFRC was cast around the required sides and fully compacted using the table shaker upon which the mold was sitting as shown in Figure 28.

Figure 28: Strengthening of beam specimens

The beam specimens were de-molded after 24hrs and inserted into a curing tank where they were moist cured for 28 days as shown in Figure 29.

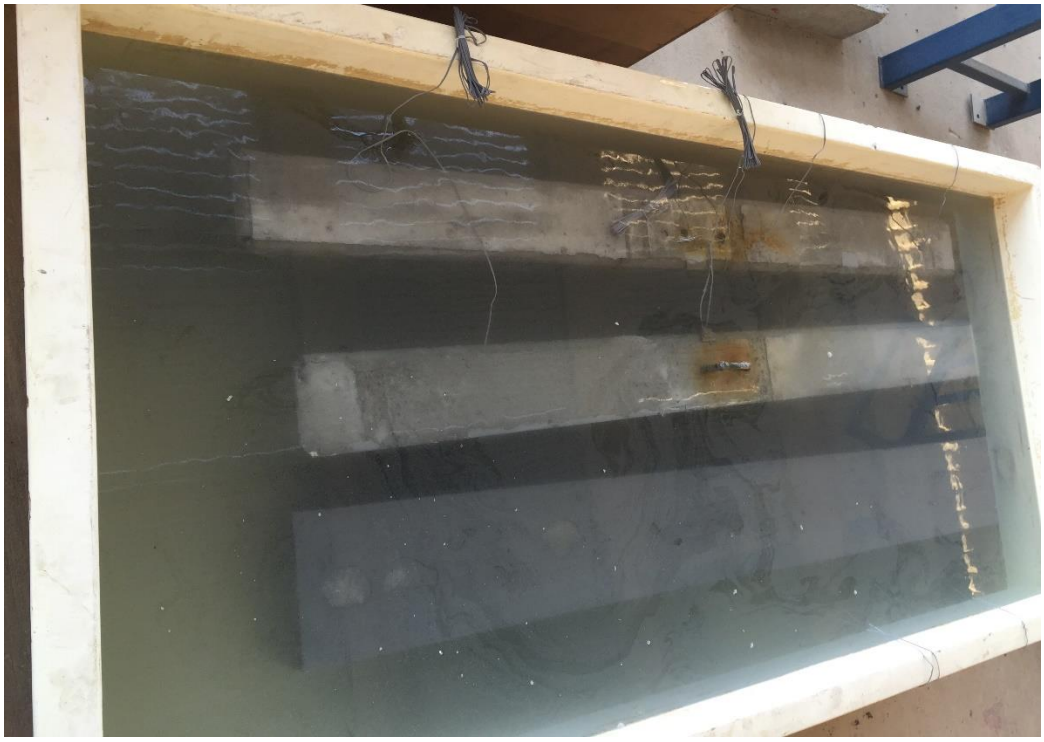

Figure 29: Curing of strengthened beam specimens

3.5.2.2 Using Epoxy Adhesive

In this method, UHPFRC strips were produced by casting fresh UHPFRC separately in molds having the desired dimension (i.e. corresponding to the dimension of the beam surface for which it will be attached to) as shown in Figure. 30.

Figure 30: Cast UHPFRC strips

Figure 31: UHPFRC strips

The strips were de-molded after 24hrs as shown in Figure 31 and moist cured for 28 days inside a curing tank. After curing, the prefabricated strips were bonded to the desired beam surfaces using the epoxy adhesive as shown in Figures. 32 and 33 “FOSROC NITOBOND EP”. The bond is air cured for 7 days in air temperature of between 25 - 31°C

Figure 32: Bonding of UHPFRC using epoxy adhesive “FOSROC Nitobond EP”

Figure 33: Strengthened beams specimens using epoxy adhesive bonding

3.6 Flexural Testing Of Beam Specimens

The beam specimens were tested under flexure in a four-point loading arrangement as shown in Figures. 34 and 35. Linear variable differential transducers were used to measure displacement at the midspan while concrete strain gauges were used for measuring longitudinal of concrete around the midspan region. Similarly, strain gauges attached to reinforcing bars in the case of RC beams was used to monitor deformation of reinforcing steel.

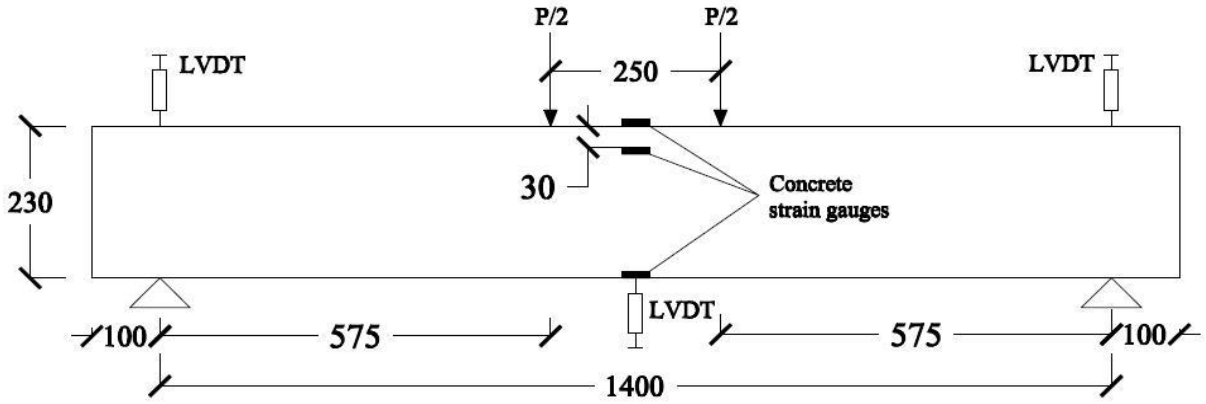

Figure 34: Instrumentation of beam flexural strength test

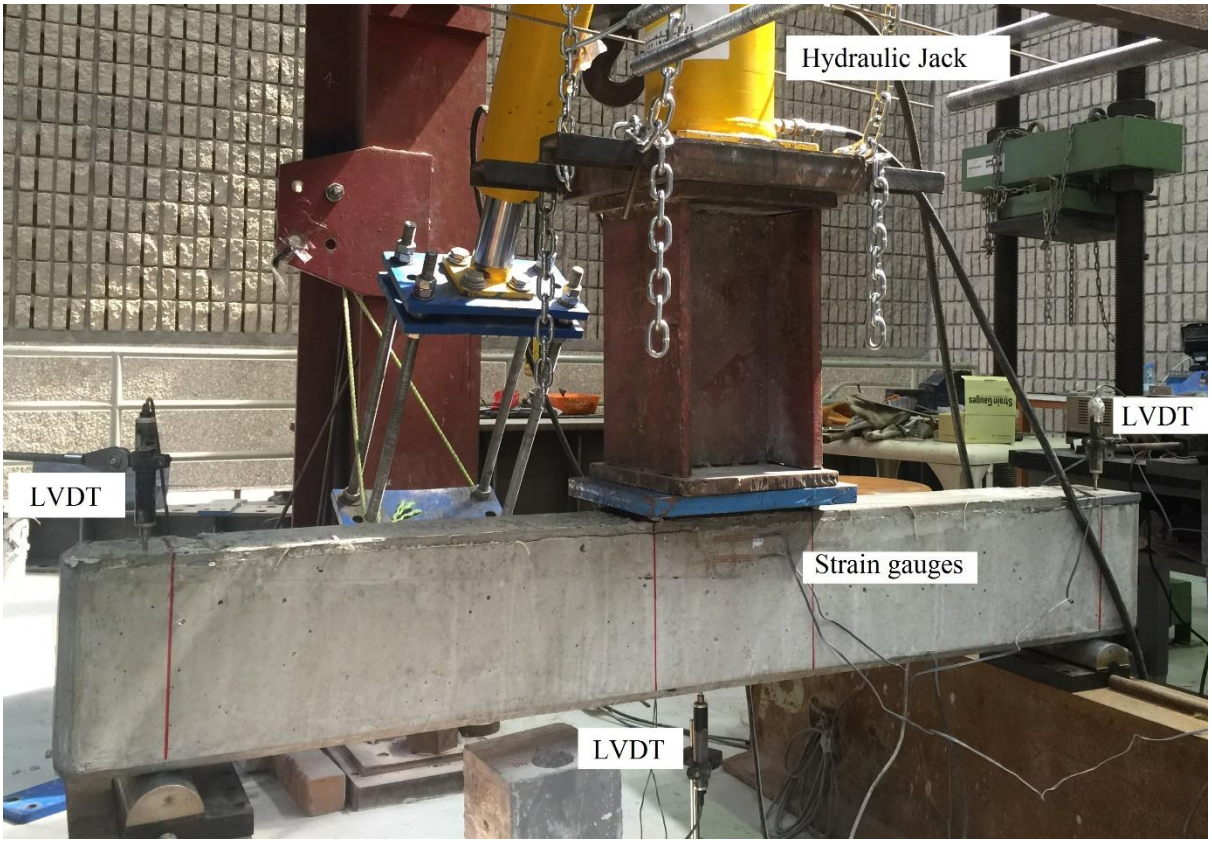

Figure 35: Beam test set-up

CHAPTER 4

EXPERIMENTAL RESULTS AND DISCUSSION

4.1 General

Experimental test results were presented and analysed in this chapter. The test result shows the effectiveness of using UHPFRC jacketing in increasing the moment capacity of both plain and reinforced concrete beams specimens. Also, results of bond strength show that UHPFRC has high bond strength but is affected by the type surface preparation.

4.2 Material Mechanical Properties

Mechanical properties of both normal concrete and UHPFRC determined in the laboratory were presented as shown in Table 3.

Table 3: Mechanical properties of concrete and UHPFRC

Property	**Concrete (MPa)**	**UHPFRC (MPa)**
Compressive strength	54	128
Modulus of Elasticity	34,000	46,000
Split tensile strength	6	17
Flexural Strength	4	15

4.2.1 UHPFRC Uniaxial Compressive Strength Test

The uniaxial compressive strength test conducted on 75 *150mm cylinders is as shown in Figure 36. The data obtained from this test is used in calibrating the finite element and the analytical models.

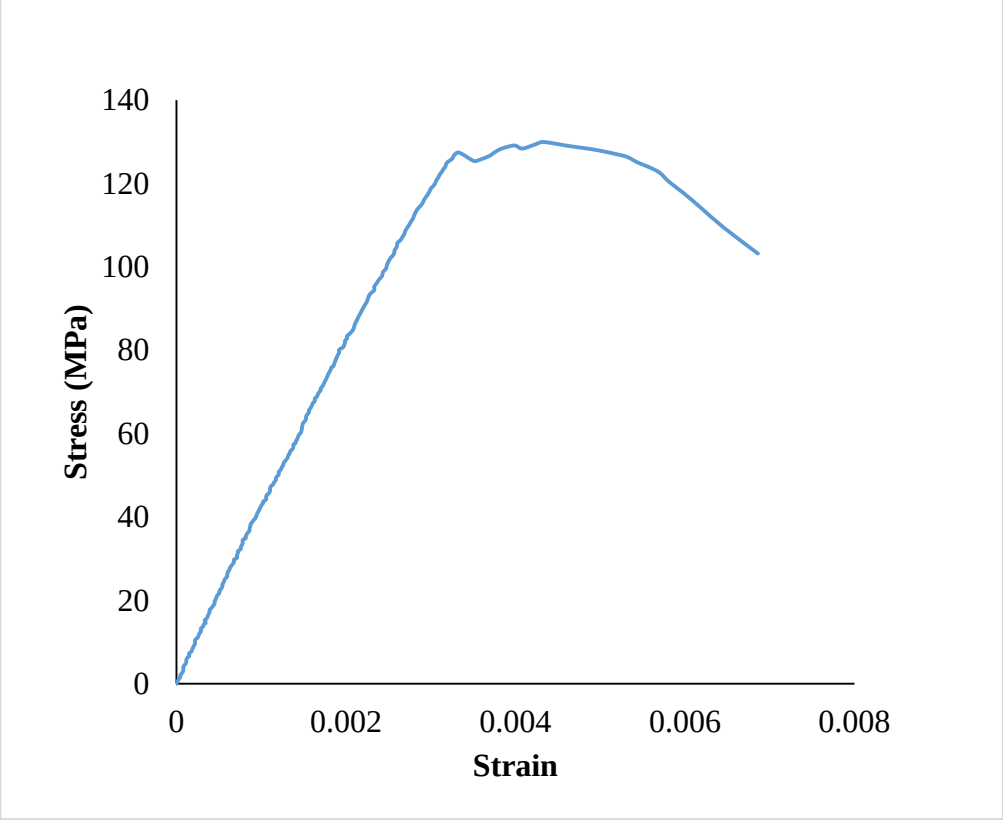

Figure 36: Uniaxial compressive strength behavior of UHPFRC

4.2.2 UHPFRC Uniaxial Direct Tensile Strength Test

Uniaxial direct tensile strength behavior conducted on dog bones specimens is shown in Figure 37. The behavior shows more strain hardening response when compared to normal concrete behavior

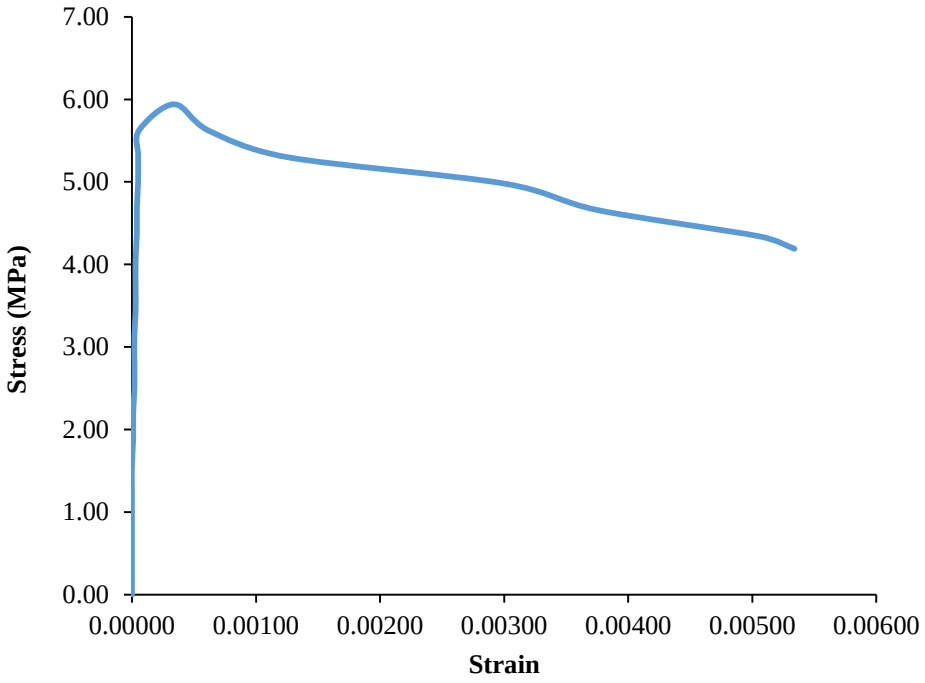

Figure 37: Uniaxial tensile behavior of UHPFRC

4.3 Bond Strength Test

To ascertain the bond strength between UHPFRC and normal concrete substrates, split cylinder tensile strength test and slant shear strength test were conducted on composite UHPFRC-normal concrete cylinders in accordance with ASTM C496 and ASTM C882 respectively.

UHPFRC is bonded to the normal concrete substrate by casting UHPFRC on halved cylinder sandblasted to a depth of 2mm and another by casting UHPFRC on the plain surface of the halved cylinder substrate while the other was by bonding UHPFRC substrate as well as a concrete substrate using an epoxy adhesive. The results of split tensile and slant

shear strength test were presented in Table 4 and compared with bond strength quality ranges provided by [29] and [30] respectively.

Table 4: Bond strength test results

Substrate Surface Preparation	**Split Cylinder Tensile Strength**		**Slant Shear Strength**	
	Average strength	Failure mode	Average strength	Failure mode
Plain surface	2.58	A	21.56	A
Sand Blasted	3.73	B	27.01	C
Epoxy bonded	5.89	C	23.15	B

where

A =Interface failure

B = Interface + partial substrate failure

C = Substrate failure

Split tensile test shows that failure occurred directly along the interface in the case of plain/smooth substrate surfaces, failure occurs at the interface and partially inside the concrete substrate in the case of sandblasted substrate surface while failure occurs within the concrete substrate in the case of bonding with an epoxy adhesive as shown in Figure 38. The test result shows that bonding with epoxy adhesive is more effecting in enhancing the tensile strength of the bond as shown in Figure 39.

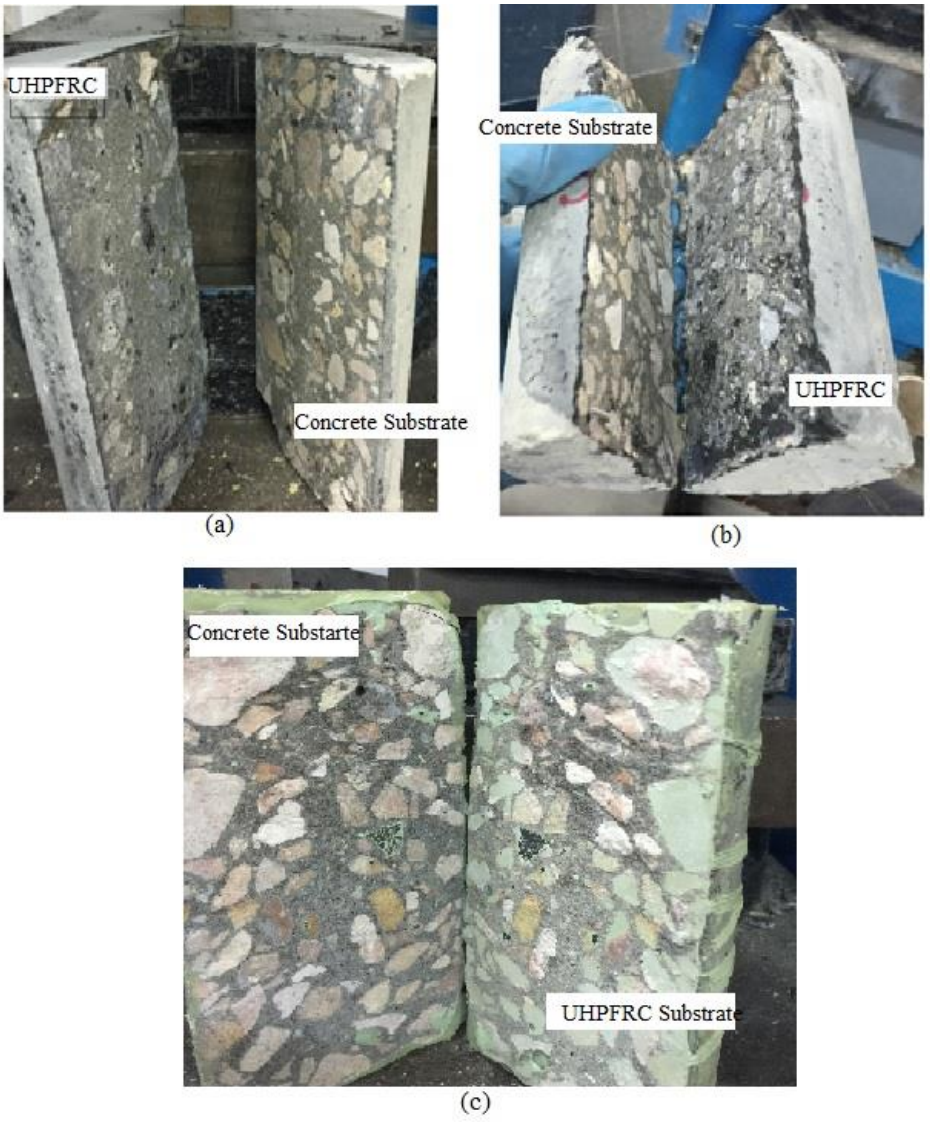

Figure 38: Split cylinder tensile strength bond test for (a) plain surface (b) sandblasted surface (c) epoxy adhesive surface preparation

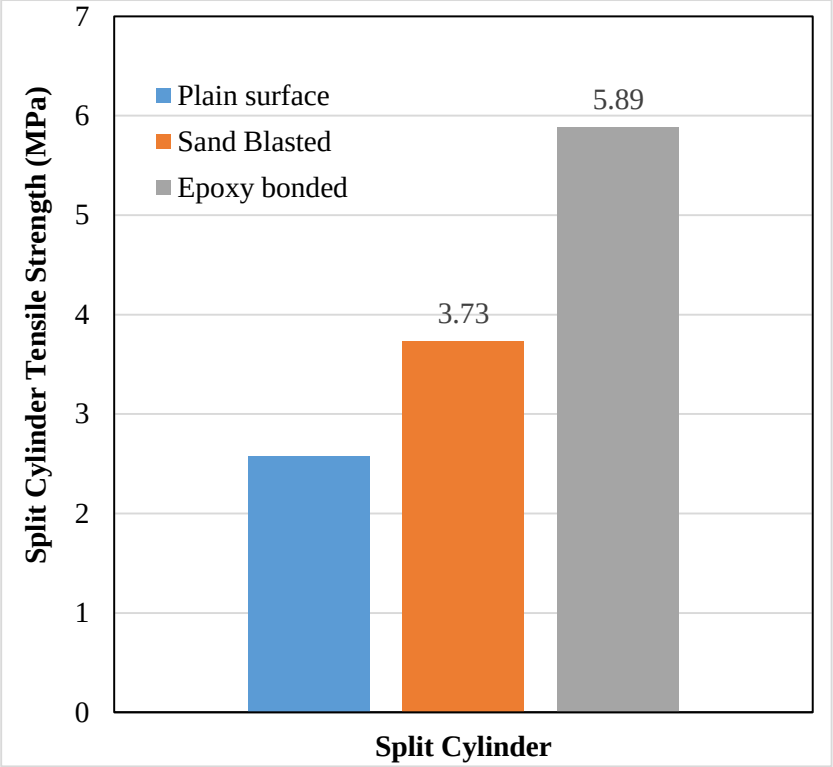

Figure 39: Split tensile bond strength test of composite UHPFRC-normal concrete

Cylinders having different interface preparationSlant shear strength test shows that failure occurred directly along the interface in the case of plain/smooth substrate surfaces and failure occurs inside the concrete substrate in the case of sandblasted substrate and an Interface + partial concrete substrate failure was observed for epoxy adhesive bonded cylinders as shown in Figure 40. The test result shows that sandblasting the concrete substrate surface is more effective in resisting shear stresses than the other two methods as shown in Figure 41.

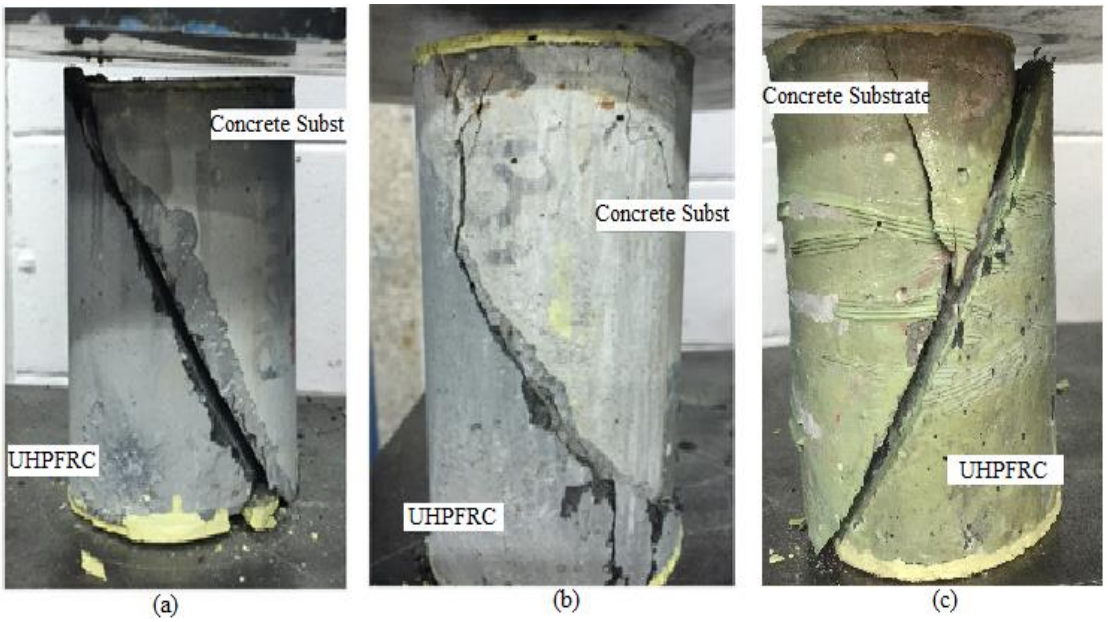

Figure 40: Slant Shear Strength bond test for (a) plain surface (a) sandblasted surface(c) epoxy adhesive surface preparations

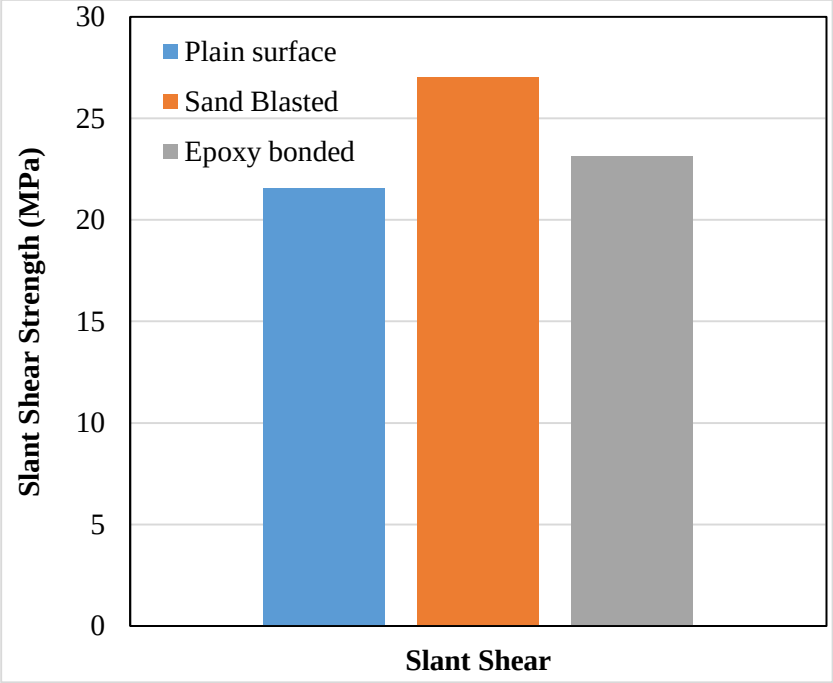

Figure 41: Slant shear strength bond strength test UHPFRC-normal concrete cylinders having different interface preparation

Results of split cylinder tensile strength test for both specimens fall under the category of "Excellent bond quality" (i.e. if tensile bond strength ≥ 2.1 MPa) as quantified by [29]. Also, the slant shear strength for both specimens indicates adequate bond strength in accordance to [30] which specifies a slant shear strength of ≥ 20.7 MPa at 28 days. These results show that UHPFRC has excellent bonding with surface of the concrete substrate.

4.4 Flexural Strength Test

The strength of concrete strengthened with UHPFRC tested in flexure under a four-point loading arrangement shows adequate enhancement in flexure for all strengthened beams specimens compared to their control specimens. Other features and properties such as crack patterns, deflections and strains also show the effectiveness of these strengthening technique.

4.4.1 Test Observations and Failure Modes

RC – Control shows traditional flexural cracking pattern characterized by vertical cracks starting from mid-span and spreading away from the mid-span as the load increases. Inclined flexural-shear cracks start to develop at the furthest locations towards the supports up to failure load. The cracks were spread over the middle 850mm span of the beam specimen as shown in Figure 1(a). As forRC – SB – BOT SJ, the specimen also shows a combination of flexural cracks and some branching flexural cracks which develops at higher load. However, the crack load is more than double that of the control and cracks were concentrated in the middle 760mm span of the beam as shown in Figure 1(b). In the case RC – SB – 2 SJ, the specimen shows fewer number of cracks compared to RC –

Control and RC – SB – BOT SJ and the cracks were spread over the middle 640mm span of the beam. A dominant flexural crack developed directly at the midspan of the beam later becomes the failure crack of the beam. RC – SB – 3 SJ specimen shows the least number and spread of cracks when compared to the previously mentioned specimens. The cracks were concentrated within the middle 350mm span of the beam specimen as shown in Figure 42(e).

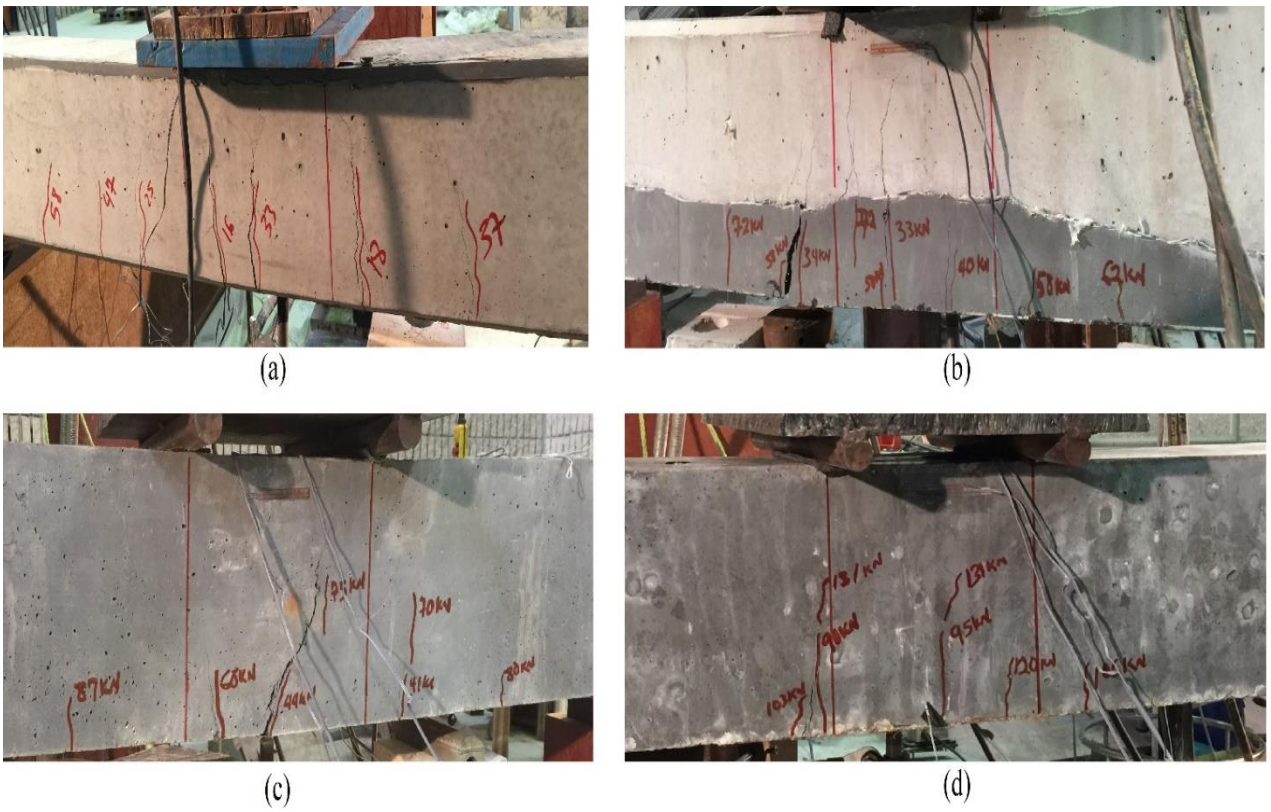

Figure 42: Crack patterns for sandblasted RC beam specimens (a) RC – Control (b) RC – SB – BOT SJ (c) RC – SB – 2 SJ (d) RC – SB – 3 SJ

The properties of the tested beams specimens were as shown in Table 5.

Table 5: Cracking properties of RC-SB beam specimens

Specimen	**Cracking Load (KN)**	**Failure Crack type**	**Crack width at Failure Load (mm)**	**Crack Width on unloading (mm)**
RC – Control	16	Pure flexural	3.5	2.5
RC – SB – BOT SJ	33	Branching flexural	11.0	8
RC – SB – 2 SJ	41	Pure flexural	6.5	5
RC – SB – 3 SJ	90	Pure flexural	1.5	0.5

For beams specimens for which prefab UHPFRC strips were attached by bonding with epoxy adhesive, RC – EP – BOT SJ shows a number of flexural cracks similar to those in RC – SB – BOT SJ and a dominant branching crack develops to become the failure crack of the beam as shown in Figure 43(b). However the cracking load was higher than in the case of RC – SB – BOT SJ. RC – EP – 2 SJ also shows similar crack pattern to RC – SB – 2 SJ with a flexural failure crack developing very close to the mid-span of the beam as shown in Figure 43(c). Similarly crack patterns for RC – EP – 3 SJ resembles that of RC – SB – 3 SJ only that the cracks were spread over a longer span of around 420mm middle span of the beam as shown in Figure 43(d). The properties of the tested beams specimens were as shown in Table 6.

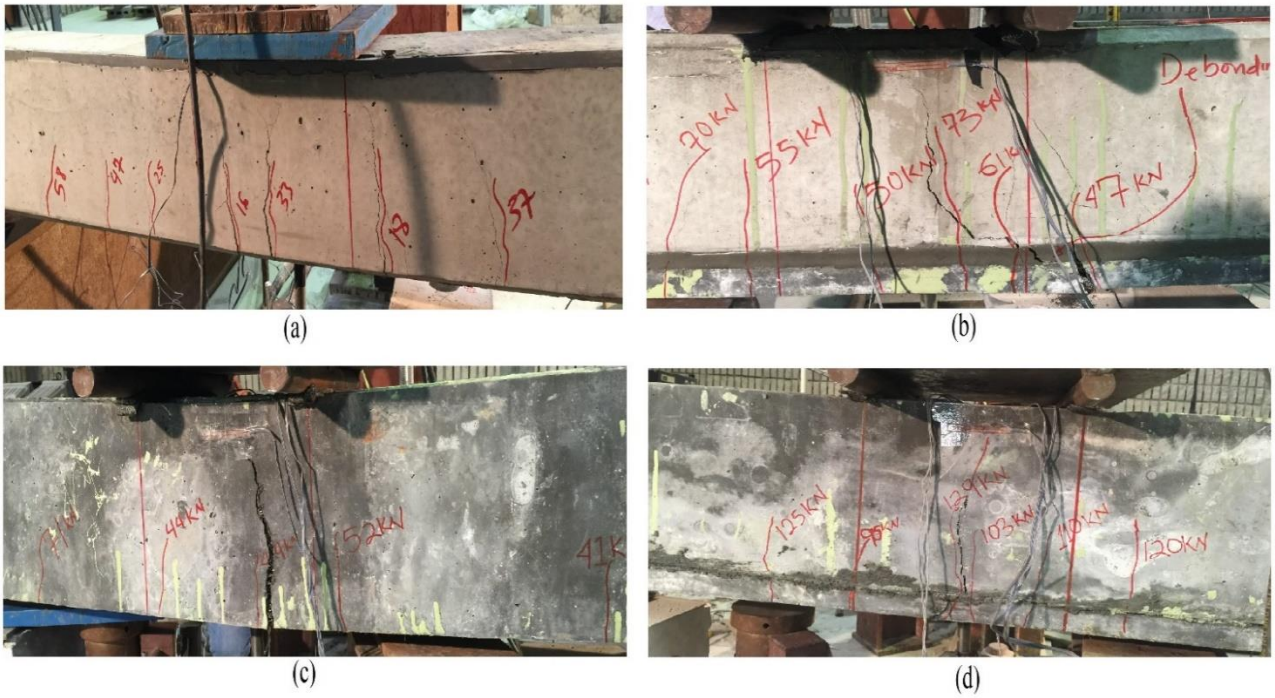

Figure 43: Crack patterns for epoxy bonded RC beam specimens (a) RC – Control (b) RC – EP – BOT SJ (c) RC – EP – 2 SJ (d) RC – EP – 3 SJ

Table 6: Cracking properties of RC-EP beam specimens

Specimen	**Cracking Load (KN)**	**Failure Crack type**	**Crack width at Failure Load (mm)**	**Crack Width on unloading (mm)**
RC – Control	16	Pure flexural	3.5	2.5
RC – EP – BOT SJ	47	Branching Flexural	7.0	5.0
RC – EP – 2 SJ	44	Pure flexural	10.5	6.0
RC – EP – 3 SJ	95	Pure flexural	3.5	1.3

In the case of plain concrete beam specimens, PC – Control failed in a very brittle manner with the development of a single flexural crack at the mid-span which goes directly throughout the entire beam as shown in Figure 44(a). PC – SB – BOT SJ's failure was also brittle with the development of a single flexural crack at a distance 220mm to the left of beam mid-span unlike in the case of PC – Control were the crack is approximately at mid-span. However, cracking load was much higher than in the case of PC – Control as shown in fig 44(b). Similarly, for PC – SB – 2 SJ a single crack was developed at mid-span similar to PC – Control which later deviates into a branching crack around mid-depth of the beam specimen. In the case of PC – SB – 3 SJ, failure is less brittle than the previous mentioned specimens with the development of two flexural cracks at about 120mm to the left of the beam mid span (similar to PC – SB – Bot SJ) as shown in Figure 44(d). Properties of the tested beams is as shown in Table 7

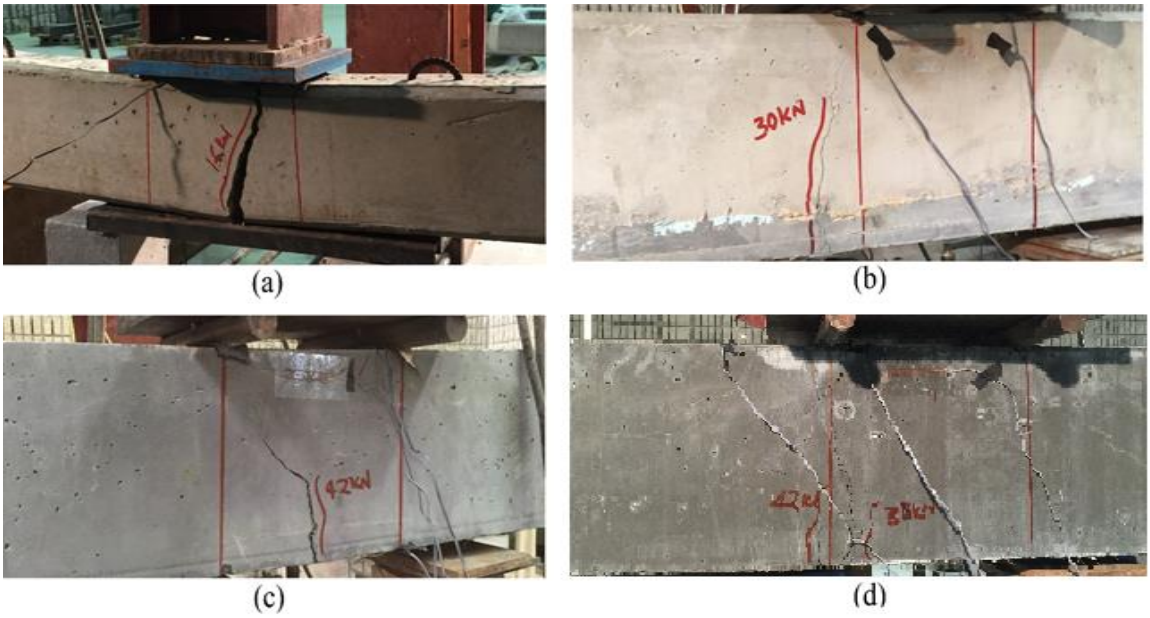

Figure 44: Crack patterns for plain concrete beam specimens (a) PC – Control (b) PC – SB – BOT SJ (c) PC – SB – 2 SJ (d) PC – SB – 3 SJ

Table 7: Cracking properties of PC beams specimens

Specimen	Cracking Load (KN)	Failure Mode (Crack type)	Crack width at Failure Load (mm)	Crack Width on unloading (mm)
PC – Control	16	Flexure	Broken	Broken
PC – SB – BOT SJ	30	Flexure	2.0	0.8
PC – SB – 2 SJ	42	Branching flexure	4.0	2.5
PC – SB – 3 SJ	38	Branching flexure	1.5	1.0

It was observed that this strengthening technique increases the cracking load of the beams specimen, decreases the number and spreading of cracks along their spans. Also, flexure-shear cracks that were observed towards the supports in the case of RC – Control were eliminated. Beam specimens strengthened on its three i.e. RC – SB – 3 SJ, RC – EP – 3 SJ, PC – SB – 3 SJ sides shows the highest enhancement whereas beams strengthened at the bottom only i.e. RC – SB – BOT SJ, RC – EP – BOT SJ, PC – SB – BOT SJ shows the least enhancement compared to their control specimens. It was also observed that beams strengthened by bonding prefab UHPFRC strips with epoxy adhesives (EP) shows higher cracking loads than their counterparts strengthened by casting UHPFRC on sand blasted surfaces (SB). This is as a results of the higher tensile strength of the epoxy adhesive which resist the hair line cracks from going through until its tensile strength is exceeded after which the cracks became visible.

4.4.2 Load Deflection Behavior

Load-deflection behavior of RC – Control was a familiar one similar to most types of normal RC beams. Load increases linearly up to yielding of the steel reinforcement at a load level of equal to 51 KN, after which it shows considerable hardening with lower stiffness and large deformations up to failure as shown in Figure 45. RC – SB – BOT SJ and RC – SB – 2 SJ shows similar behavior as RC – Control except that load increases rapidly with more improved stiffness up to yielding of reinforcement at load level equal to 64KN and 91KN respectively. After yielding, the load increase drops and the load stabilises up to failure. The specimens shows higher stiffness and less deformations due to lesser number and spread of cracks thanRC – Control. In the case ofRC – SB – 3 SJ, the beam shows higeher load increase and lesser deformation up to yield which a occurs at a higher load equal to 124KN. However, the load still keeps increasing after the yield up to 133KN with a slight reduction in stiffness, followed by a sudden decrease in load up to failure, indicating a less ductile failure compared to RC – Control, RC – SB – BOT SJ, and RC – SB – 2 SJ. Behaviors and properties of the above mentioned beams specimens are as shown in Figure 45 and Table 8 respectively

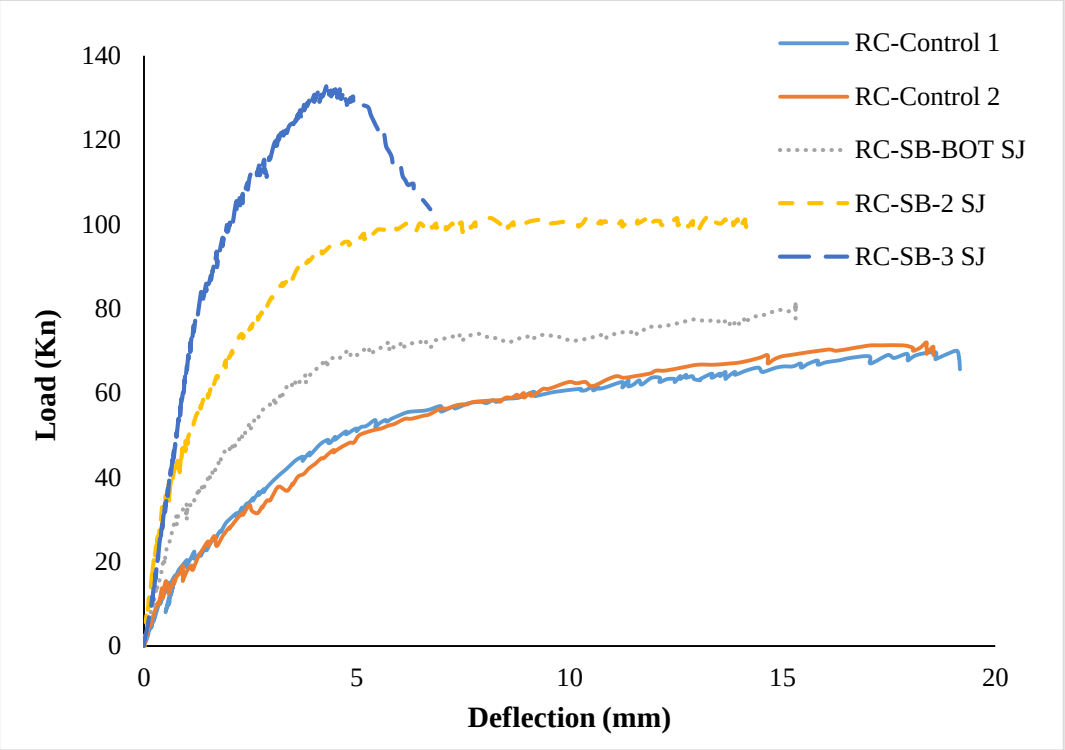

Figure 45: Load-deflection behavior for RC-SB beam specimens

Table 8: Load deflection properties RC-SB beam specimens

Specimen	Displacement at Peak Load (KN)	Displacement on unloading (mm)	Peak Load (KN)	Capacity Enhancement (%)
$RC - Control$	19.10	12.79	70	-
$RC - SB - BOT\ SJ$	15.31	10.44	81	16
$RC - SB - 2\ SJ$	13.38	9.54	102	46
$RC - SB - 3\ SJ$	4.55	2.51	132	89

Similarly, $\mathrm{RC}-\mathrm{EP}-\mathrm{BOT\ SJ}, \mathrm{RC}-\mathrm{EP}-2\ \mathrm{SJ}$and $\mathrm{RC}-\mathrm{EP}-3\ \mathrm{SJ}$ shows exactly the same behavior as their respective specimens in the $RC-SB$ group. However, $\mathrm{RC}-\mathrm{EP}-2\ \mathrm{SJ}$ shows lesser stiffness compared to $\mathrm{RC}-\mathrm{SB}-2\ \mathrm{SJ}$ which is likely due to some bond defects in the case of using epoxy adhesive. Behaviors and properties of $\mathrm{RC}-\mathrm{EP}$ beams are shown in Figure 46 and Table 9.

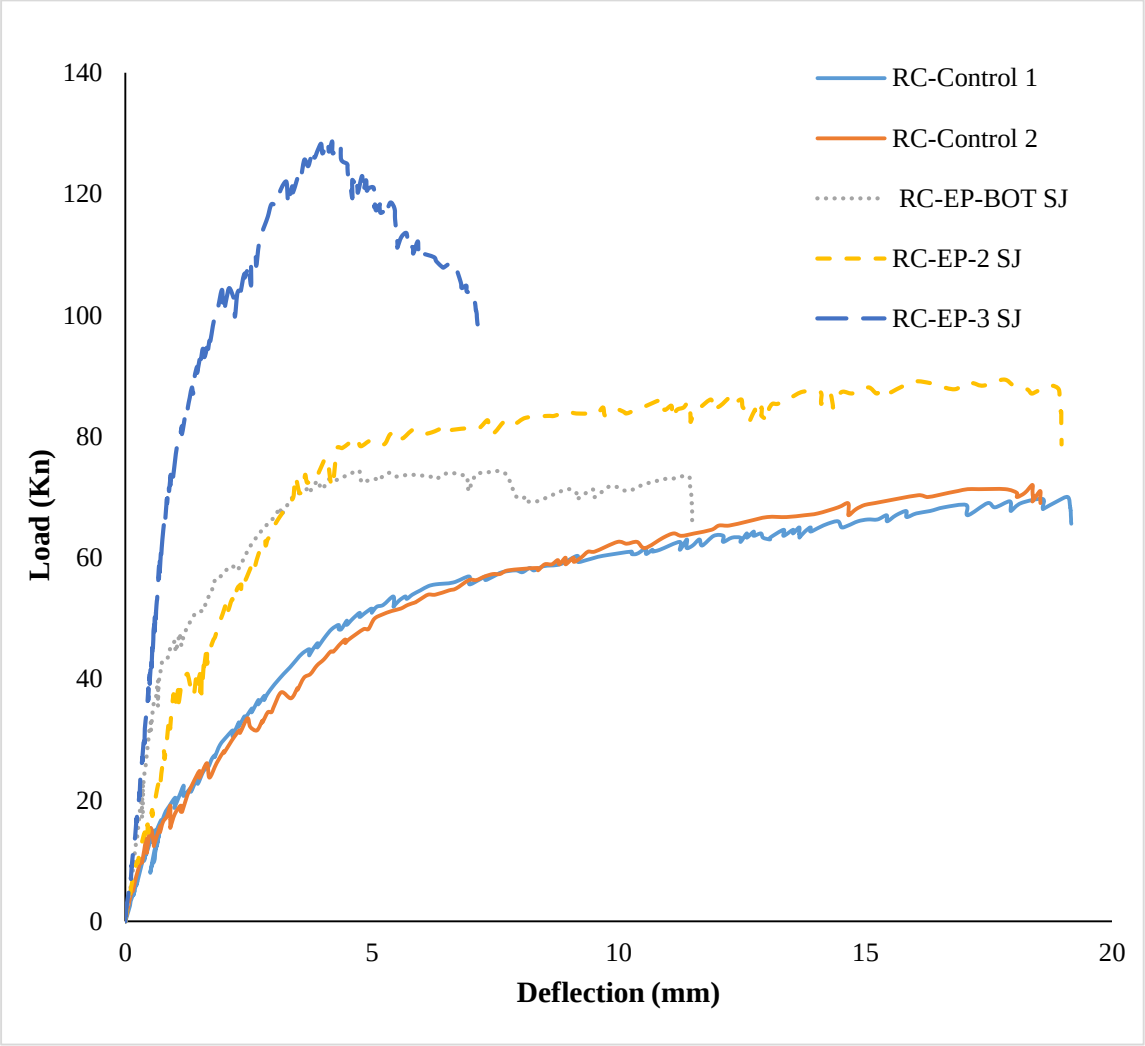

Figure 46: Load-deflection behavior of epoxy bonded RC beam specimens

Table 9: Properties tested RC – EP beams

Specimen	Displacement at Peak Load (KN)	Displacement on unloading (mm)	Peak Load (KN)	Moment Capacity Enhancement (%)
$RC - Control$	19.10	12.79	70	-
$RC - EP - BOT\ SJ$	4.73	7.55	75	8
$RC - EP - 2\ SJ$	15.7	14.07	95	36
$RC - EP - 3\ SJ$	4.35	4.29	129	85

In the case plain concrete (PC) beam specimens having no steel reinforcement, PC – Control shows a very brittle collapse as shown in Figure 48 once the elastic range of the beam was exceeded (at a very small deflection < 1mm) which splits the beam into two halves. PC – SB – BOT SJ shows similar brittle behavior but with a more elastic response by reaching a higher load capacity and mid-span deflection compared to PC – Control as shown in Figure 48. Despite showing similar brittle failure, PC – SB – 2 SJ and PC – SB – 3 SJ however shows considerable amount of softening and undergoes higher amount of deflection without breakage of the specimens. Properties of tested PC-SB beams are shown in Table 10.

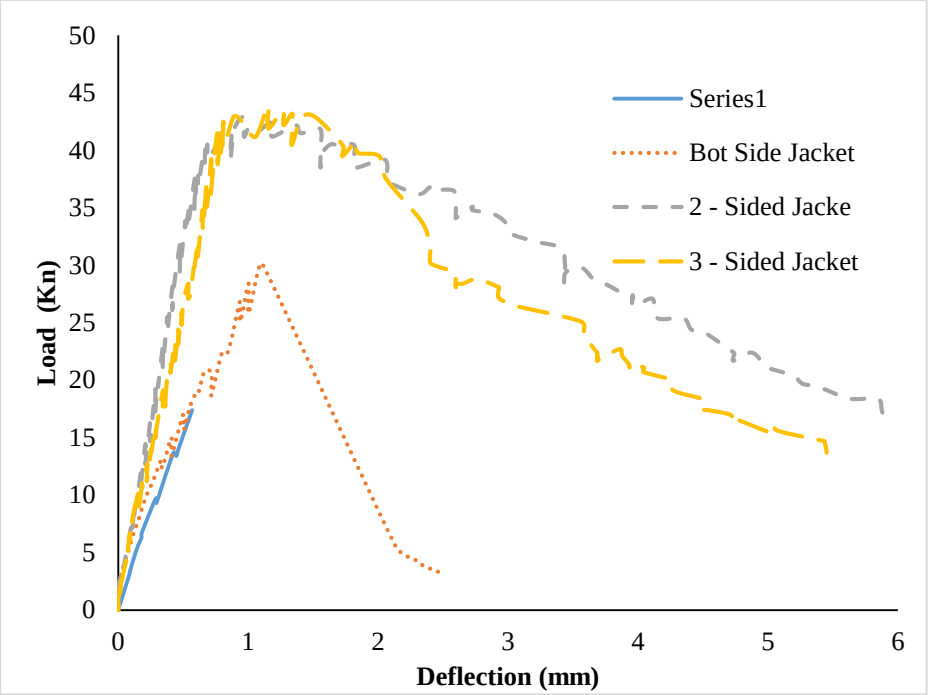

Figure 47: Load-deflection behavior of epoxy bonded RC beam specimens

Table 10: Load-deflection properties of tested plain concrete (PC) beams

Specimen	**Displacement at Peak Load (KN)**	**Residual Displacement (mm)**	**Peak Load (KN)**	**Moment Capacity Enhancement (%)**
$PC - Control$	0.57	Broken	17.4	-
$PC - SB - BOT\ SJ$	1.11	2.34	30.1	73
$PC - SB - 2\ SJ$	0.96	5.07	42	142
$PC - SB - 3\ SJ$	1.27	4.68	44	153

4.4.3 Effect of Strengthening Configuration

Results show that beams strengthened with UHPFRC jacket on 3-sides (3 SJ) gives the highest load increment of about 89 and 153% for RC and PC beams respectively. While strengthening on the bottom side only (BOT SJ) gives the least load increment of 16 and 73% for RC and PC beams respectively as shown in Figure. 48. For the same strengthening technique, it was observed that PC shows higher percentage increase in failure load than in the case of RC beams. Failure load increase of 73, 142 and 153% was observed for $PC-SB-BOT\ SJ$, $PC-SB-2\ SJ$ and $PC-SB-3\ SJ$ respectively, while 16, 46 and 89% increase was observed for $RC-SB-BOT\ SJ$, $RC-SB-2\ SJ$ and $RC-SB-3\ SJ$ respectively as shown in Figure 48. This is due to the fact that reinforcing steel in RC beams has much higher tensile strength $f_y = 610\ MPa$ than UHPFRC $f_t = 6\ MPa$ as such the beams becomes less sensitive to the effect of UHPFRC jackets compared to PC beams.

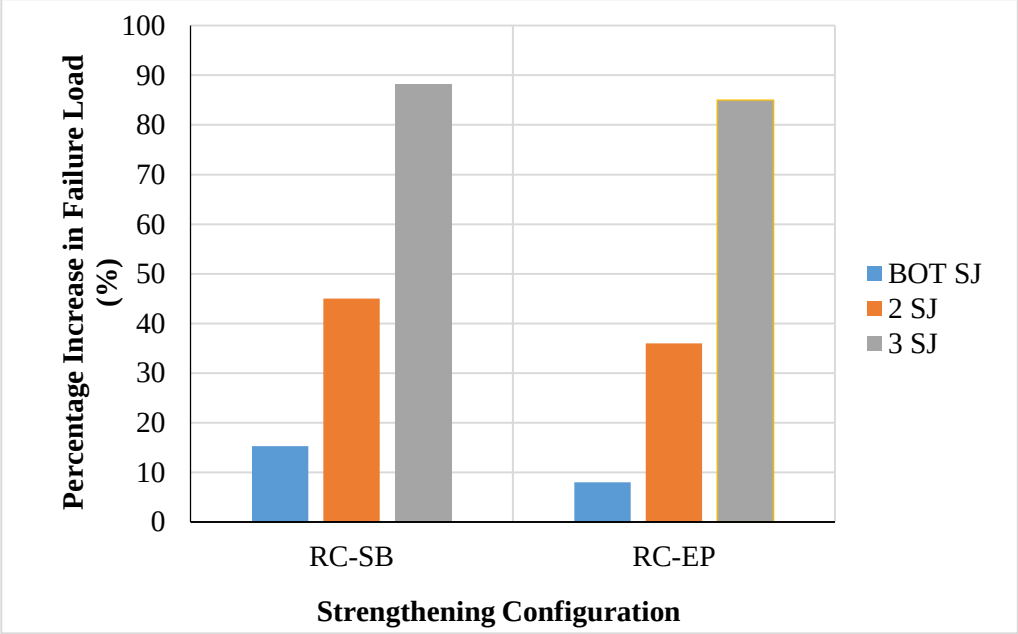

Figure 48: Effect of strengthening configuration on failure load of RC and PC specimens

CHAPTER 5

FINITE ELEMENT MODELLING

5.1 General

Both concrete and UHPFRC's behavior are non-linear and complex. However, the availability of computer-based finite element packages has made it possible to model and analyze these complex behaviors. A 3D finite element model of the beam specimens were modelled using the non-linear finite element package ABAQUS to predict the behavior of the beams specimens under flexure. The concrete damage plasticity model was used to model both the normal and UHPFRC. The behavior of the materials were simulated by directly inputting the stress-strain experimental results into the selected models.

5.2 Material Models

The elastic behavior of steel was modelled as an isotropic linear elastic material up to yield point using the elastic material model in Abaqus while the inelastic part was modelled using the plastic material model with isotropic hardening. Both concrete and UHPFRC were modelled using the concrete damage plasticity.

5.2.1 Concrete Damage Plasticity

The concrete damage plasticity is a very strong and versatile model capable of predicting concrete behavior under both static and dynamic loading. It operates on two mechanisms i.e. tensile cracking and compressive crushing of concrete. In tension, the concrete uses a

multi-axial damage elasticity model and a multi-axial plasticity model with the non-associated flow and and isotropic scalar hardening in compression. Damage states in tension and in compression are characterized independently by two hardening variables known as equivalent plastic strains in tension and compression. Cracking caused by tension and crushing caused by compression are caused by increasing values of theses hardening variables, the variables control the evolution of the yield surface and degradation of elastic stiffness.

The model behavior in uniaxial tension and compression are shown in Figure 50 and 51

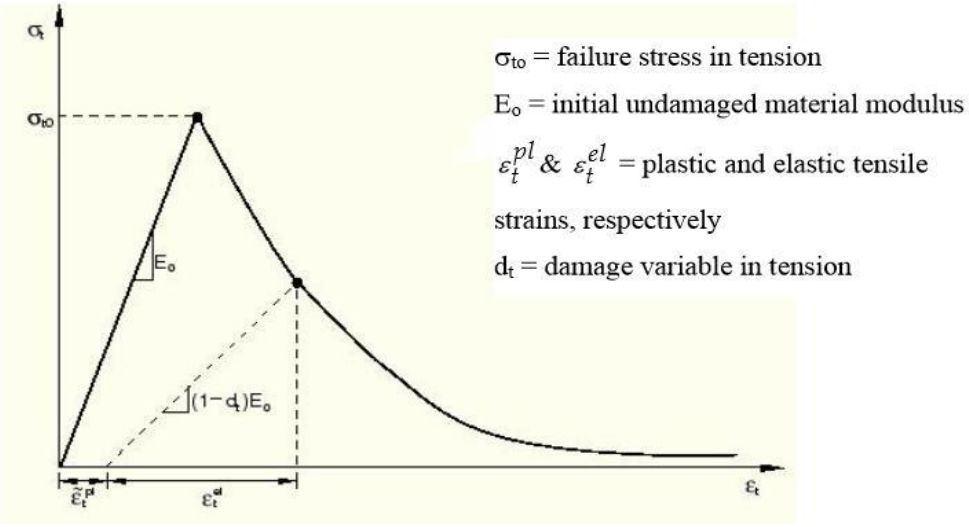

Figure 49: Uniaxial tensile stress-strain curve in tension (Abaqus User Manual)

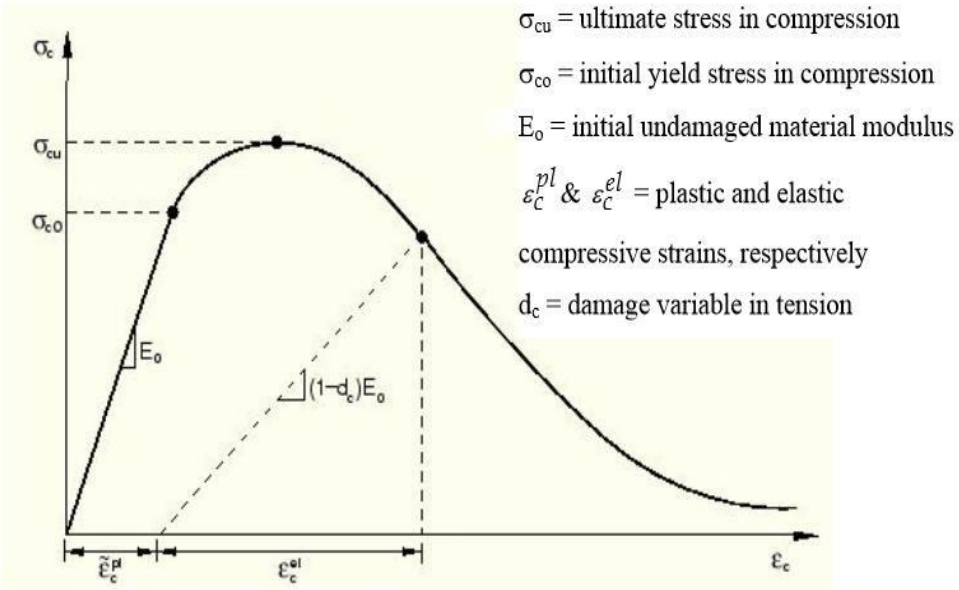

Figure 50: Uniaxial compressive stress-strain curve in tension (Abaqus User Manual)

The concrete damage plasticity model uses the following definition for the yield surface and flow potential.

5.2.1.1 Yield Surface

The yield condition used by the model was based on the yield function developed Lubiner et al [31] with modification made by Lee et al [32] The yield function is given in terms of the effective stresses in the form of

$$F = \left(\bar{\sigma}, \tilde{\varepsilon}^{pl}\right) = \frac{1}{1-\alpha}\left(\bar{q} - 3\alpha\bar{p} + \beta(\tilde{\varepsilon}^{pl})\langle\hat{\bar{\sigma}}_{max}\rangle - \gamma\langle-\hat{\bar{\sigma}}\rangle\right) - \bar{\sigma}_c(\tilde{\varepsilon}^{pl}) = 0 \qquad (3)$$

Where

$\bar{p} =$ Is the effective hydrostatic pressure

$$\bar{p} = \frac{1}{3}\bar{\sigma}: I \qquad (4)$$

$q =$ Is the Mises equivalent stress

$$q = \sqrt{\frac{1}{3}\bar{S} : \bar{S}} \tag{5}$$

$\bar{S} =$ Is the deviatoric part of effective stress

$$\bar{S} = \bar{p}I + \bar{\sigma} \tag{6}$$

$\alpha \; and \; \gamma$ are material constants

$$\alpha = \frac{\left(\frac{\sigma_{b0}}{\sigma_{c0}}\right)-1}{2\left(\frac{\sigma_{b0}}{\sigma_{c0}}\right)-1}; \quad 0 \leq \alpha \leq 0.5, \quad \gamma = \frac{3(1-K_c)}{2K_c-1} \tag{7}$$

$$\beta = \frac{\overline{\sigma_c}\left(\tilde{\varepsilon}_c^{pl}\right)}{\overline{\sigma_t}\left(\tilde{\varepsilon}_t^{pl}\right)}(1-\alpha) - (1+\alpha) \tag{8}$$

$\frac{\sigma_{b0}}{\sigma_{c0}}$ = ratio of initial equibiaxial compressive yield stress to initial compressive yield stress

K_c = ratio of second stress invariant on the tensile meridian to that on the compressive meridian at yield for any given values of pressure invariant p

$\hat{\bar{\sigma}}_{max}$ = maximum principal effective stress

The evolution of the yield surface is controlled by two hardening variable $\tilde{\varepsilon}_c^{pl} \; and \; \tilde{\varepsilon}_t^{pl}$ which are the equivalent tensile and compressive strains which controls the failure mechanism in tension and compression respectively.

5.2.1.2 Flow Rule and Potential

The concrete damage plasticity model assumes non-associated potential plastic flow that is continuous and smooth where the flow direction uniquely defined by Drucker-Prager hyperbolic function is used to define the flow potential G

$$G = \sqrt{(\epsilon\sigma_{t0}tan\Psi)^2 + \bar{q}^2} - \bar{p}tan\Psi \quad (8)$$

Where

Ψ = the dilation angle measure in p-q plane at high confining pressure in degrees

σ_{t0} = the uniaxial tensile strength at failure

ϵ = eccentricity parameter, defining the rate at which the function approaches the asymptote.

The flow rule is given as

$$d\varepsilon_{ij}^{pl} = d\lambda \frac{\partial G}{\partial \sigma_{ij}} \quad (9)$$

5.2.1.3 Input Parameters for Concrete Medical Model

The concrete damage plasticity model requires the following input parameters for defining the concrete material model

Dilation angle Ψ

Eccentricity parameter ϵ

The ratio initial equibiaxial compressive yield stress to initial uniaxial compressive yield stress $\frac{\sigma_{b0}}{\sigma_{c0}}$

The ratio of tensile-compressive meridian K.

The viscosity parameter

Uniaxial compressive yield stress – inelastic values as shown in Figures 52 and 54 while uniaxial tensile yield stress – cracking strain values as shown in Figures 53, 54 and 55.

The following parameters were used, which are the Abaqus default values to define the concrete damage plasticity models.

Table 11: Damage plasticity parameters for normal concrete

Normal Concrete							
Mass density (kg/m^3)	Young modulus (MPa)	Poisson ratio	Ψ (°)	ϵ	$\frac{\sigma_{b0}}{\sigma_{c0}}$	K	Viscosity parameter
2.4E-06	2.78E+3	0.15	36	0.1	1.16	0.667	0

Table 12: Damage plasticity parameters for UHPFRC

UHPFRC							
Mass density (kg/m^3)	Young modulus (MPa)	Poisson ratio	Ψ (°)	ϵ	$\frac{\sigma_{b0}}{\sigma_{c0}}$	K	Viscosity parameter
2.5E-06	45.8E+3	0.15	36	0.1	1.16	0.667	0

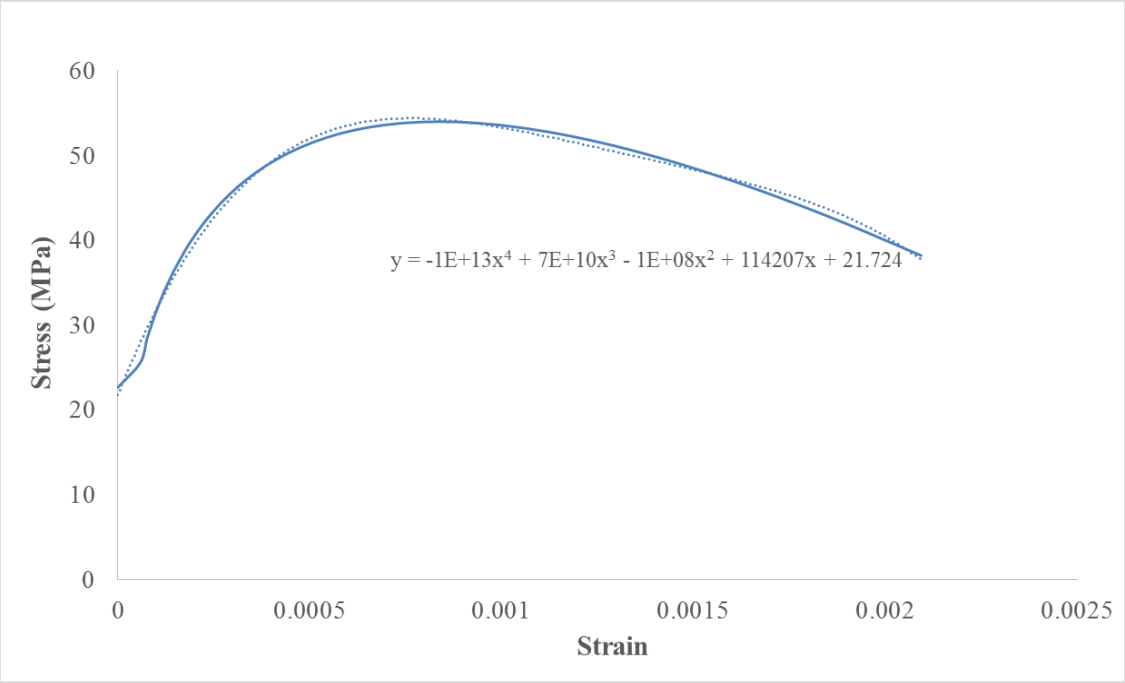

Figure 51: Non-linear compressive behavior of concrete

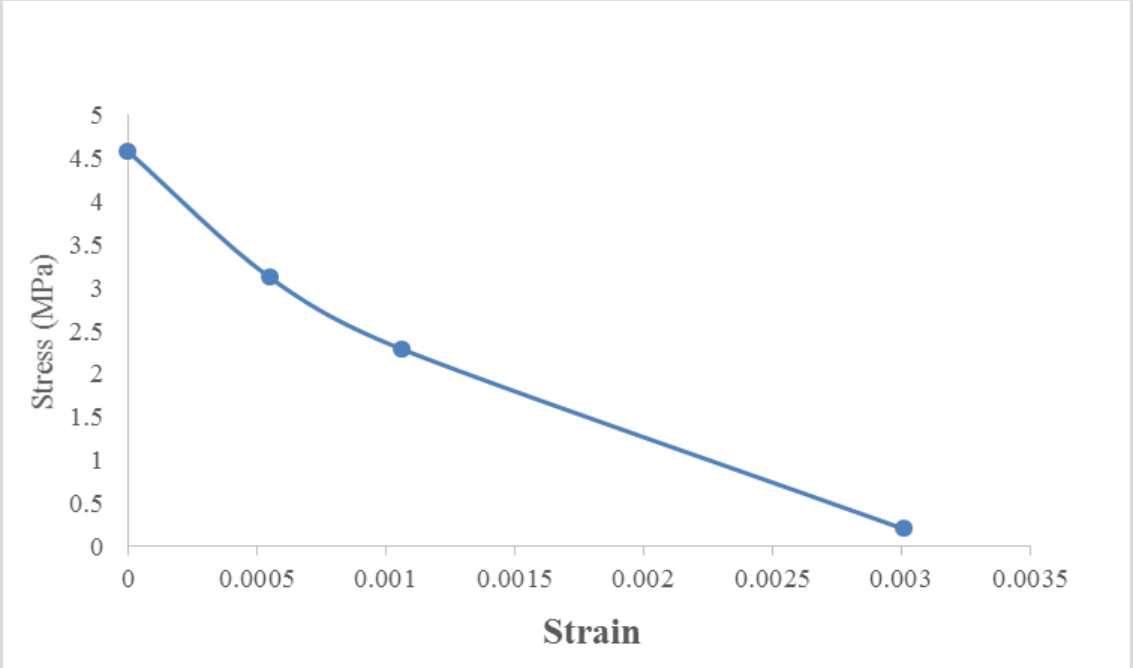

Figure 52: Non-linear tensile behavior of concrete

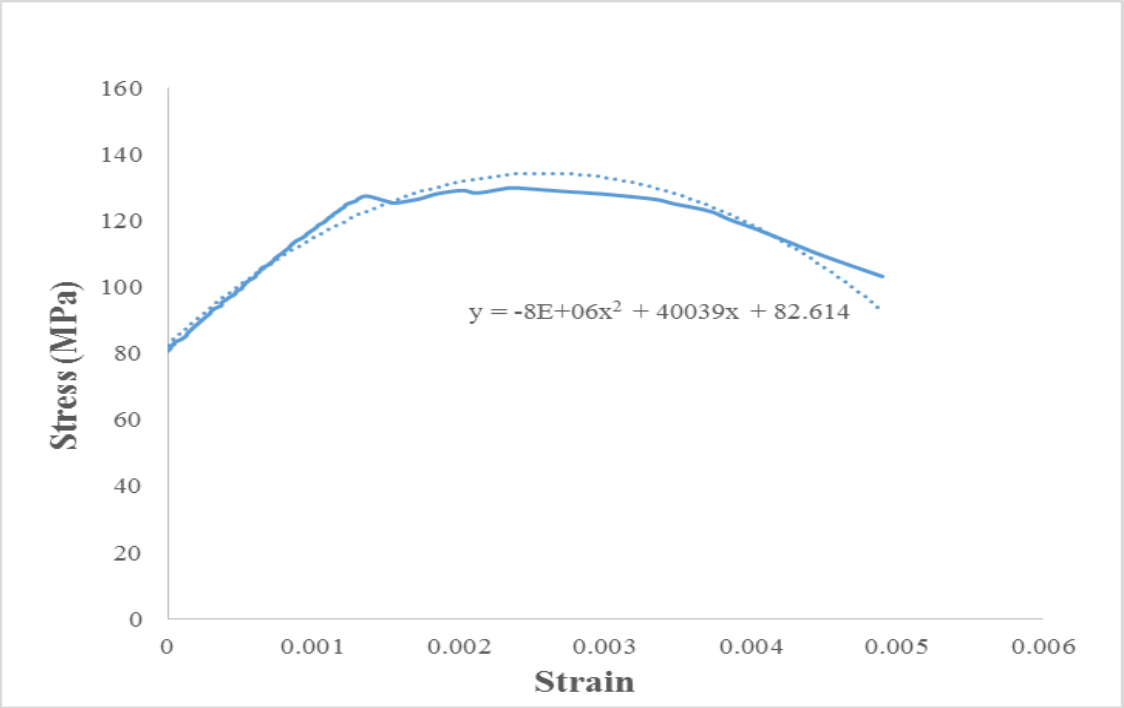

Figure 53: Non-linear compressive behavior of UHPFRC

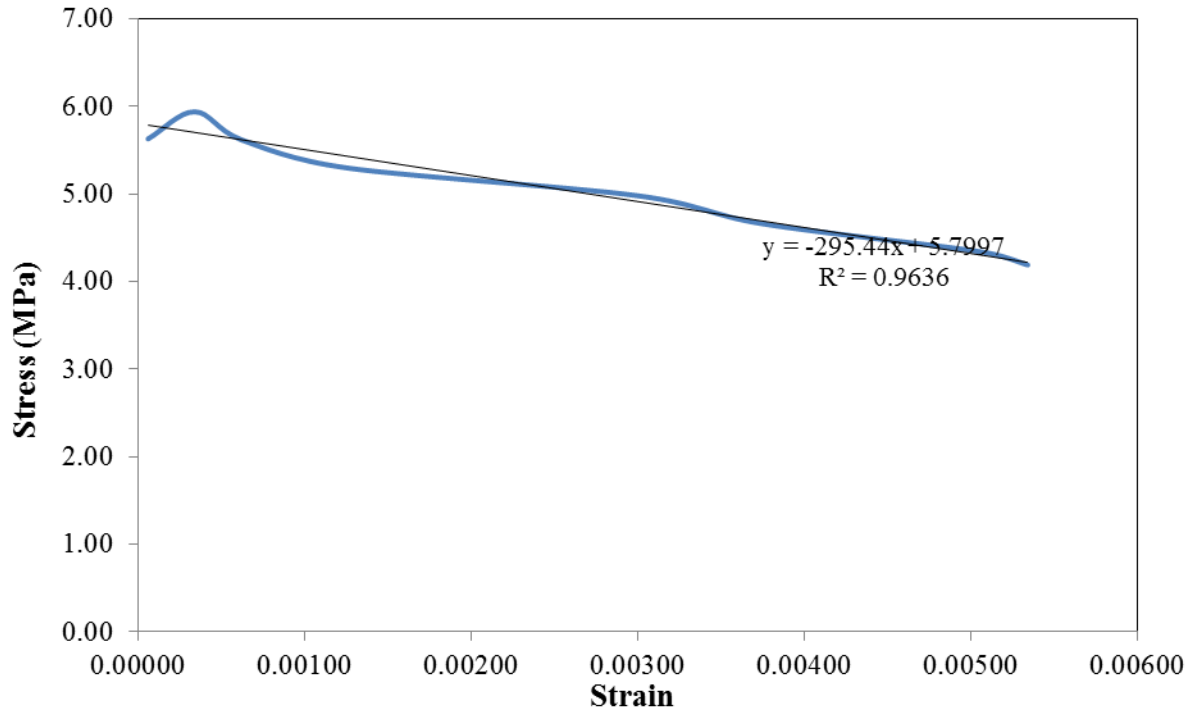

Figure 54: Non-linear tensile behavior of UHPFRC

5.3 Model Constraints

A Certain number of constraints were applied to model the beam specimens. These constraints define the interactions between the various parts of the model as well as define constraints on the analysis of degrees of freedom between regions of the model.

5.3.1 Tie Constraint

The tie constraint allowed us to fuse together the UHPFRC jacket and the normal concrete beam even if the meshes created on the surfaces of the regions of normal concrete and UHPFRC jacket are different. The UHPFRC surfaces were selected as the master surface been the harder surfaces while the concrete beam surfaces were selected as the slave surfaces. This constraint makes the translation and rotational motion as well as other active degrees of freedom equal for a joined concrete-UHPFRC surfaces.

5.3.2 Embedded Region Constraint

To model the interaction between steel reinforcement and concrete beam, the embedded region constraint was used. This constraint embed the steel rebars and stirrups referred to as embedded region in the model inside the concrete referred to as the host region. The constraint uses the geometric relationship between the nodes of the embedded elements and the host element. The translational degrees of freedom of the embedded nodes are constrained to the interpolated values of the corresponding degrees of freedom of the host element. A truss-in-solid was used to model the embedded element-in-host element (i.e. steel reinforcement-in-concrete).

5.4 Model Analysis

An explicit dynamic analysis was used to analyze the model. This is due to the fact that an explicit dynamic analysis provides for flexibility to the solver in applying the load by defining amplitude for load application, thereby eliminating convergence problem of static analysis. The explicit dynamic procedure performs a large number of small time increment efficiently by using an explicitly central-difference time integration, thereby allowing the solution to proceed without iterations and without required tangent stiffness matrices. The analysis also simplifies the treatment of contact problems.

5.5 Meshing Elements

5.5.1 3 – D Stress Elements

A 3 – D stress 8 – nodded linear brick element (solid continuum) shown in Figure 56 and 57 was used to model both the normal concrete and UHPFRC. This element type can be used for both linear analyses and for complex non-linear analysis involving contact, plasticity, and large deformations.

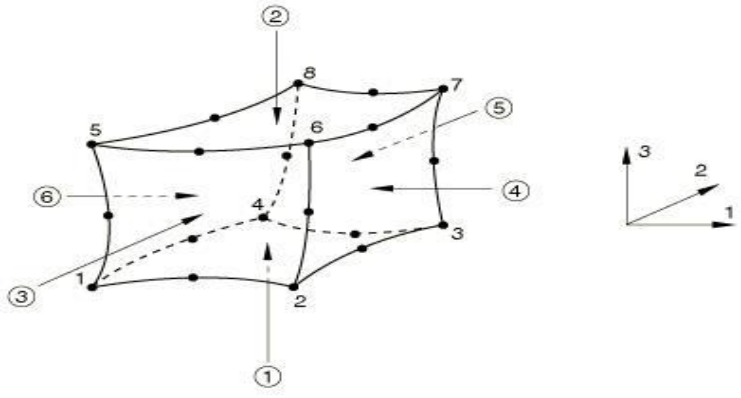

Figure 55: A 3 – D stress 8 – nodded element

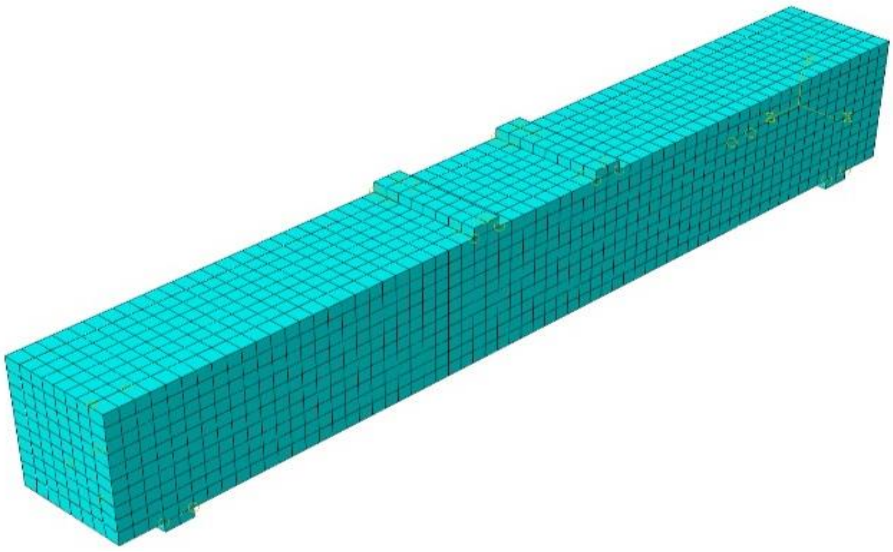

Figure 56: Discretized beam using the 3 – D stress 8 – nodded element

5.5.2 Truss Elements

A 3 – nodded linear 3 – D truss element shown in Figure 58 was used to model the steel reinforcing bars and stirrups. The element is a long, slender structural member that transmit only axial load. It allows the definition of cross-sectional area of the truss element which can be used to define the cross-sectional area of the steel reinforcement.

Figure 57: 2 – nodded linear 3 –D truss element

5.6 Finite Element Modelling Results

The stress distribution and damage along the 3D-model of the specimens were presented and the load-displacement results of the finite element model were plotted and compared with that of the experiment for each specimen.

Comparison of experimental and finite element model (FEM) load deflection behavior shows that the FEM captures both load increase and stiffness of RC-Control and PC-Control with high precision as shown in Figures 59 and 63 respectively. Similarly in the case of $\mathrm{RC-SB/EP-BOT\ SJ}$ and $\mathrm{RC-SB/EP-2\ SJ}$ in figure 60 and 61 respectively, the FEM was able to predict the experimental behavior with high accuracy. $\mathrm{RC-SB/EP-3\ SJ}$ FEM shows similar behavior with the experiment, however, an overlapping in stiffness by the FEM was observed just after the elastic range as shown in Figure 62. This makes the FEM fail at a lower load than the experimental failure load. This difference is likely due to the fact that both experimental failure load and stiffness of the beam were highly affected by the orientation and concentration of steel fibers in the path of crack propagation. However, this effect is not taken into account by the FEM as it works based on stress-strain results of small UHPFRC specimens whose steel fiber orientation and concentration might be far different from that of the beam specimens. Similar effects were observed in the case of PC specimens$\mathrm{PC-SB-BOT\ SJ}$, $\mathrm{PC-SB-2\ SJ}$ and $\mathrm{PC-SB-3\ SJ}$ as shown in Figures 64, 65 and 66 respectively. This is because PC beams are even more sensitive to steel fiber orientation and concentration across crack paths since they lack steel reinforcing bars. This effect of steel fibers orientation and concentration usually arises during mixing and due to the effect of vibration during compaction.

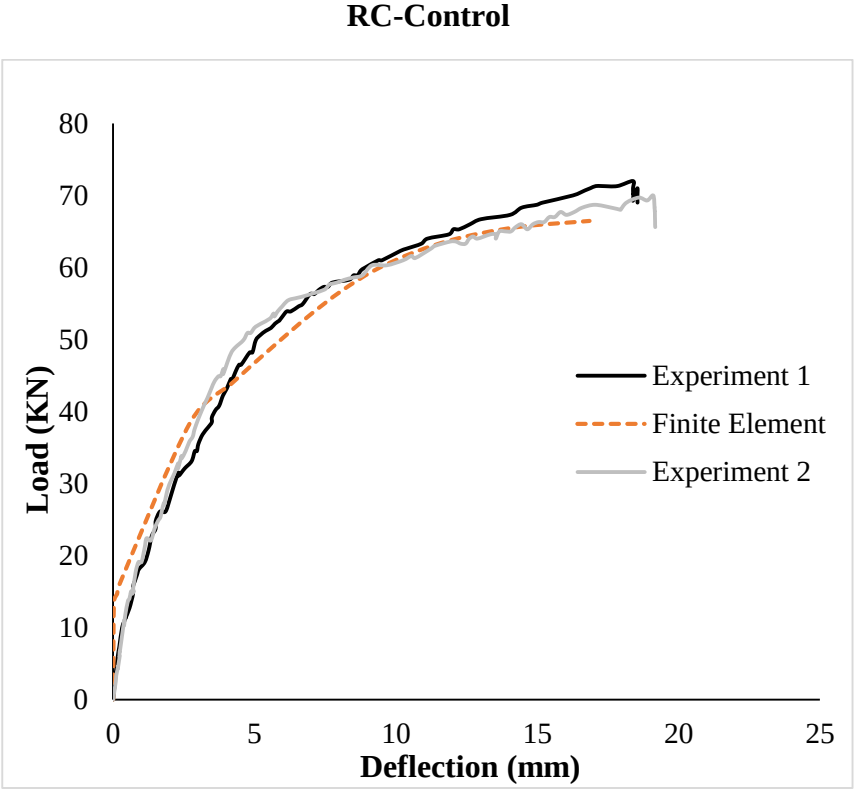

Figure 58: Finite element and experimental load deflection behavior for RC-Control

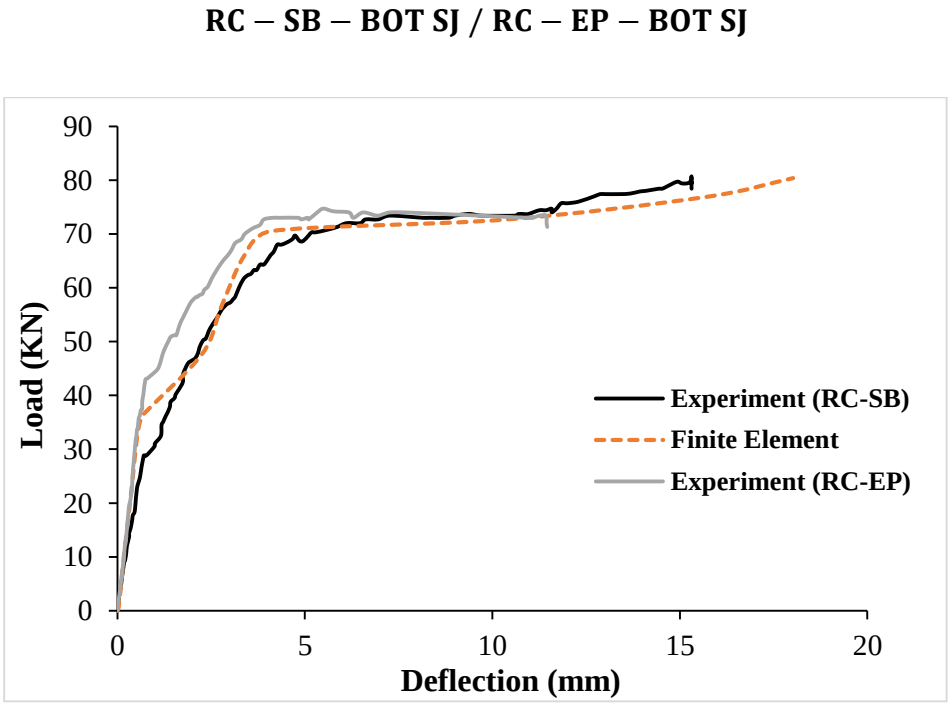

Figure 59: Finite element and experimental load-deflection behavior for RC-SB/EP-BT SJ

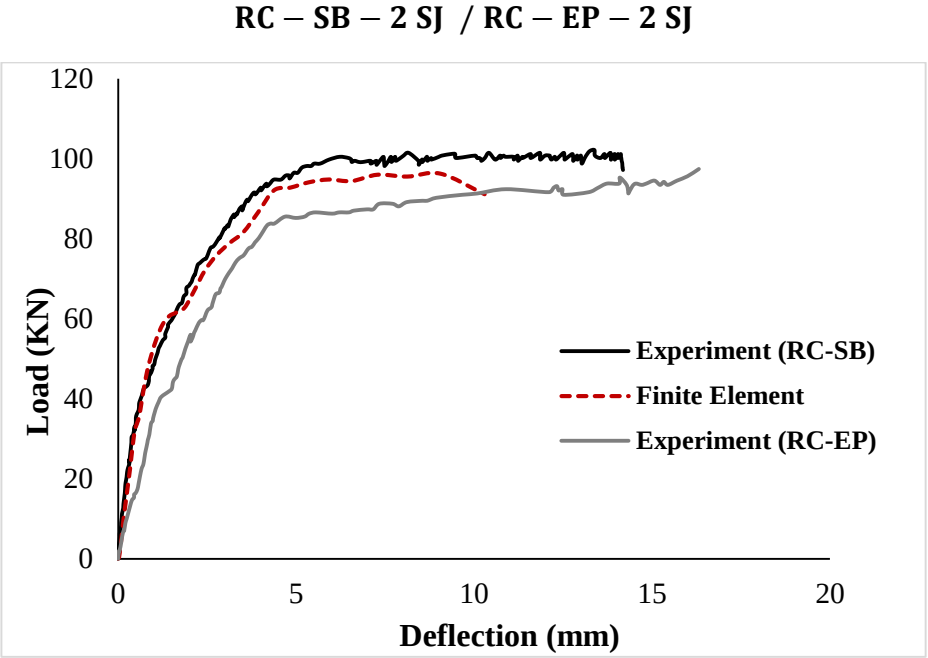

Figure 60: Finite element and experimental load-deflection behavior for RC – SB/EP – 2 SJ

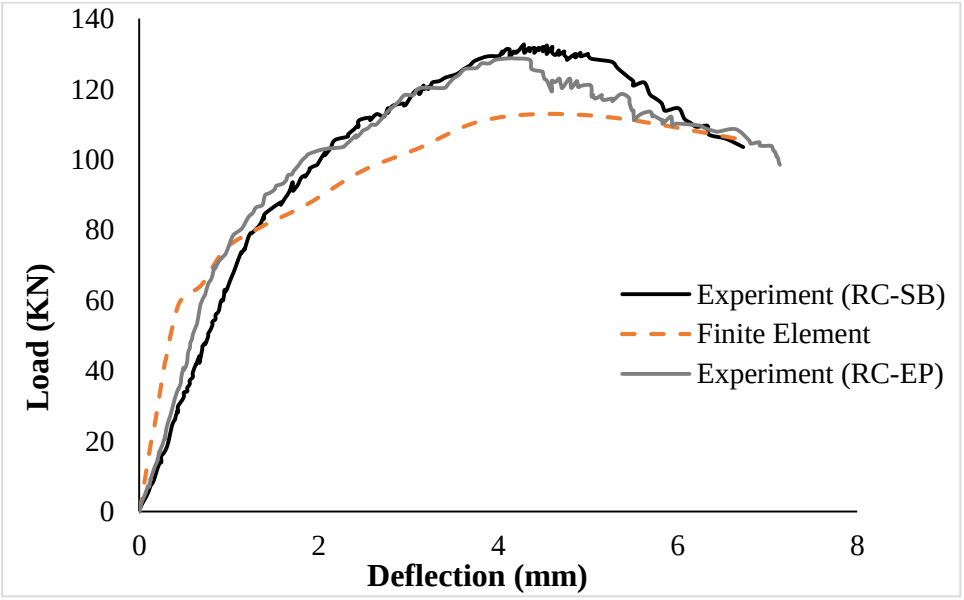

Figure 61: Finite element and experimental load-deflection behavior for RC – SB/EP – 3 SJ

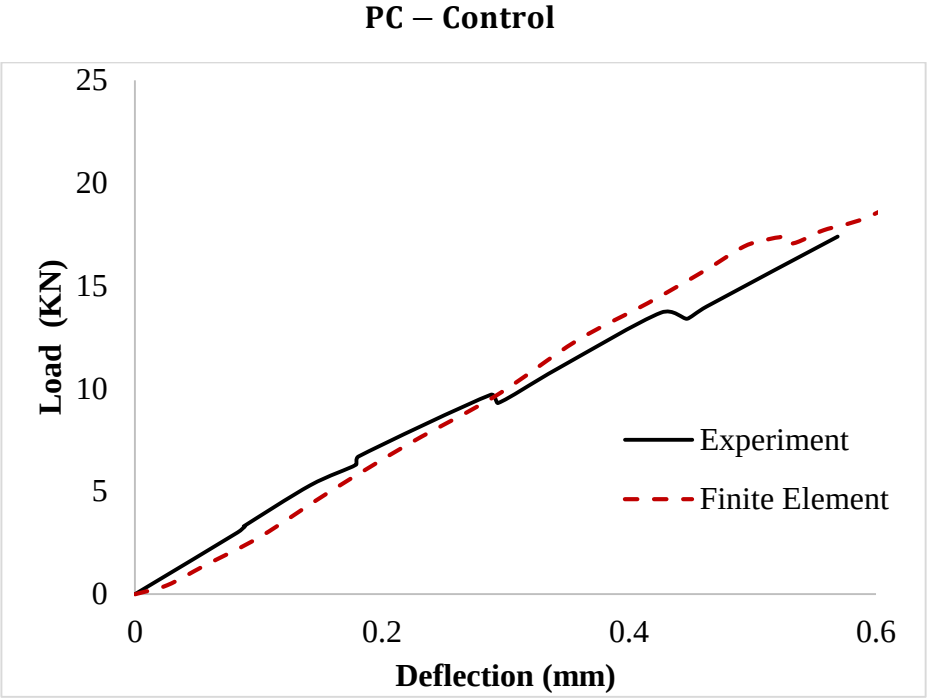

Figure 62: Finite element and experimental load-deflection behavior for PC-Control

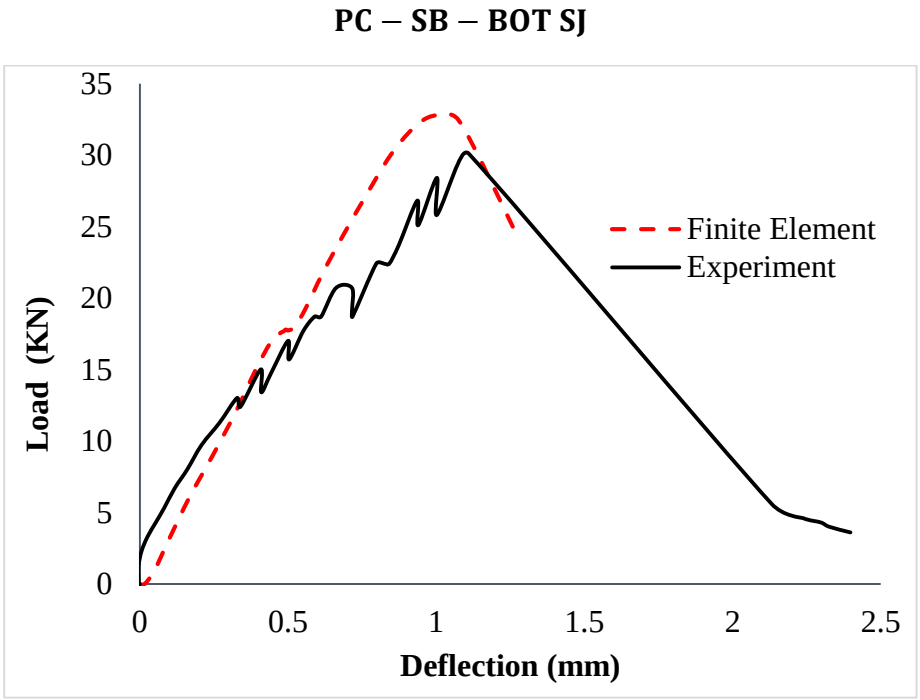

Figure 63: Finite element and experimental load deflection behavior for PC-SB-BOT SJ

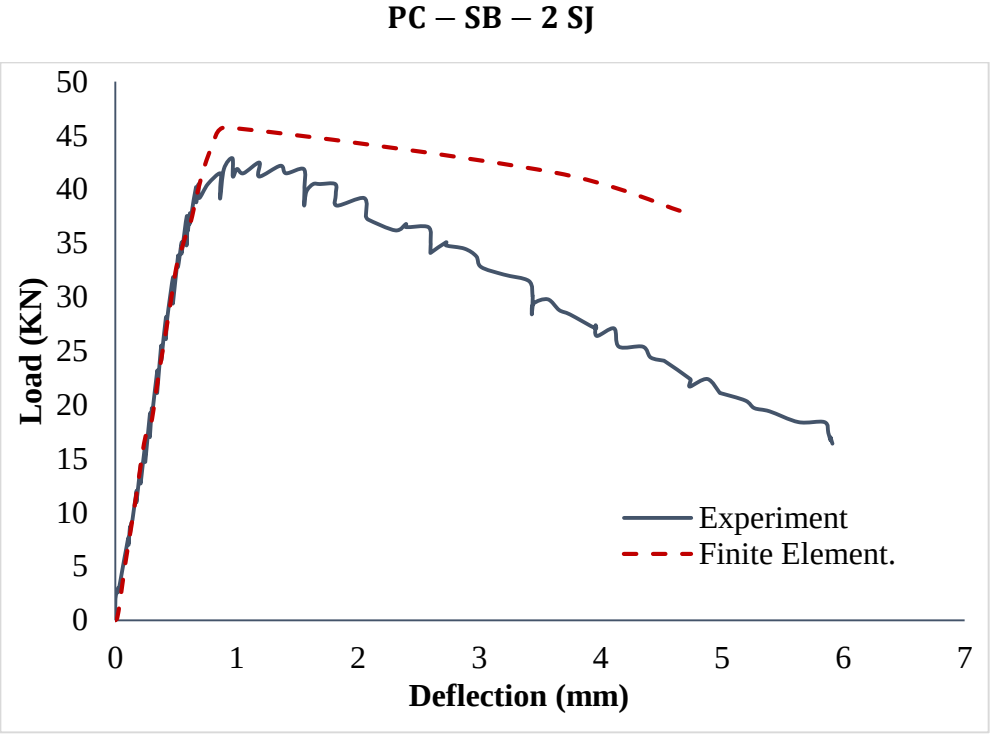

Figure 64: Finite element and experimental load-deflection behavior for PC-SB-2 SJ

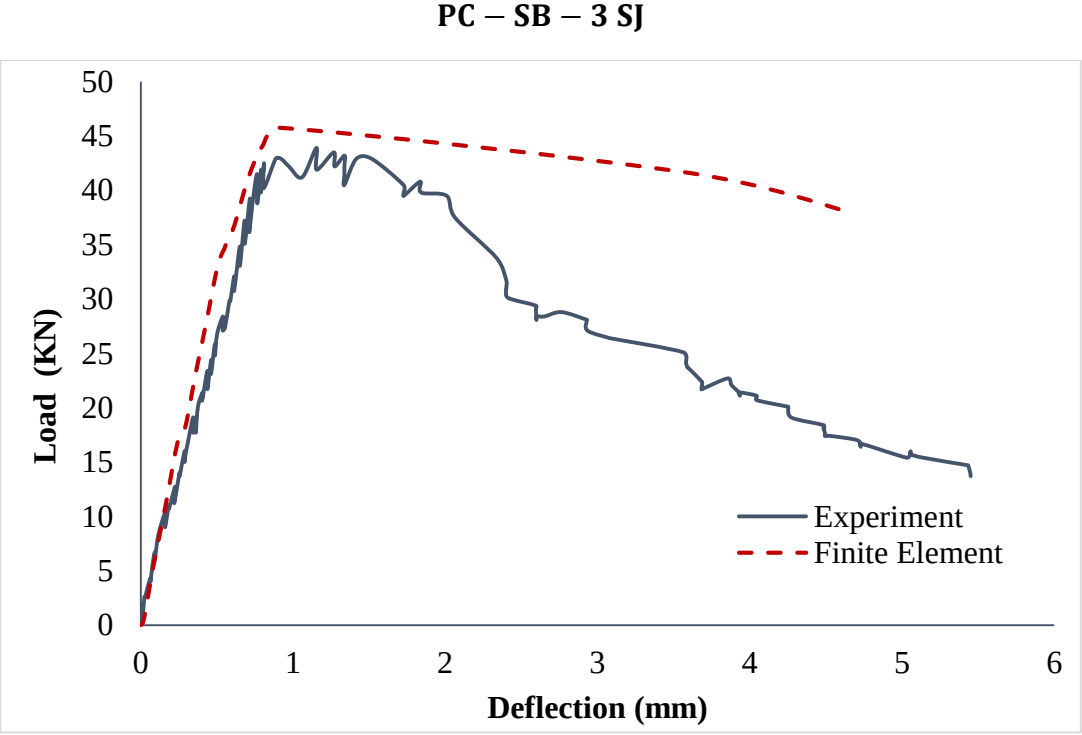

Figure 65: Finite element and experimental load-deflection behavior for PC-SB-3 SJ

Figures 67, 69, 71 and 73 shows crack experimental FEM crack patterns for RC-Control, $RC-SB-BOT\ SJ$, $RC-SB-2-SJ$ and $RC-SB-3\ SJ$ respectively. It was observed that there is high resemblance between the experimental and FEM crack pattern. This further shows that how effective the FEM was in predicting the behavior of the beams specimens. Also, steel stresses were shown in Figures 68, 70, 72 and 74 for $RC-$ Control, $RC-SB-BOT\ SJ$, $RC-SB-2-SJ$ and $RC-SB-3\ SJ$ respectively. It was observed that steel has already yielded as it was observed in the case of experiment tests.

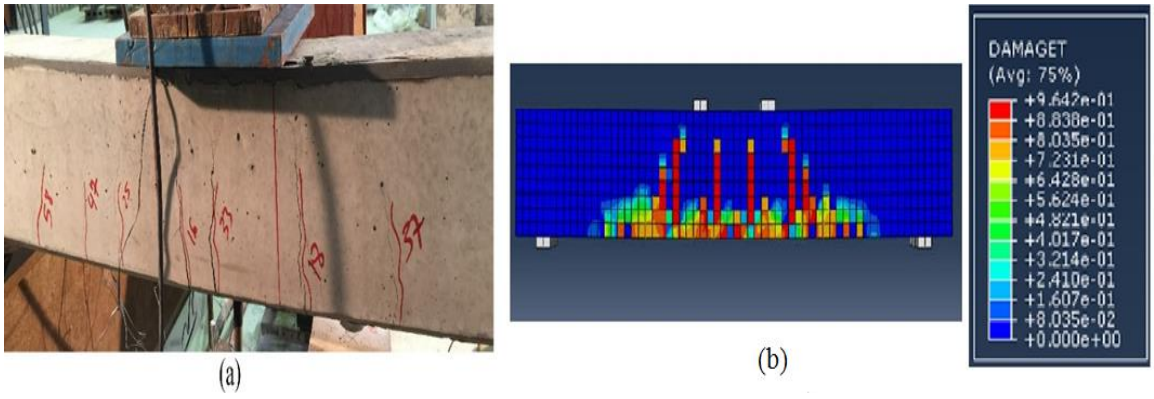

Figure 66: Crack Pattern for RC-Control (a) experiment (b) FEM

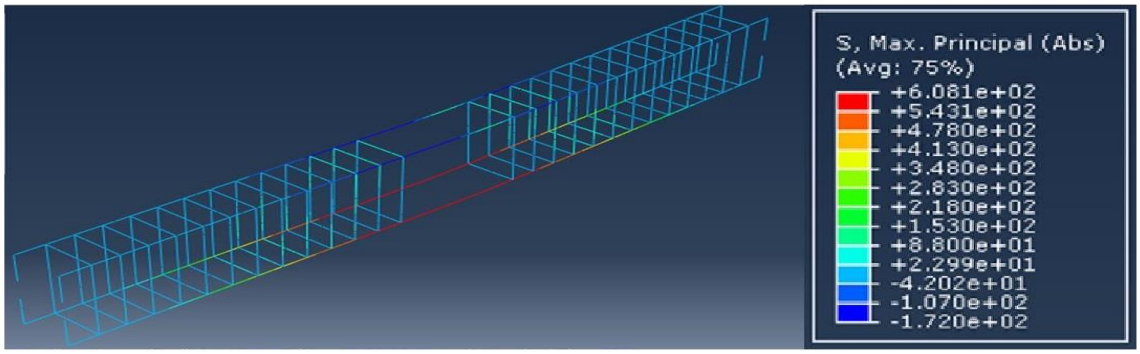

Figure 67: Stress distribution in steel at failure for RC-Control

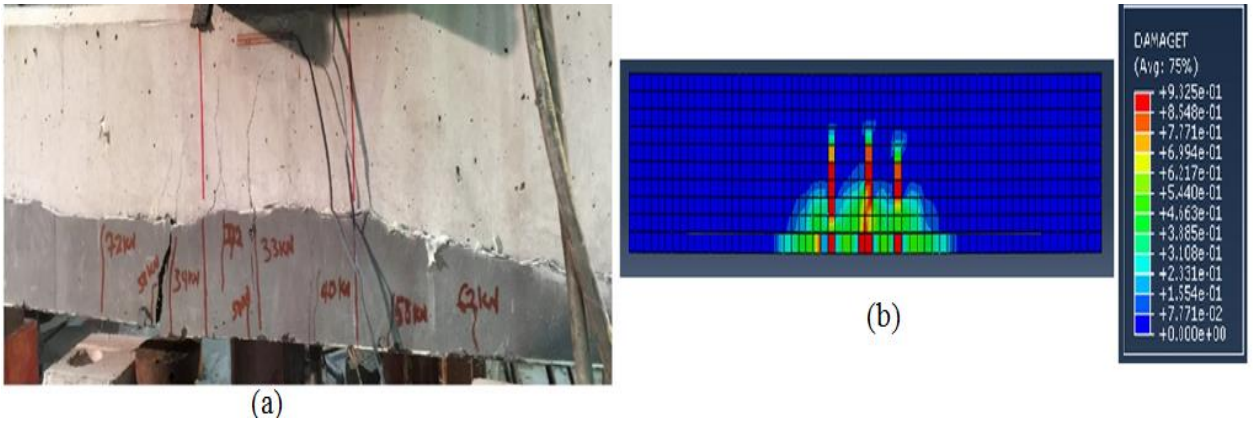

Figure 68: Crack Pattern for RC-BOT SJ (a) experiment (b) FEM

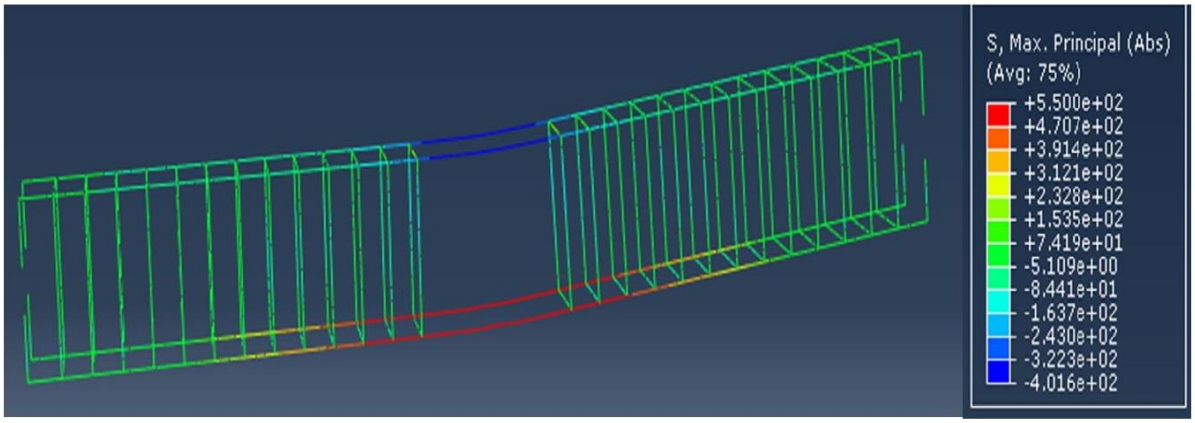

Figure 69: Stress distribution in steel at failure for RC-BOT SJ

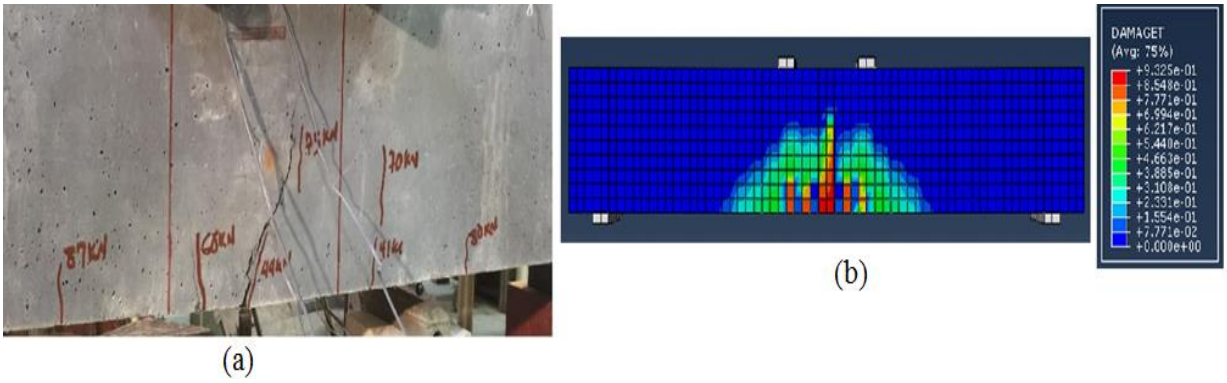

Figure 70: Crack Pattern for RC-2 SJ (a) experiment (b) FEM

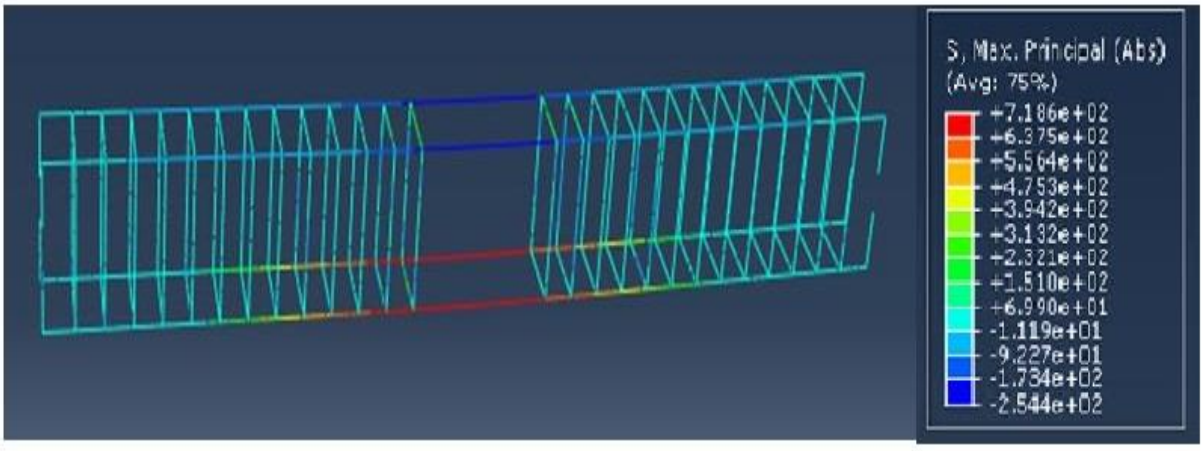

Figure 71: Stress distribution in steel at failure for RC-2 SJ

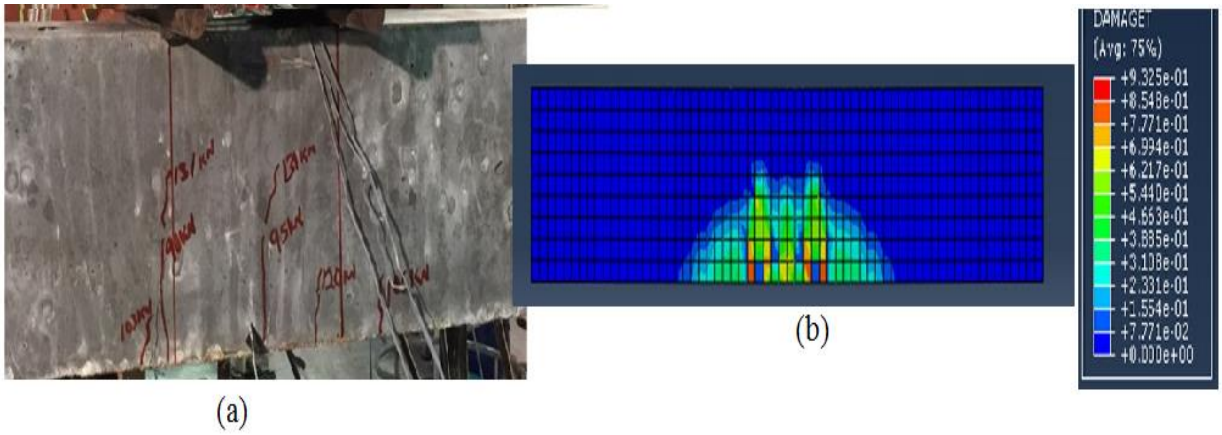

Figure 72: Crack Pattern for RC-3 SJ (a) experiment (b) FEM

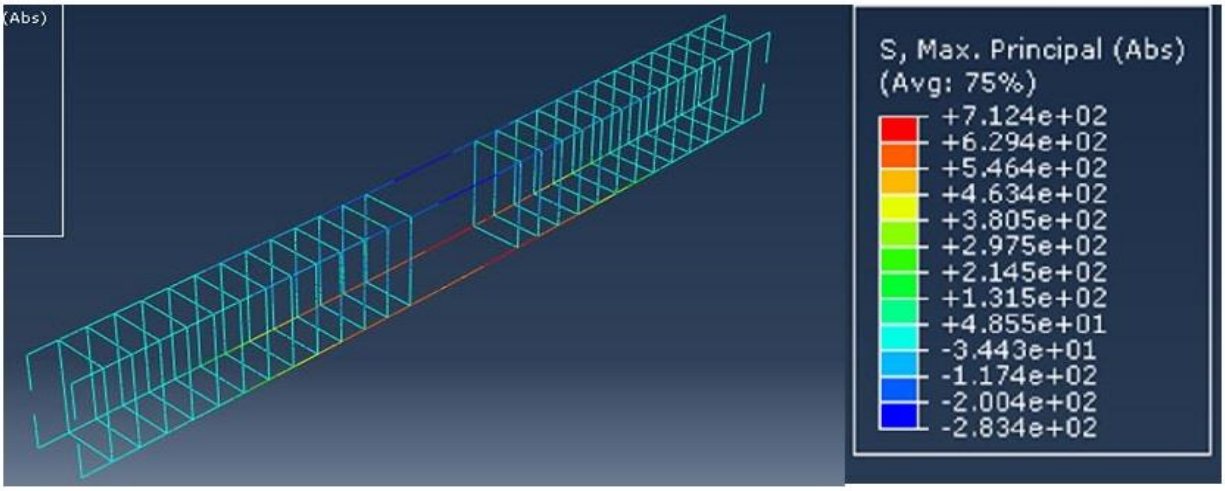

Figure 73: Stress distribution in steel at failure for RC-3 SJ

Figure 75, 76, 77 and 78 shows below shows crack pattern for PC-Control, PC-SB-BOT SJ, PC-SB-2 SJ and PC-SB-3 SJ respectively showing high resemblance between experimental and FEM pattern.

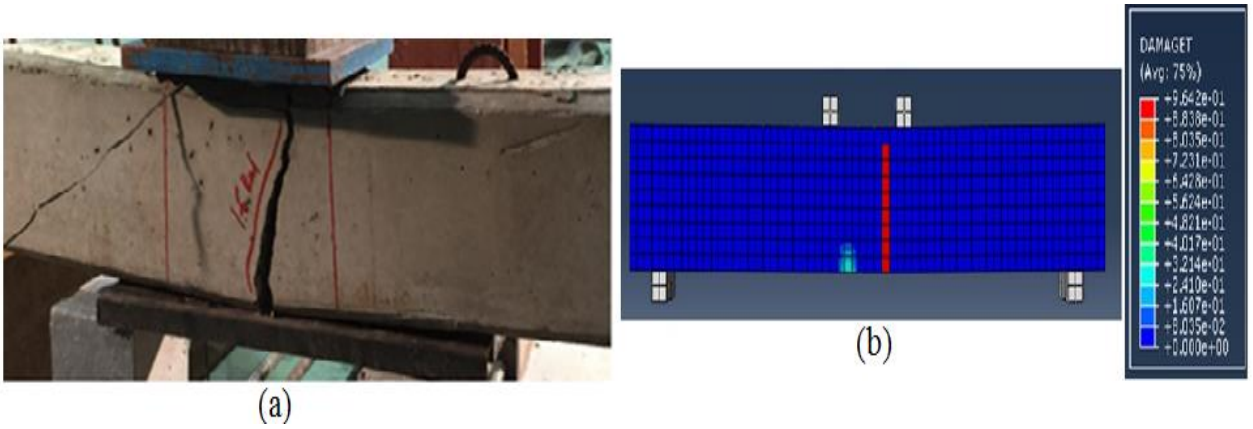

Figure 74: Crack Pattern for PC-Control (a) experiment (b) FEM

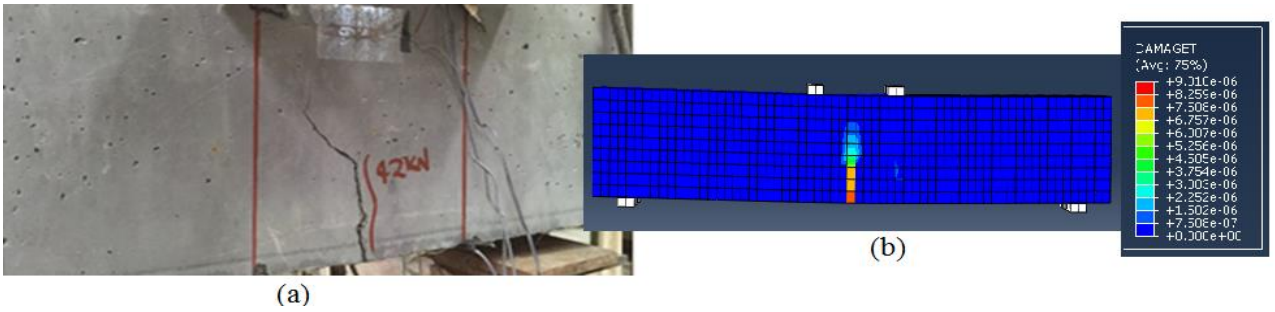

Figure 75: Crack Pattern for PC-SB-2 SJ (a) experiment (b) FEM

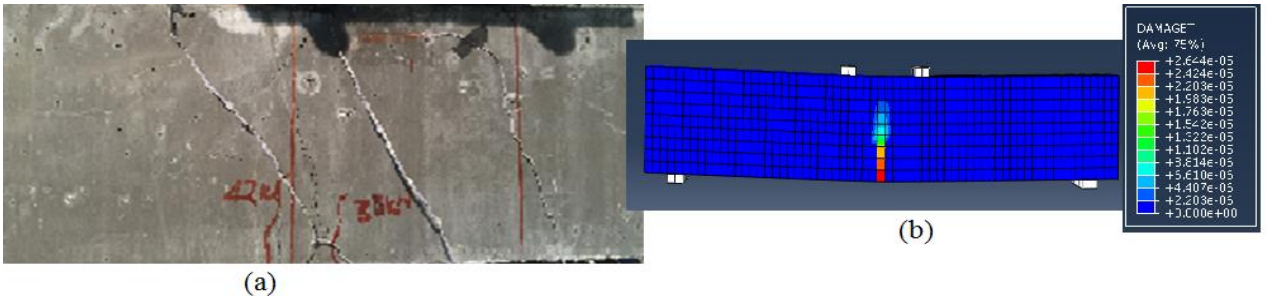

Figure 76: Crack Pattern for PC-SB-3 SJ (a) experiment (b) FEM

CHAPTER 6

ANALYTICAL/MECHANISTIC MODEL

6.1 General

The flexural behavior of both the control and UHPFRC strengthened beam specimens were determined using an analytical/mechanistic model of their cross section. The analysis uses internal stresses based on the sectional stress-strain distribution to predict internal forces. Failure moment is calculated from the internal forces at equilibrium of the member at that particular cross section. The model is developed based on the materials test results expressed as material laws that serve as inputs to the model.

6.2 Review of Related Models

An analytical model for predicting the flexural behavior of a conventional RC beam strengthened with surface mounted FRP bars/strips base on beam bending theory was developed by Sharaky et al [33]. The model was able to predict stresses and deformations with good agreement from the experimental results. Another flexural model was developed by Esmaeel and Joaquin [34] to predict flexural capacities of RC beams strengthened using hybrid composite plates (HPC). They computed the flexural capacities using both equivalent rectangular stress block and using nonlinear stress block and compared the results. They conclude that the results show good agreement with a difference of less than 5%. To predict the flexural and shear capacities of RC beams strengthened with CFRP, El-Ghandour [35] develop an analytical model where the concrete was modelled using a modified rectangular stress block developed by [Collins and Mitchell] while the CFRP was

modelled using linear elastic stress-strain curve up to failure. Their predicted capacities were found to be in close agreement with experimental results. Alaee and Karihaloo [18] developed an analytical model to predict the moment resistance and load-deflection behavior of damaged RC beams retrofitted with UHPFRC known as CARDIFRC. It was observed that the load-deflection behavior of the control specimens were adequately predicted while prediction is very good for retrofitted beam specimens. For predicting the behavior of a conventional RC beam strengthened at the tension side with UHPFRC. Ruano et al [20] also developed an analytical model based on the bending beam theory. However, the model was found to overestimates the force of the beams by 7% and 30% for beams with and without steel reinforcing bar in UHPFRC respectively. Another model was developed by Noshiravani and Bryhwiler [19] based on the assumption that the shear capacity of the of the composite beams is equal to the shear resistance provided by the NSC/HSC beam neglecting shear reinforcement plus the shear resistance provided by the steel fibres in the UHPFRC layer. The model shows some reasonable ability to predict the shear strength of the specimens

.

6.3 Analytical Model for RC Beams

The moment capacity of both control and UHPFRC strengthened beam specimens were analysed using an analytical/mechanistic model of their cross section. The analysis uses internal stresses based on the sectional stress-strain distribution to predict internal forces. Failure moment is calculated from the internal forces at equilibrium of the member at that particular cross section. The model is developed based on the materials test results expressed as material laws that serves as input data to the model. A bi-linear stress-strain

curve was used for modelling the steel reinforcing bars in tension (i.e. elastic perfectly plastic) as shown in Figure. 77(a). UHPFRC behaviour in tension is modelled by a bi-linear stress-strain curve resembling the experimental behaviour as shown in Figure. 77(b). Concrete in compression is represented using the Whitney stress block (i.e. equivalent rectangular stress distribution) in accordance to ACI Code Section 10.2.7 as shown in Figure. 77(c). Also UHPFRC in tension is represented by an equivalent rectangular stress block for high strength concrete proposed by [29]

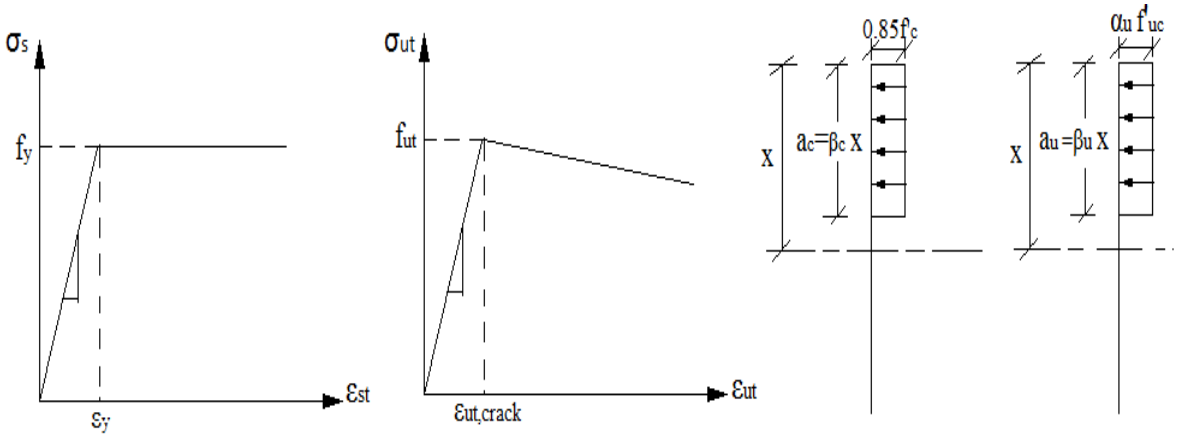

(a) (b) (c) (d)

Figure 77: Material laws (a) steel tensile behavior (b) UHPFRC tensile behavior (c) concrete compressive stress distribution (d) UHPFRC compressive stress distribution

Where

$$\beta_c = 0.85 - 0.05\frac{f_c' - 28}{7} \quad f_c' > 28MPa \qquad (10)$$

$$\alpha_u = \begin{cases} 0.85 & f_{uc}' \le 69MPa \\ 0.85 - 0.0029(f_{uc}' - 69) \ge 0.75 & f_{uc}' > 69MPa \end{cases} \quad [29] \qquad (11)$$

$$\beta_u = \begin{cases} 0.85 & f_{uc}' \le 28MPa \\ 0.85 - 0.00725(f_{uc}' - 28) \ge 0.65 & f_{uc}' > 28MPa \end{cases} \quad [29] \qquad (12)$$

The analytical model is based on the assumptions of flexure theory of reinforced concrete beams;

1) Plane sections remain plane and the beams specimen show monolithic behaviour.
2) The material behaviors are described by material laws.
3) Linear strain distribution through the full depth of the beam.
4) Tensile strength of normal concrete is neglected
5) Deformations are small.
6) Shear deformations are not considered.
7) Compression steel contribution is not considered, its location is very close to the neutral axis for all cases, thereby making it ineffective.
8) There is perfect bond between concrete, reinforcement and UHPFRC.

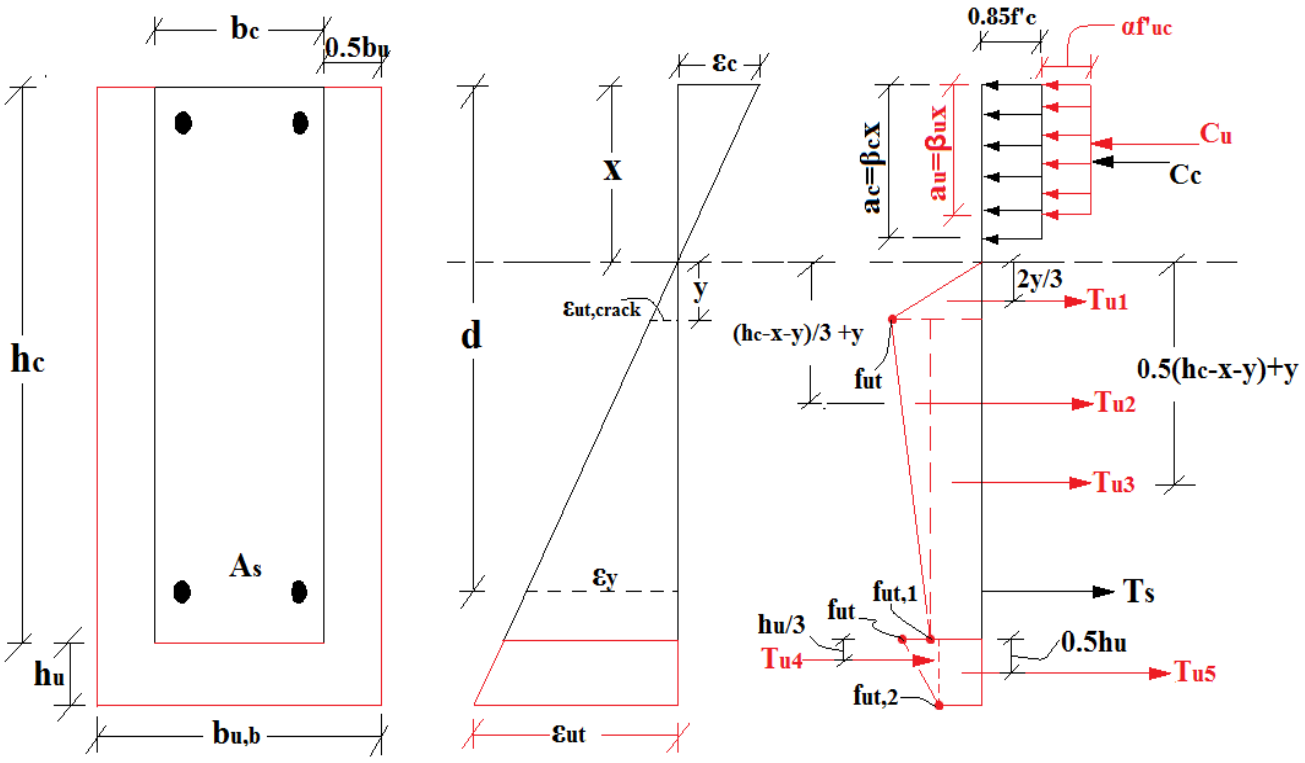

Figure 78: Analytical model definition

Internal forces were expressed as the product of stress and the cross sectional area covered by the stresses as shown in equations (13) – (20)

$$C_c = 0.85 f_c' \beta_c x b_c \tag{13}$$

$$C_u = \alpha_u f_{uc}' \beta_u x b_u \tag{14}$$

$$T_s = A_s f_y \tag{15}$$

$$T_{u1} = 0.5 f_{ut}\, b_u\, y \tag{16}$$

$$T_{u2} = 0.5\left(f_{ut} - f_{ut,1}\right).\, b_u (h_c - x - y) \tag{17}$$

$$T_{u3} = b_u (h_u - x - y) f_{ut,1} \tag{18}$$

$$T_{u4} = 0.5\, h_u \left(f_{ut} - f_{ut,2}\right) b_{u,b} \tag{19}$$

$$T_{u5} = h_u b_{u,b} f_{ut,2} \tag{20}$$

Strain at the bottom of the beam is selected ε_{ut} and equations (13) – (18) are simplified and expressed in terms of the neutral axis depth x. The value of x at failure is obtained by iteration until equilibrium of forces is attained i.e.

$$\Sigma\, F = (C_c + C_u) - (T_s + T_{u1} + T_{u2} + T_{u3} + T_{u4} + T_{u5}) = 0 \tag{21}$$

The predicted flexural moment capacity is computed by taking moment of forces about the neutral axis location

$$M_{pred} = C_c \left(x - \frac{a_c}{2}\right) + C_u \left(x - \frac{a_u}{2}\right) + T_s (d - x) + T_{u1} \left(\frac{2y}{3}\right) + T_{u2} \left[\frac{1}{3}(h_c - x - y) + y\right] +$$

$$T_{u3} \left[\frac{1}{2}(h_c - x - y) + y\right] + T_{u4} \left(h_c + \frac{1}{3} h_u\right) + T_{u5} \left(h_c + \frac{1}{2} h_u\right) \tag{22}$$

The procedure for computing the predicted moment capacities of the beams is as shown in Figure. 79.

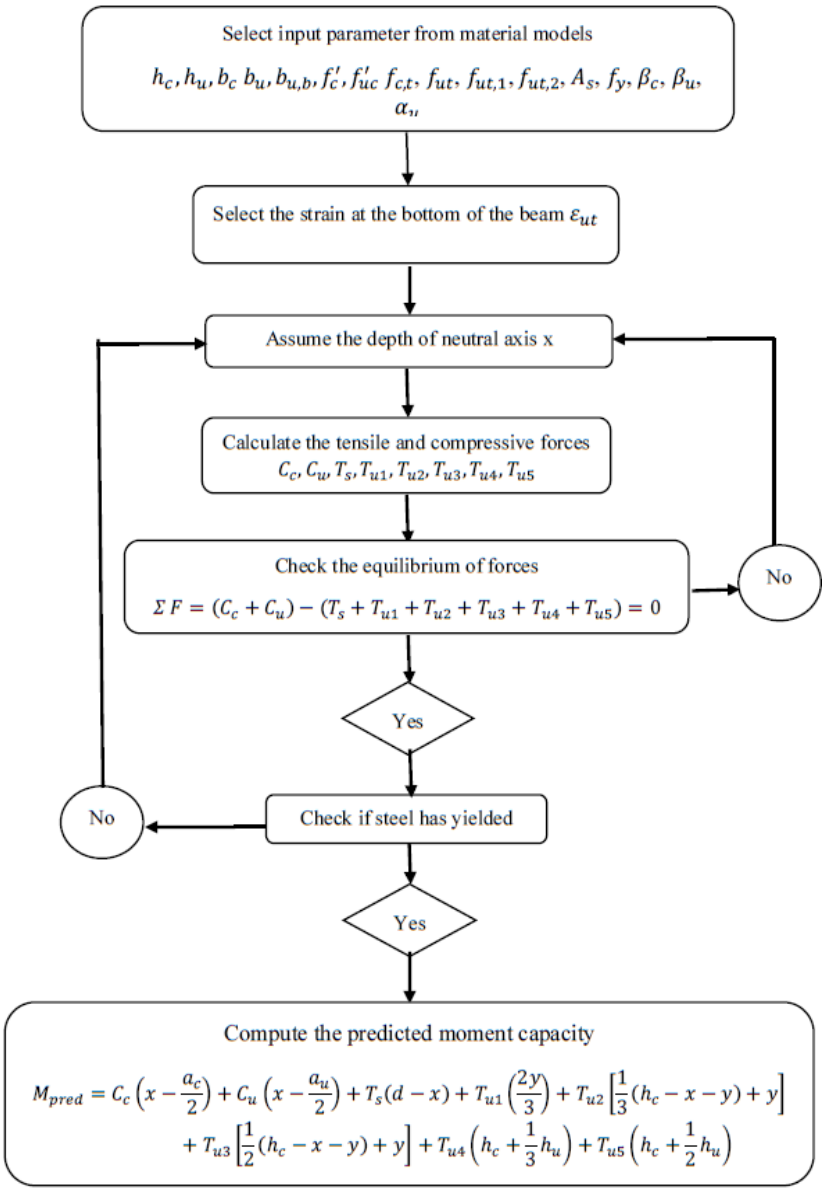

Figure 79: Analytical model flow chart for RC beams

Results of moment capacities predicted using the analytical model of the beam specimens were presented and compared with the experimental test result in Table 13. The results shows good agreement for both type of strengthening techniques

Table 13: Analytical model results of tested beam specimens

Specimen	$\mathbf{M_{Exp}}$	$\mathbf{M_{pred}}$	$\frac{\mathbf{M_{Exp}}}{\mathbf{M_{pred}}}\ \boldsymbol{ratio}$
$\mathrm{RC-Control\ 1}$	20.1	18.3	1.094
$\mathrm{RC-Control\ 2}$	19.8	18.3	1.081
$\mathrm{RC-SB-BOT\ SJ}$	23.3	24.6	0.953
$\mathrm{RC-SB-2\ SJ}$	29.3	26.5	1.109
$\mathrm{RC-SB-3\ SJ}$	37.9	35.7	1.065
$\mathrm{RC-EP-BOT\ SJ}$	21.6	24.6	0.878
$\mathrm{RC-EP-2\ SJ}$	27.3	26.5	1.030
$\mathrm{RC-EP-3\ SJ}$	37.1	35.7	1.039

Difference between analytical and experimental failure load was 9.4 and 7.8% for $\mathrm{RC-Control\ 1}$ and $\mathrm{RC-Control\ 2}$ respectively. Also, a difference of 4.9, 10.8 and 6.4% for $\mathrm{RC-SB-BOT\ SJ}$, $\mathrm{RC-SB-2\ SJ}$ and $\mathrm{RC-SB-3\ SJ}$ respectively while the difference of 13.3, 3.3 and 4% were obtained for $\mathrm{RC-EP-BOT\ SJ}$, $\mathrm{RC-EP-2\ SJ}$ and $\mathrm{RC-EP-3\ SJ}$ respectively as shown Figure. 80.

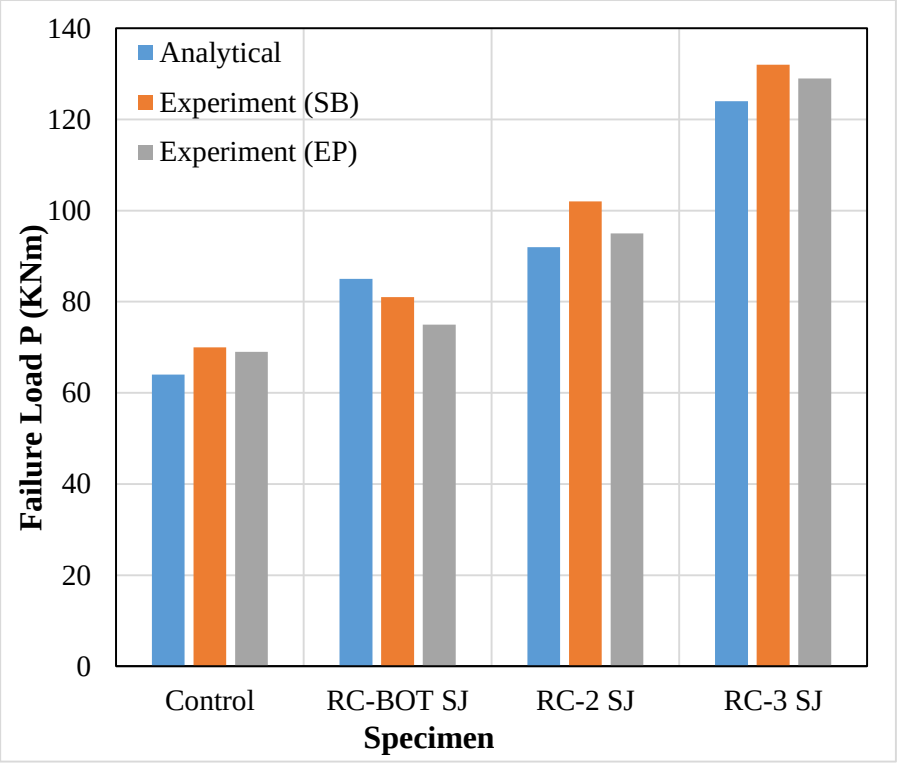

Figure 80: Comparison between analytical model and experimental failure loads

6.4 Analytical Model for PC Beams

The moment capacity of both control and UHPFRC strengthened beam specimens were analyzed using an analytical/mechanistic model of their cross section. The analysis uses internal stresses based on the sectional stress-strain distribution to predict internal forces. Failure moment is calculated from the internal forces at equilibrium of the member at that particular cross section. The model is developed based on the materials test results expressed as material laws that serve as input data to the model. UHPFRC and concrete behaviors in tension are modelled by a bilinear stress-strain curve resembling the experimental behavior as shown in Figure. 81. Concrete and UHPFRC in compression are

modelled to have linear response as was obtained results of deformations during conducting the experiment.

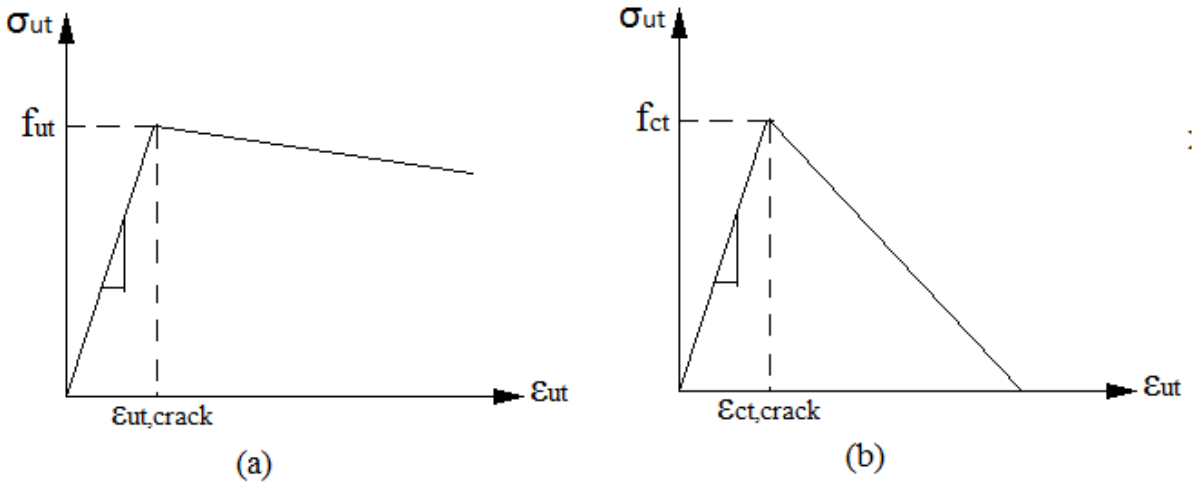

Figure 81: Material laws (a) UHPFRC tensile behavior (b) concrete tensile behavior

The analytical model is based on the following assumptions for bending;

1) Plane sections remain plane and the beams specimen show monolithic behavior.
2) The material behaviors are described by material laws.
3) Linear strain distribution through the full depth of the beam.
4) Tensile strength of concrete is taken into account
5) Deformations are small.
6) Shear deformations are not considered.
7) There is perfect bond between concrete, reinforcement and UHPFRC.

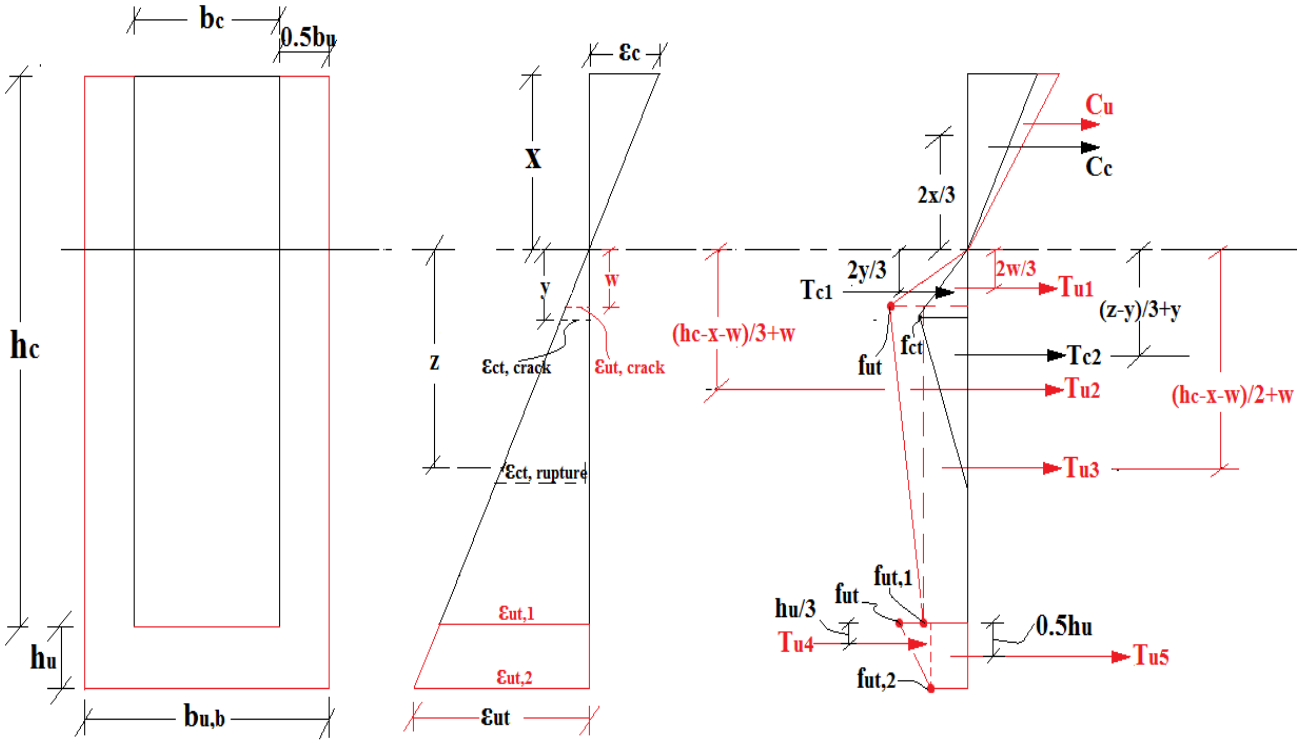

Figure 82: Analytical model definition of PC beams

For a given tensile strain at the bottom of the beamε_{ut}, the remaining strain, stress are deduced from the uniaxial tensile strength test curves. While others are computed in terms of the neutral axis position x as given in equation (23) – (27).

Using Similar triangles

$$\varepsilon_c = \frac{\varepsilon_{ut,2} \times x}{(h_c - x + h_u)} \tag{23}$$

$$w = \frac{\varepsilon_{ut,crack} \times (h_c - x + h_u)}{\varepsilon_{ut,2}} \tag{24}$$

$$y = \frac{\varepsilon_{ct,crack} \times (h_c - x + h_u)}{\varepsilon_{ut,2}} \tag{25}$$

$$\varepsilon_{ut,1} = \frac{\varepsilon_{ut,2} \times (h_c - x)}{(h_c - x + h_u)} \tag{26}$$

$$z = \frac{\varepsilon_{ct,rupture} \times (h_c - x + h_u)}{\varepsilon_{ut,2}} \quad (27)$$

Internal forces are expressed as the product of stress and the cross-sectional area covered by the stresses as shown in equations (28) – (36)

$$C_c = \frac{1}{2} b_c \, x(\varepsilon_c E_c) \quad (28)$$

$$C_u = \frac{1}{2} b_u \, x(\varepsilon_c E_u) \quad (29)$$

$$T_{c1} = \frac{1}{2} b_c \, y \, f_{ct} \quad (30)$$

$$T_{c2} = \frac{1}{2} b_c \, (z - y) \, f_{ct} \quad (31)$$

$$T_{u1} = \frac{1}{2} b_u w \, f_{ut} \quad (32)$$

$$T_{u2} = \frac{1}{2} b_u (h - x - w) \times (f_{ut} - f_{ut,1}) \quad (33)$$

$$T_{u3} = b_u (h - x - w) f_{ut,1} \quad (34)$$

$$T_{u4} = \frac{1}{2} b_{u,b} h_u \times (f_{ut} - f_{ut,2}) \quad (35)$$

$$T_{u5} = b_{u,b} h_u \, f_{ut,2} \quad (36)$$

The forces given in equations (28) – (34) are simplified and expressed in terms of the neutral axis depth x. The value of x at failure is obtained by iteration until equilibrium of forces is attained

$$\sum Forces = (C_c + C_u) - (T_{c1} + T_{c2} + T_{u1} + T_{u3} + T_{u4} + T_{u5}) = 0 \quad (37)$$

The predicted flexural moment capacity is computed by taking moment of forces about the neutral axis location

$$M_{pred} = C_c \times \left(\frac{2}{3}x\right) + C_u\left(\frac{2}{3}x\right) + T_{c1}\left(\frac{2}{3}y\right) + T_{c2}\left(\frac{1}{3}(z-y)+y\right) + T_{c1}\left(\frac{2}{3}w\right) +$$

$$T_{u2}\left(\frac{1}{3}(h_c - x - w) + w\right) + T_{u3}\left(\frac{1}{2}(h_c - x - w)\right) + T_{u4}\left(h_c - x + \frac{1}{3}h_u\right) +$$

$$T_{u5}\left(h_c - x + \frac{1}{2}h_u\right) \quad (38)$$

The procedure for computing the predicted moment capacities of the beams is as shown in Figure. 83.

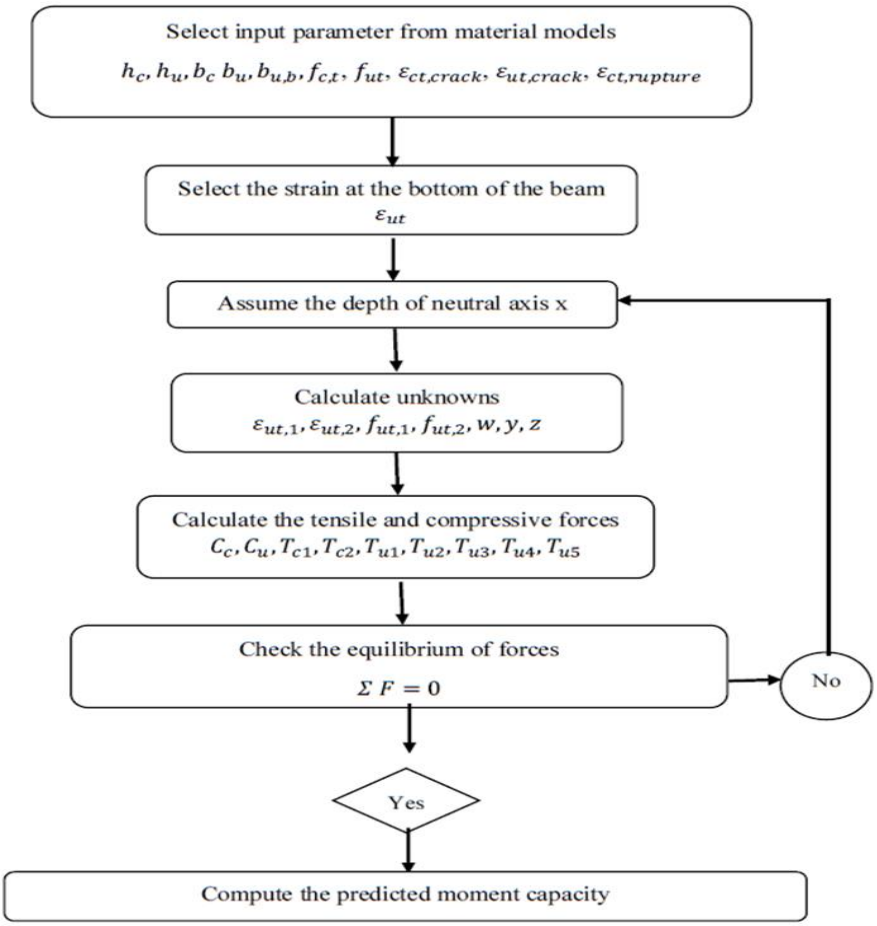

Figure 83: Analytical model flow chart for PC beams

Results of moment capacities predicted using the analytical model of the beam specimens were presented and compared with the experimental test result in Table 14. The results show good agreement for both type of strengthening techniques

Table 14: Analytical model results of tested PC beam specimens

Specimen	M_{Exp}	M_{pred}	$\frac{M_{Exp}}{M_{pred}}$ **ratio**
$PC - Control\ 1$	4.9	5.2	0.942
$PC - SB - BOT\ SJ$	8.6	8.9	0.966
$PC - SB - 2\ SJ$	12.0	9.8	1.224
$PC - SB - 3\ SJ$	12.6	13.6	0.924

Figure 84: shows comparison between experimental and analytical model failure load.

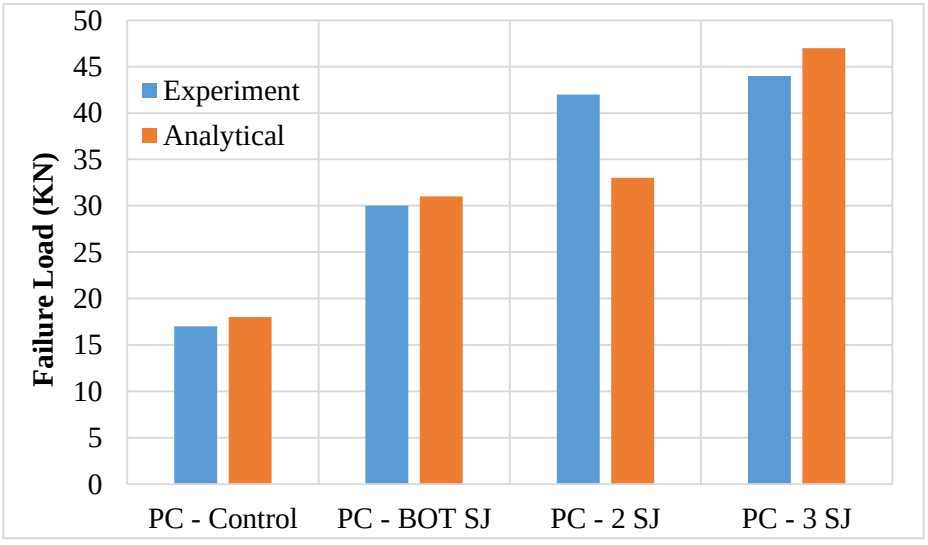

Figure 84: Comparison between experimental and analytical failure load of PC beam specimens

CHAPTER 7

CONCLUSIONS AND RECOMMENDATIONS

7.1 General

With the aim of investigating the flexural behavior of concrete beams strengthened with UHPFRC, an exploratory investigation has been carried out to develop ways of applying UHPFRC jacket to concrete beams in different configurations. Two concepts were explored (i) by sandblasting of concrete surface then casting fresh UHPFRC to the required surface. (ii) by using epoxy adhesive to attach prefab UHPFRC strips to the concrete beam. Two types of concrete beams were investigated (i) reinforced concrete (RC) beams (ii) plain concrete (PC) beams. Both concept (i) and (ii) were applied on RC beams while only concept (ii) was applied on PC beams.

Test results shows great enhancement in the flexural moment capacity for both RC and PC beams for all configurations of UHPFRC strengthening. No significant difference was observed regarding the two concepts of applying UHPFRC jackets to the beams used as both proved effective. Further studies are required for possible application of this techniques in practice.

7.2 Conclusions

1) Bond strength tests shows that UHPFRC has good bonding property even without surface preparation of the concrete substrate. However, concrete substrates whose surface is roughened by sand blasting followed by casting fresh UHPFRC around it shows higher bond strength under compression and shear. While specimens for which

concrete and UHPFRC substrates were bonded with epoxy adhesive shows higher bond strength in tension

2) The use of UHPFRC strengthening has increased the stiffness of the concrete beams under service condition i.e. deformations were under applied loads when compared to the control beam specimens.
3) UHPFRC strengthening helps to delay cracking load, crack propagation and spread when compared the control concrete beam specimens. This is due to the high tensile strength and strain hardening property of UHPFRC
4) The strengthened beam shows monolithic behavior i.e. no debonding occurs for both concepts used to apply the UHPFRC jackets. However, a flexural crack was observed to branched out and propagate over a short distance along the interface was in case of epoxy bonded prefab UHPFRC strips ($RC - EP - 2\ SJ$).
5) Beam specimens strengthened on its three sides shows the highest capacity enhancement whereas beams strengthened for all types of concrete beams and for all concepts of applying UHPFRC jacket.
6) The use of UHPFRC strengthening increases the stiffness of the concrete beams under service condition i.e. deformations under applied loads were lower when compared to the control beam specimens. Beams strengthened on the three side shows highest increase in stiffness compared to other beams of the same concrete beam type.

7) The results of finite element modelling (FEM) shows good agreement with the experimental test results particularly for RC beams specimens. The FEM predict peak load and deflections close to the experimental test values.
8) The analytical model is able to predict the moment capacity of the strengthened beams with high accuracy for all types of concrete beams. the model provide an effective tool to determine the moment capacity for strengthened concrete beams strengthened with UHPFRC jacketing irrespective of the material property of UHPFRC mix used.

7.3 Recommendations for future work

1) This research works was conducted for reinforced and plain beam beams. There is need for similar research works on other RC elements particular on columns, walls and slabs.
2) There is need to develop closed form design equations for flexural strengthening of reinforced and plain concrete beams with UHPFRC as well as design guidelines if the material is to be adopted for practical purposes.
3) Performance of the strengthened concrete beams under fatigue loading particularly cyclic loading should be investigated with more emphasis giving to the interface condition.
4) Behavior and performance of the strengthened concrete beams under fire load should be investigated with respect to its effect on strength, stiffness and interface condition. Knowledge of such behavior and performance will be an invaluable design parameter.

5) Also, there is need to investigate the behavior and performance of the strengthened concrete beams particularly at the interface under seismic loading, blast loading as well as impact loading.
6) Most or all the works reviewed here have been conducted under one environmental condition. There is need to check performance (particularly interface condition) under varying environmental condition such as freezing and thawing, wetting and drying etc.

REFERENCES

[1] Hazem A. El-Enein, Hossein Azimi, Khaled Sennah, Faouzi Ghrib (2014). Flexural strengthening of reinforced concrete slab–column connection using CFRP sheets. Construction and Building Materials, Vol. 57, pp 126 – 137.

[2] G. Monti, M. A. Liotta (2005). FRP strengthening in shear: Tests and design equations. ACI Structural Journal, Vol. 230, pp 543 – 562.

[3] Rahman S, Molyneaux T, Patnaikuni I. Ultra – high performance concrete, recent applications and research. Aust J Civ Eng 2005; 2(1):13–20

[4] Hakeem, I.Y.A., Characterization of an ultra-high performance concrete, King Fahd University of Petroleum & Minerals (Saudi Arabia), MSc Thesis, 2011.

[5] Lubbers, A., "MS Thesis "Bond Performance of Ultra- High Performance Concrete and Prestressing Strands", Ohio University, August, 2003.

[6] Luaay Hussein, Lamya Amleh (2015). Structural behavior of ultra-high performance fiber reinforced concrete-normal strength concrete or high strength concrete composite members. Construction and Building Materials, Vol. 93, pp. 1105 – 1116.

[7] Habel K, Denarié E, Bruhwiler E. Experimental investigation of composite ultra-high performance fiber-reinforced concrete and conventional concrete members. ACI Struct J 2007; 104(1):10–20

[8] Martinola G, Meda A, Plizzari GA, Rinaldi Z. Strengthening and repair of RC beams with fiber reinforced concrete. Cement Concrete Compos 2010; 32(9):731–9.

[9] A. P. Lampropoulos, S.A. Paschalis, O. T. Tsioulou, S. E. Dritsos (2016). Strengthening of reinforced concrete beams using ultra-high performance fiber reinforced concrete (UHPFRC). Engineering Structures, Vol. 106, pp. 370 – 384.

[10] Bassam A. Tayeh, B. H. Abu Bakar, M. A. Megat Johari, Yen Lei Voo (2013). Utilization of ultra-high performance fiber concrete (UHPFC) for rehabilitation - A review. 2nd International Conference on Rehabilitation and Maintenance in Civil Engineering. Procedia Engineering, Vol. 54, pp. 525 – 538.

[11] Graybeal, B. Ultra-High Performance Concrete. TechNote, FHWA-HRT-11-038, Federal Highway Administration, McLean, VA, 2011.

[12] US Department of Transportation (2006). Material characterization of ultra-high performance concrete. Tech. Note: FHWA – HRT – 06 – 103.

[13] Bassam A. Tayeh, B. H. Abu Bakar, M. A. Megat Johari, Yen Lei Voo (2013). Evaluation of bond strength between normal concrete substrate and ultra-high performance fiber concrete as a repair material. 2nd International Conference on Rehabilitation and Maintenance in Civil Engineering. Procedia Engineering, Vol. 54, pp. 554 – 563.

[14] Tohru Makita, Eugen Brühwiler (2014). Tensile fatigue behavior of ultra-high performance fibre reinforced concrete combined with steel rebars (R-UHPFRC). International Journal of Fatigue, Vol. 59, pp. 145 – 152.

[15] Voort V (2008). Design and field testing of tapered H-shaped Ultra High Performance Concrete piles, Iowa State University.

[16] Ahlborn, T.M., Harris, D.K., Misson, D.L., and Peuse, E.J. (2012). Strength and durability characterization of ultra-high performance concrete under variable curing conditions. Transportation Research Record – Design of Structures, Journal of the Transportation Research Board – Structures 2011, TRR No. 2251, 68-75.

[17] Prabhat Ranjan Prem, A. Ramachandra Murthy, G. Ramesh, B. H. Bharatkumar and Nagesh R. Iyer (2015). Flexural behavior of damaged rc beams strengthened with ultra-high performance concrete. Advances in Structural Engineering, Vol. 3, pp. 2057 – 2069.

[18] Farshid Jandaghi Alaee, Bhushan Lal Karihaloo (2003). Retrofitting of reinforced concrete beams with CARDIFRC. Journal of Composites for Construction, Vol. 7, pp. 174.

[19] Talayeh Noshiravani, Eugen Brühwiler (2013). Experimental investigation on reinforced ultra-high performance fiber-reinforced concrete composite beams subjected to combined bending and shear. ACI Structural Journal, Vol. 110 No.2, pp. 251 – 262.

[20] Gonzalo Ruano, Facundo Isla, Rodrigo Isas Pedraza, Domingo Sfer, Bibiana Luccioni (2014). Shear retrofitting of reinforced concrete beams with steel fiber reinforced concrete. Construction and Building Materials, Vol. 54, pp. 646 – 658.

[21] Thaer Jasim Mohammed, B. H. Abu Bakar, N. Muhamad Bunnori (2016). Torsional improvement of reinforced concrete beams using ultra high-performance

fiber reinforced concrete (UHPFC) jackets – Experimental study. Construction and Building Materials, Vol. 106, pp. 533–542.

[22] I. Iskhakov, Y. Ribakov, K. Holschemacher, T. Mueller (2013). High performance repairing of reinforced concrete structures. Materials and Design, Vol. 44, pp. 216 – 222.

[23] K. Habel, E. Denarié, E. Brühwiler (2007). Experimental investigation of composite UHPFRC-concrete members. ACI Structural Journal, Vol. 104 No.1, pp. 93–101.

[24] M. Bastien-Masse, E. Brühwiler (2014). Ultra high performance fiber reinforced concrete for strengthening and protecting bridge deck slabs. Bridge Maintenance, Safety, Management and Life Extension – Chen, Frangopol & Ruan (Eds) Taylor & Francis Group, London.

[25] Oesterlee C. 2010. Structural response of reinforced UHPFRC and RC composite members. Doctoral Thesis, No. 4848, Ecole Polytechnique Fédérale de Lausanne, Switzerland.

[26] Thierry Thibaux (2008). Strengthening of Huisne bridge using ultra-high performance fiber reinforced concrete. Tailor Made Concrete Structures. Taylor & Francis Group, London, ISBN 978-0-415-47535-8

[27] C.T. Liu, J.S. Huang (2009). Fire performance of highly flowable reactive powder concrete. Construction and Building Materials, Vol. 23, pp. 2072–2079.

[28] Y.S. Tai, H.H. Pan, Y.N. Kung (2011). Mechanical properties of steel fiber reinforced reactive powder concrete following exposure to high temperature reaching 800˚C, Nuclear Engineering Des. Vol. 241, pp. 2416–2424.

[29] M. M. Springkel, C. Ozyildirim (2000), Evaluation of high performance concrete overlays placed on route 60 over Lynnhaven inlet in Virginia. Technical Note: VTRC 01-R1, Virginia department of transportation

[30] G. Chynoweth, R. R. Stankie, W. L. Allen, R. R. Anderson, W. N. Babcock, P. Barlow (1996). Concrete repair guide. ACI Committee, Concrete Repair Manual, Vol. 546R pp. 287 – 327.

[31] J. Lubiner, J. oliver, S. Oller, E. Onale (1989). A plastic-damage model for concrete. International Journal Solids Structures, Vol. 25, No. 3, pp. 299-326.

[32] Lee, J., & Fenves, G. L. (1998). Plastic-damage model for cyclic loading of concrete structures. Journal of Engineering Mechanics, ASCE, 124 (8), 892–900.

[33] I.A. Sharaky, L. Torres, H.E.M. Sallam (2014). Experimental and analytical investigation into the flexural performance of RC beams with partially and fully bonded NSM FRP bars/strips. Composite Structure, Vol. 122, pp. 113-126.

[34] E. Esmaeeli and J. A. O. Barros (2015). Flexural strengthening of RC beams using hybrid composite plate (HPC): Experimental and analytical study. Journal of Composites, part B, Vol. 79, pp. 604-620.

[35] A.A El-Ghandour (2010). Experimental and analytical investigation of CFRP flexural and shear strengthening efficiencies of RC beams. Construction and Building Materials Vol. 25, pp. 1419-1429

APPENDIX: ANALYRICAL MODELS

A1: RC-Control

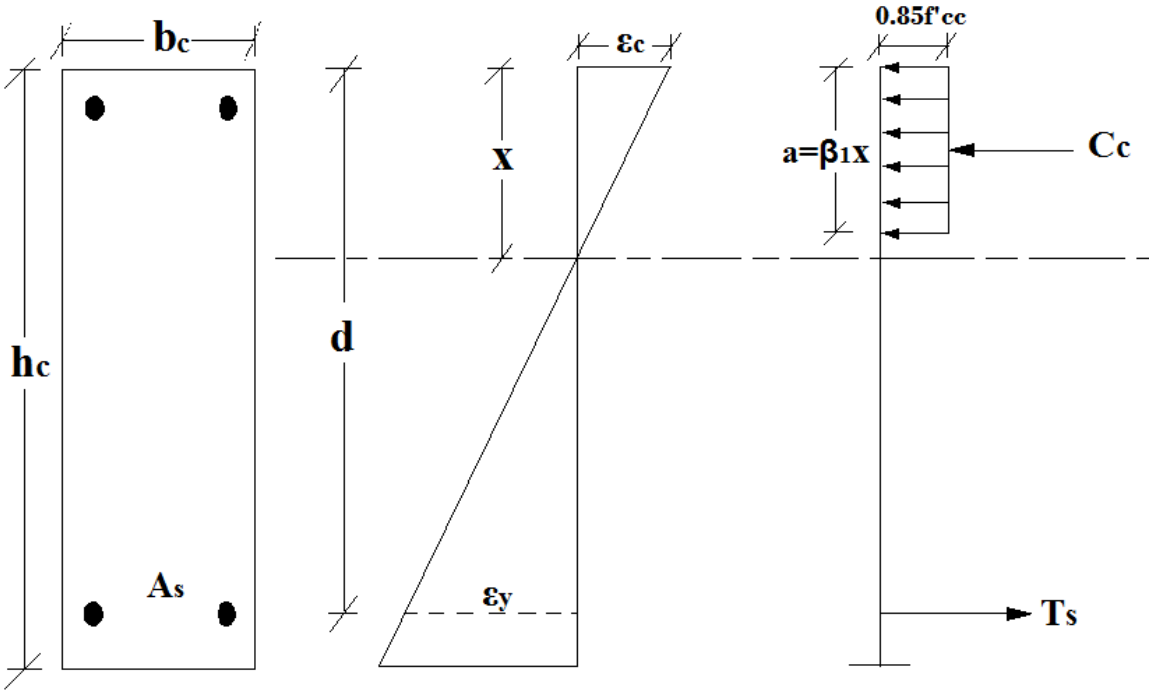

Figure 85: Analytical model definition for RC-Control

Inputs Data:

$f'_{cc} = 45\ MPa$

$f'_{uc} = 0$

$\varepsilon_y = 0.003$

$\varepsilon_{ut} = 0$

$f_y = 610\ MPa$

$E_s = 200{,}000$

$h_c = 230mm$

$b_u = 0$

$b_c = 140mm$

$h_u = 0$

$b_u = 0$

A 2: RC – BOT SJ

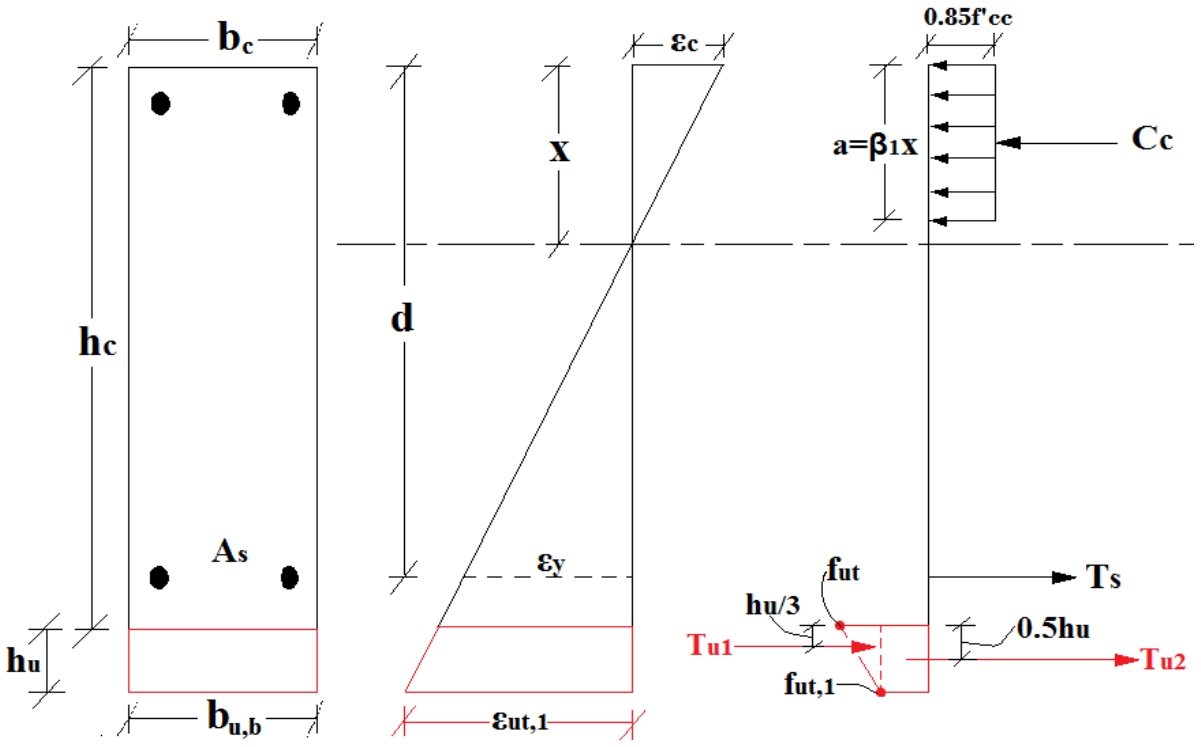

Figure 86: Analytical model definition for $RC - BOT\ SJ$

Input Data:

$f'_{cc} = 45\ MPa$

$f'_{uc} = 0$

$\varepsilon_y = 0.003$

$\varepsilon_{ut} = 0.005$

$f_y = 610\ MPa$

$f_{ut,1} = f_{ut,crack} = 7MPa$

$f_{ut,2} = 4.6MPa$

$E_s = 200{,}000MPa$

$h_c = 230mm$

$b_u = 0$

$b_c = 140mm$

$h_u = 30mm$

$b_{u,b} = 140mm$

A 2: RC − 2 SJ

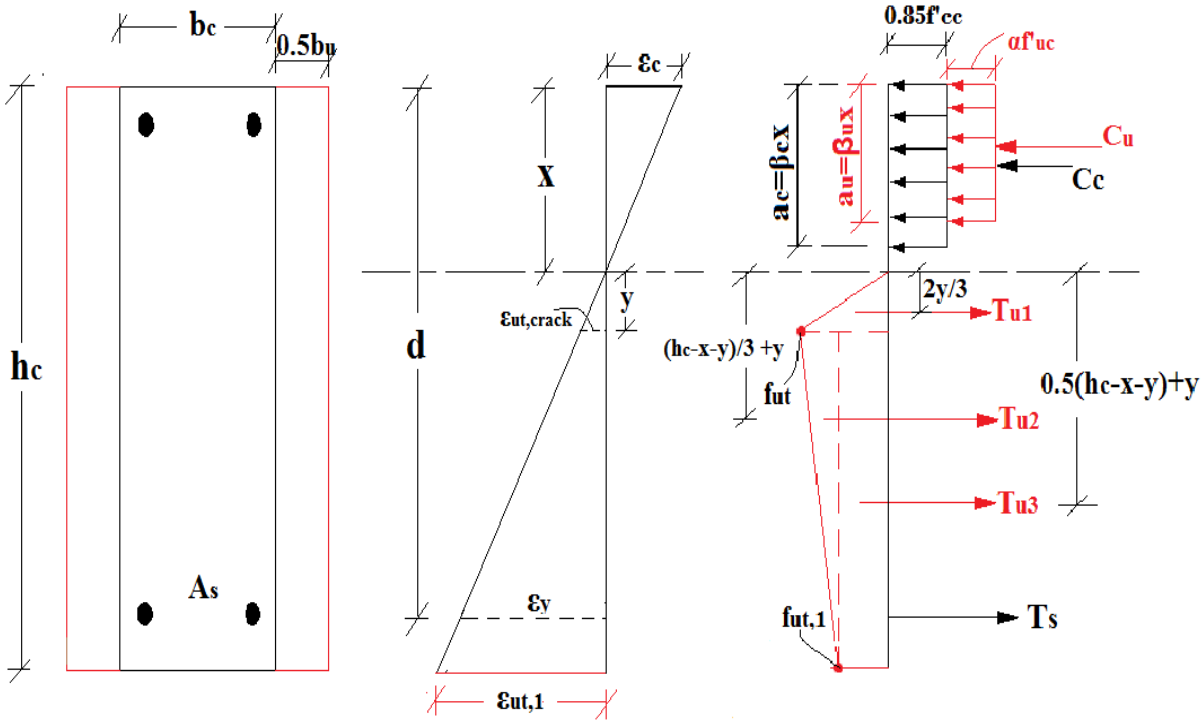

Figure 87: Analytical model definition for $RC - 2\ SJ$

Input Data:

$\varepsilon_y = 0.003$

$\varepsilon_{ut} = 0.006$

$f'_{cc} = 45\ MPa$

$f'_{uc} = 128MPa$

$f_y = 610\ MPa$

$f_{ut,1} = f_{ut,crack} = 7MPa$

$f_{ut,2} = 4.6MPa$

$E_s = 200{,}000MPa$

$h_c = 230mm$

$b_u = 60MPa$

$b_c = 140mm$

$h_u = 0$

$b_{u,b} = 0$

A4: RC − 3 SJ

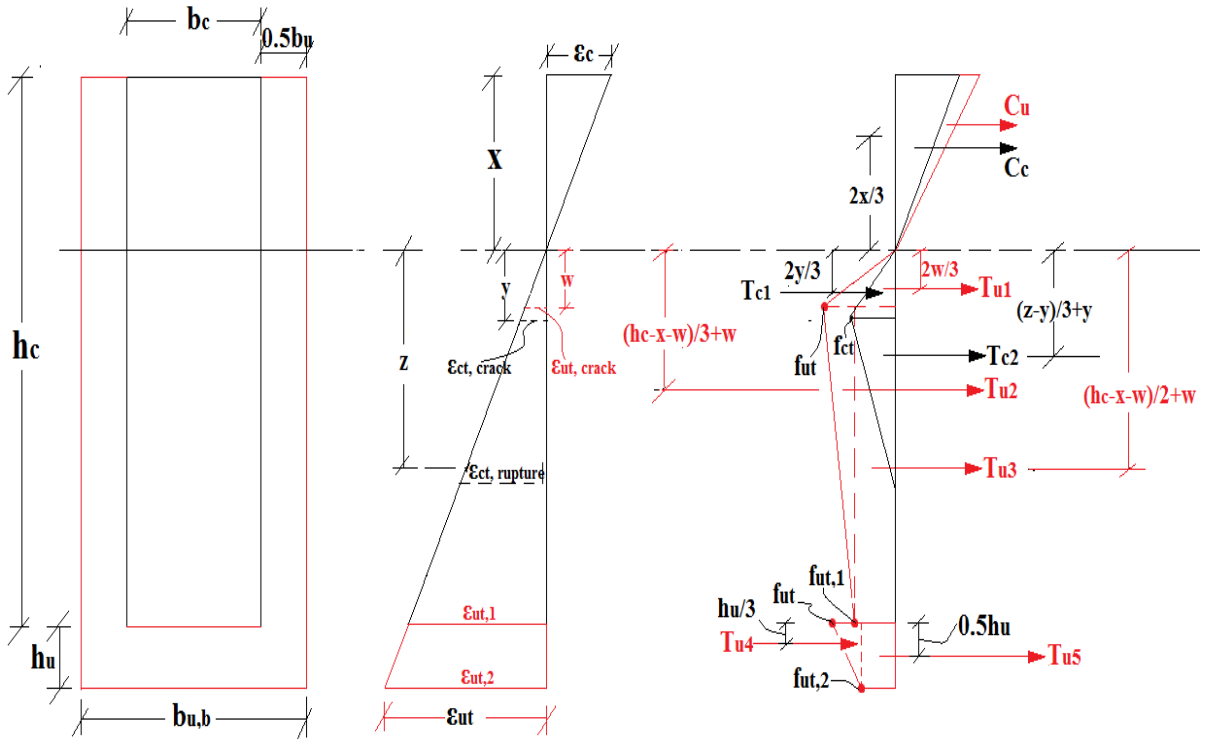

Figure 88: Analytical model definition for $RC - 3\ SJ$

Input Data:

$\varepsilon_y = 0.003$

$\varepsilon_{ut} = 0.007$

$f'_{cc} = 45\ MPa$

$f'_{uc} = 128MPa$

$f_y = 610\ MPa$

$f_{ut,1} = f_{ut,crack} = 7MPa$

$f_{ut,2} = 5MPa$

$f_{ut,3} = 7MPa$

$f_{ut,4} = 4.2MPa$

$E_s = 200{,}000MPa$

$h_c = 230mm$

$b_u = 60MPa$

$b_c = 140mm$

$h_u = 30mm$

$b_{u,b} = 230mm$

A5: PC − Control

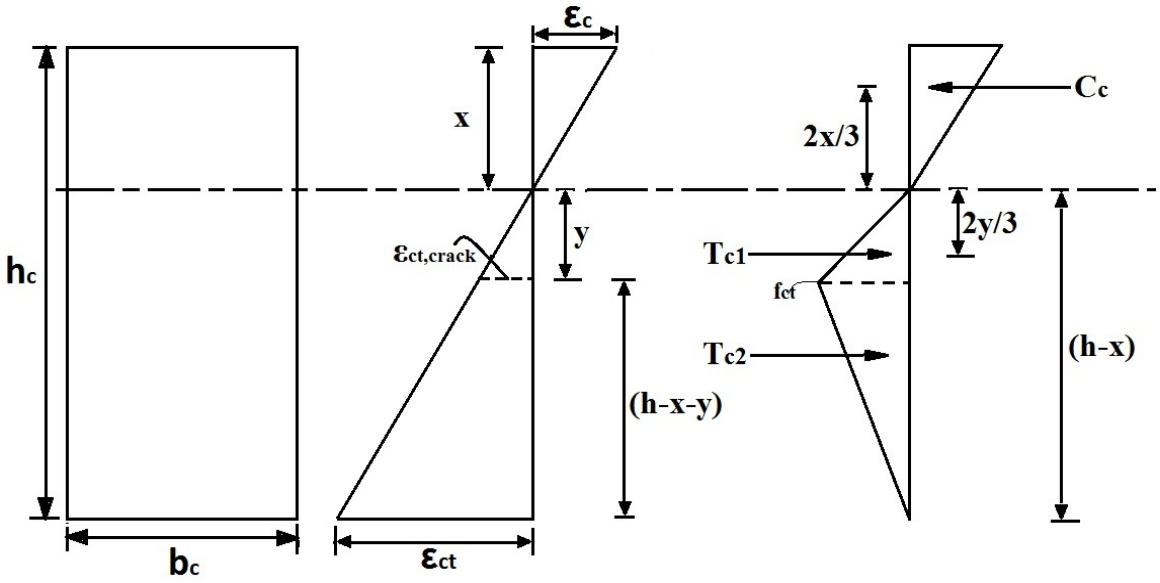

Figure 89: Analytical model definition for PC − Control

Inputs Data:

$\varepsilon_{ct,crack} = 0.00015$

$\varepsilon_{ct} = 0.0013$

$f_{ct} = 4.14\text{MPa}$

$E_c = 31{,}500\text{MPa}$

$h_c = 230\text{mm}$

$b_u = 0$

$b_c = 140\text{mm}$

$h_u = 0$

$b_u = 0$

A6: PC – SB – BOT SJ

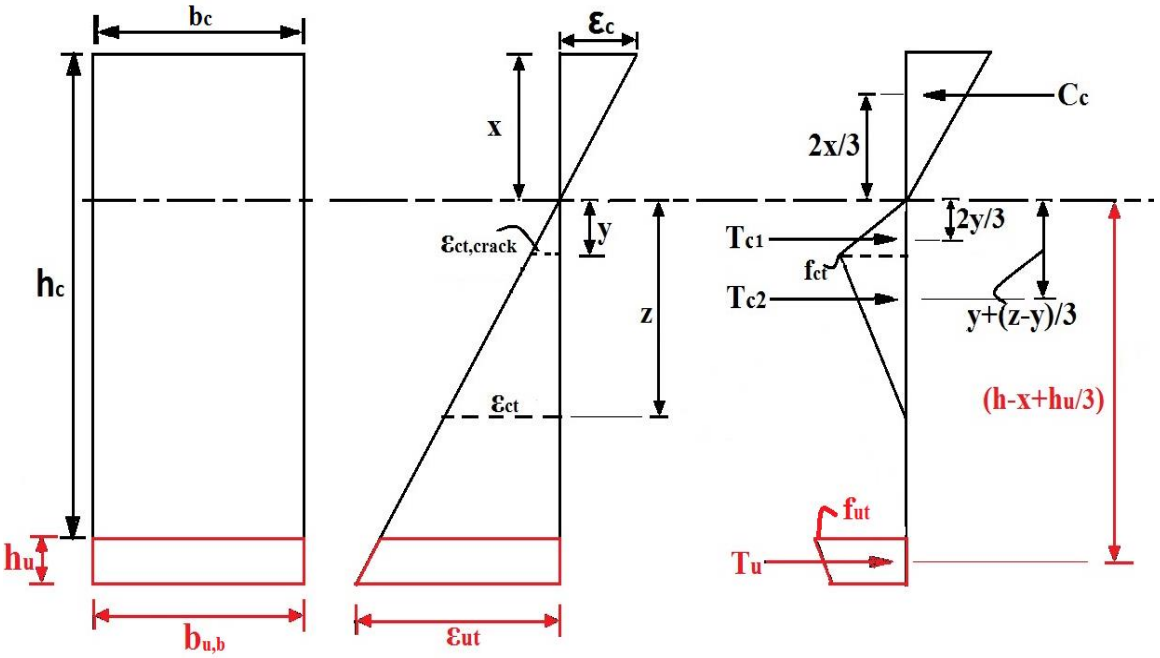

Figure 90: Analytical model definition for PC – BOT SJ

Input Data:

$\varepsilon_{ct,crack} = 0.00015$

$\varepsilon_{ut} = 0.0015$

$f_{ct} = 4.14\text{MPa}$

$f_{ut} = 6\text{MPa}$

$E_c = 31{,}500\text{MPa}$

$h_c = 230\text{mm}$

$b_u = 0$

$b_c = 140\text{mm}$

$h_u = 30\text{mm}$

$b_{u,b} = 140\text{mm}$

A7: PC – BS – 2 SJ

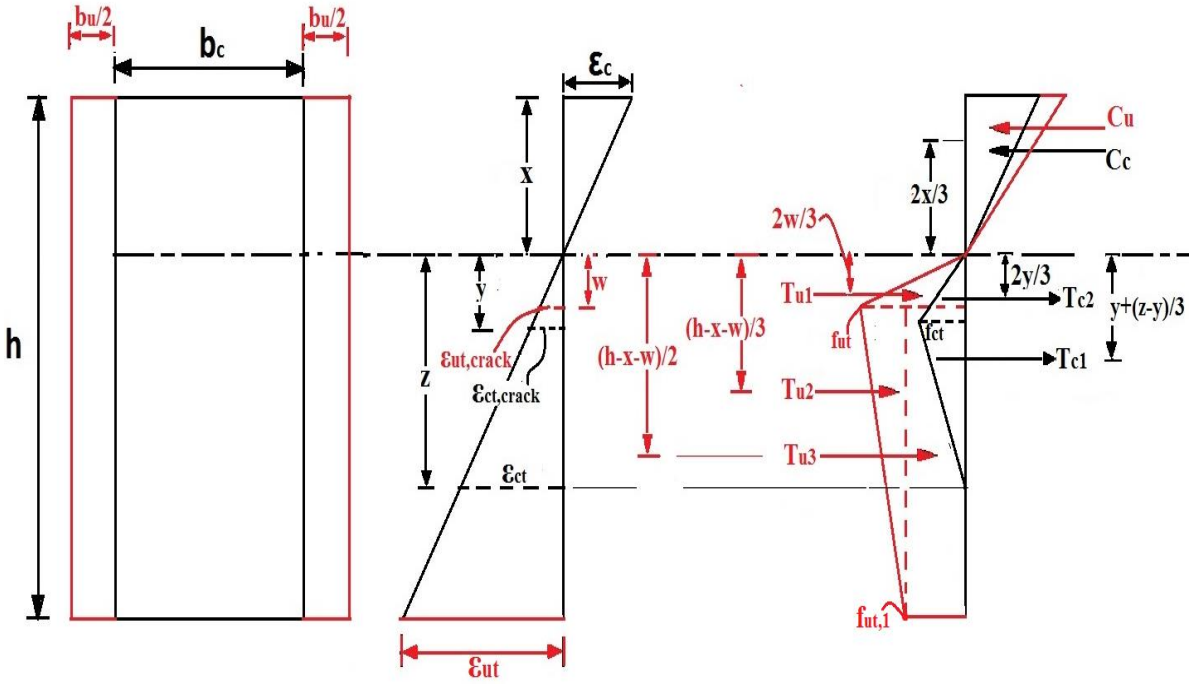

Figure 91: Analytical model definition for PC – SB – 2 SJ

Input Data:

$\varepsilon_{ct,crack} = 0.00015$

$\varepsilon_{ut} = 0.0015$

$f_{ct} = 4.14\text{MPa}$

$f_{ut} = 6\text{MPa}$

$f_{ut,1} = 5\text{MPa}$

$E_c = 31{,}500\text{MPa}$

$h_c = 230\text{mm}$

$b_u = 60\text{mm}$

$b_c = 140\text{mm}$

$h_u = 0\text{mm}$

$b_{u,b} = 0$

PC – SB – 3 SJ

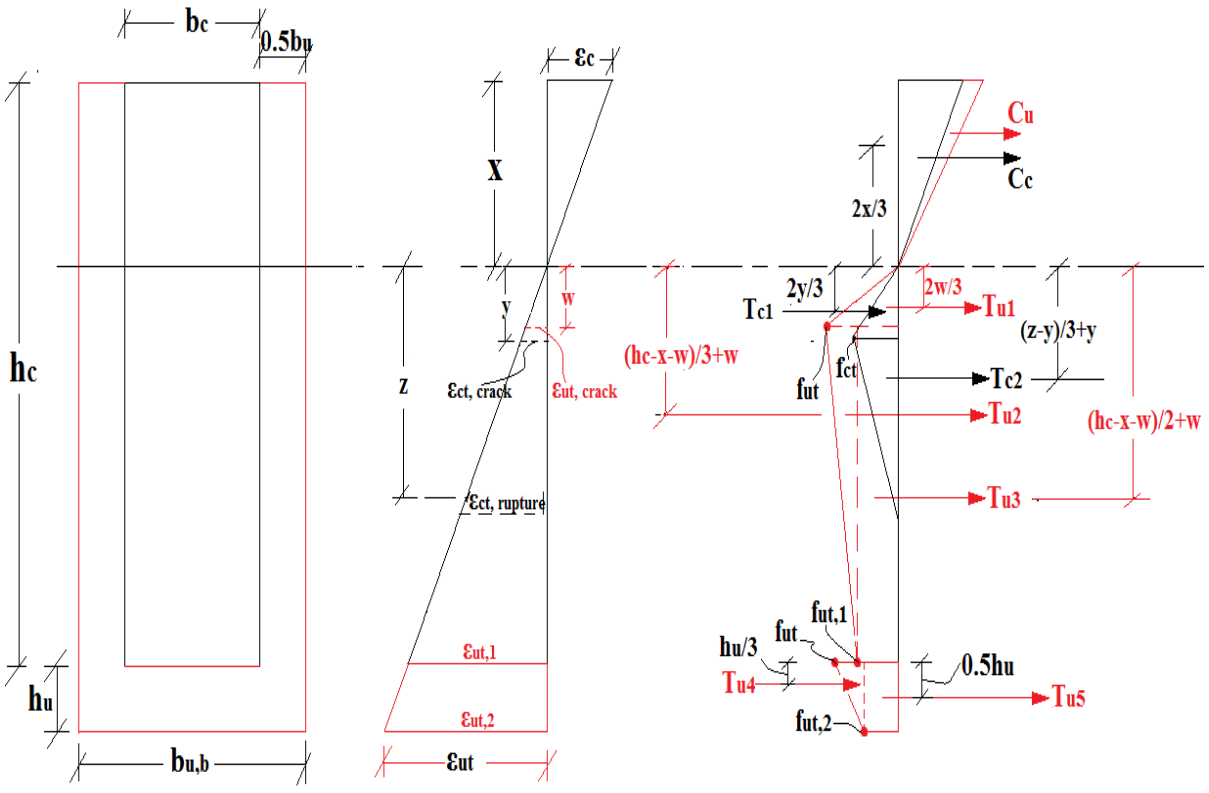

Figure 92: Analytical model definition for PC – SB – 3 SJ

Input Data:

$\varepsilon_{ct,crack} = 0.00015$

$\varepsilon_{ut} = 0.0015$

$f_{ct} = 4.14\text{MPa}$

$f_{ut} = 6\text{MPa}$

$f_{ut,1} = 4.5\text{MPa}$

$f_{ut,2} = 4.2\text{MPa}$

$E_c = 31{,}500\text{MPa}$

$h_c = 230\text{mm}$

$b_u = 60\text{mm}$

$b_c = 140\text{mm}$

$h_u = 0\text{mm}$

$b_{u,b} = 0$

VITAE

Name:	Muhammad Nura Isa
Nationality:	Nigeria
Date of Birth:	7th August 1989
Email:	mnisheshe@gmail.com
Address:	Dankura Street, Zoo Road, Kano, Nigeria
Academic Background:	(1) M.S. Civil Engineering; King Fahd University of Petroleum and Minerals (KFUPM), Saudi Arabia. (2) B.Eng Civil Engineering; Bayero University Kano (BUK), Nigeria.
Awards:	His Excellency Governor Rabiu Musa Kwankwaso Prize for the Best Graduating Student in the Department of Civil Engineering BUK 2010/2011 Academic Session